Technical University of Munich

Master's Thesis

Investigation of Finite Element Methods for a 4D Hybrid Plasma Model / Untersuchung von Finite-Elemente-Methoden für ein 4D hybrides Plasmamodell

Author:
Florian Holderied

Referees:
1. Prof. Dr. Sibylle Günter
2. Dr. Stefan Recksiegel

Munich 2019

Masterarbeit vorgelegt der Fakultät für Physik der Technischen Universität München zur Erlangung des akademischen Grades des *Master of Science* (M. Sc.).

Autor	Florian Holderied
Bearbeitungszeit	01. Februar 2018 bis 31. Januar 2019
durchgeführt bei	Max-Planck-Institut für Plasmaphysik (IPP) Boltzmannstraße 2 D-85748 Garching
Gutachter	1. Prof. Dr. Sibylle Günter 2. Dr. Stefan Recksiegel
Betreuer	Dr. Xin Wang Dr. Ahmed Ratnani Dr. Stefan Possanner

Abstract

Two different numerical methods which both belong to the well-known class of finite element methods have been applied on a four-dimensional (one dimension in space and three dimensions in velocity space) hybrid plasma model for electrons in a stationary, neutralizing background of ions. Here, the term hybrid means that (energetic) electrons with velocities close to the phase velocity of the model's characteristic waves are treated kinetically whereas electrons that are much slower than the phase velocity are treated with fluid equations. The two numerical methods, which belong on the one hand to the class of standard finite elements and on the other hand to the more modern class of finite element exterior calculus (FEEC) [1, 2], have been implemented in Python, tested successfully by using results from the analytical theory and compared in terms of long-term energy conservation which is expected on the continuous level. Regarding the latter, it turned out that FEEC applied on the model yields better results which is due to fact that the spatial discretization leads to a large system of ordinary differential equations in time that exhibits a non-canonical Hamiltonian structure for which special time integration schemes with good conservation properties exist [3, 4].

Contents

List of Figures

1 Introduction

1.1 Fusion energy and energetic particles

„Bringing the power of the sun to earth". This dream of human kind of an abundant, safe and emission-free source of energy has become noticeably stronger in the last decades due to global problems such as climate change, a fast growing global population, the finite amount of fossil fuels such as coal, oil and gas on earth and the unsolved problem of storing the large amounts of long-living nuclear waste produced by conventional nuclear power plants that work with nuclear fission. Nuclear fusion, the process with which the sun gains its energy, combines the advantages of having an almost infinite amount of the fuel on earth and not producing harmful exhaust fumes and long-living nuclear waste. For a future fusion reactor, the above-mentioned fuel will be Deuterium (D) and Tritium (T) due to the large reactivity of the reaction

Figure 1.1: *Reactivity of some common fusion reactions dependent on the temperature T. At $T = 10\,keV$ one observes a two orders of magnitude larger reactivity of the D-T reaction compared to the other reactions [5].*

$$\,^2_1\mathrm{D} + \,^3_1\mathrm{T} \rightarrow \,^4_2\mathrm{He}\,(3.52\,\mathrm{MeV}) + \,^1_0\mathrm{n}\,(14.06\,\mathrm{MeV}). \tag{1.1}$$

This can be seen in fig. 1.1, where the reactivities with respect to the temperature of some common fusion reactions are compared. Deuterium can easily be extracted from sea water whereas Tritium, which is unstable and does therefore not exist in vast amounts in nature, can be generated by a reaction involving Lithium and neutrons which come out of the reaction (1.1) [5, 6].

However, bringing two positively charged ions close enough together in order to overcome the repulsive Coulomb barrier by quantum tunneling requires much thermal energy of $T \gtrsim 10\,\mathrm{keV}$[1]. At this temperature, a gas can be considered as completely ionized and shows a distinctly different behavior compared to a neutral gas which is why this state of matter gets the new name *plasma* [5].

In order to achieve a self-sustained fusion plasma (*ignition*), the self-heating power of the plasma by the formed $3.52\,\mathrm{MeV}$ α-particles ($P_{\mathrm{fus},\alpha}$) must be larger than all the losses P_{loss} during a characteristic confinement time τ_{c}. For a homogeneous plasma in a volume V this condition reads

$$P_{\mathrm{fus},\alpha} \geq P_{\mathrm{loss}} = \frac{3}{2}\frac{T(n_{\mathrm{e}} + n_{\mathrm{DT}})V}{\tau_{\mathrm{c}}}. \tag{1.2}$$

---

[1]We suppress the Boltzmann constant k_{B}, i.e. the temperature T denotes actually the energy $k_{\mathrm{B}}T$.

In the range $T \approx 10-20\,\text{keV}$, where the D-T-reactivity can be approximated by a parabola (i.e. $\sim T^2$, in the logarithmic plot 1.1 this results in a straight line), this leads to the famous *Lawson criterion*

$$n_{\text{e}} \cdot T \cdot \tau_{\text{c}} \geq 3 \cdot 10^{24}\,\text{eVsm}^{-3}, \tag{1.3}$$

where $n_{\text{e}} = n_{\text{DT}}$ is the electron/D-T number density and $T = T_{\text{i}} \approx T_{\text{e}}$ the ion/electron temperature [5, 7]. This means that the *Lawson criterion* allows to vary n_{e} and τ_{c} over wide ranges as long as the product $n_{\text{e}}\tau_{\text{c}}$ is large enough to overcome the lower limit for some fixed temperature T.

The concept of inertial confinement is the approach of a large $n_{\text{e}} \approx 10^{31}\,\text{m}^{-3}$ and a low $\tau_{\text{c}} \approx 10^{-10}$ s. The idea of this method is to heat the target on a time scale where it is confined by its own inertia [8]. This can for instance be achieved with very strong laser pulses [9]. In contrast to that, the concept of magnetic confinement works with a low $n_{\text{e}} \approx 10^{21}\,\text{m}^{-3}$ and a large $\tau_{\text{c}} \approx 5$ s. This method uses a strong helically shaped magnetic field that forces the charged particles of the fusion plasma on orbits around its field lines due to the Lorentz force. However, reaching a stable plasma configuration, meaning that the hot plasma does not touch the wall of a fusion device due to perturbations which are unstable and therefore grow in time, is a challenging task which is why ignition has not been achieved yet [5].

The closer experiments reach this goal, the more important becomes the understanding of effects of energetic particles on the keV background plasma. This is because reaching such high temperatures involves additional heating beyond the ohmic limit with e.g. neutral beam injection (NBI), ion and electron resonance heating (ICRH, ECRH), which, together with the $3.52\,\text{MeV}$ α-particles in case of fusion, leads to an enhanced population of energetic particles that can possibly destabilize the plasma [10, 11].

The plasma model which will be considered in this thesis belongs to this particular class of energetic particles interacting with a thermal background plasma and has the aforementioned property that energetic particles lead to a destabilization of originally stable plasma waves [13, 14].

1.2 Hierarchy of plasma models

Nowadays, with the help of super computers, quite realistic numerical simulations of energetic particle phenomena become possible and have already been carried out with various codes (see for instance ref. [12]). Such codes implement a certain mathematical plasma model which is typically a set of partial differential equations (PDEs) that describe the time evolution of a set of plasma quantities dependent on some given initial configuration. The challenge of solving such a system of equations is to find a good balance between accuracy on the one hand and efficiency on the other hand since computational resources are limited and often expensive. This means that one tries to find a model which is able to describe the physics of interest with the least computational costs possible.

There are three basic classes of plasma models that form a hierarchy in terms of accuracy and computational costs meaning that they become on the one hand less and less accurate, however „easier" to solve (see [5, 15] for basic plasma descriptions):

1. **_Microscopic models_**: Such models describe a plasma really as what it is, namely a collection of freely movable electrons and ions. This means that one would have to solve an equation of motion of the form

$$m_i \frac{\mathrm{d}\mathbf{v}_i}{\mathrm{d}t} = \sum_j q_i(\mathbf{E}_j + \mathbf{v}_i \times \mathbf{B}_j) + q_i(\mathbf{E}_0 + \mathbf{v}_i \times \mathbf{B}_0) \tag{1.4}$$

for every single plasma particle i with mass m_i and charge q_i which is subjected to the Lorentz force due to the electromagnetic fields $\mathbf{E}_j$ and $\mathbf{B}_j$ generated by all the other particles j as well as due to external fields $\mathbf{E}_0$ and $\mathbf{B}_0$. However, this is not possible and also not of interest for several reasons: First, solving this model would require the knowledge of positions and velocities of all particles at some point in time, which is of course not possible. Second, even if one had this information, the amount of needed computations which is of the order N^2, where N being the number of particles, would take billions of years with current computers. And third, the knowledge of every single particle position and velocity is not of interest as this cannot be measured in experiments. Here, only macroscopic quantities such as temperature, pressure or the mean velocity of the plasma are accessible.

2. **_Statistical/kinetic models_**: Here, the quantity of interest is the distribution function $f_\alpha = f_\alpha(\mathbf{x}, \mathbf{v}, t)$ of some plasma species α (e.g. $\alpha = \mathrm{e}$ for electrons or $\alpha = \mathrm{i}$ for ions) which represents a statistical mean of a large number of microscopic realizations of indistinguishable particles in the six-dimensional phase space. The distribution function then gives the number of particles $\mathrm{d}N_\alpha$ which are located in the interval $[\mathbf{x}, \mathbf{x} + \mathrm{d}^3\mathbf{x}]$ and have velocities in the interval $[\mathbf{v}, \mathbf{v} + \mathrm{d}^3\mathbf{v}]$, i.e.

$$\mathrm{d}N_\alpha = f_\alpha \mathrm{d}^3\mathbf{x}\mathrm{d}^3\mathbf{v}. \tag{1.5}$$

The time evolution of the distribution function obeys the _Boltzmann_ equation

$$\frac{\partial f_\alpha}{\partial t} + \mathbf{v} \cdot \nabla f_\alpha + \frac{q_\alpha}{m_\alpha}(\mathbf{E} + \mathbf{v} \times \mathbf{B}) \cdot \nabla_\mathbf{v} f_\alpha = \sum_\beta C^{\alpha/\beta}(f_\alpha), \tag{1.6}$$

where we have already used that in plasma physics one deals with a statistical ensemble of charged particles of mass m_α and charge q_α which are subjected to the Lorentz-force due to the presence of a macroscopic electric field $\mathbf{E} = \mathbf{E}(\mathbf{x}, t)$ and a macroscopic magnetic field $\mathbf{B} = \mathbf{B}(\mathbf{x}, t)$.

The collision operator $C^{\alpha/\beta}$ on the right-hand side of eq. (1.6) takes into account collisions between different particle species, including itself, and has the effect of bringing a non-equilibrium distribution function back to an time-independent equilibrium state. A commonly used collision operator in plasma physics is the _Landau_ operator which is built from the fact that two-particle interactions in plasmas are dominated by small-angle Coulomb collisions. However, under certain circumstances, e.g. very high temperatures like in the core of a fusion plasma or high-frequency phenomena, the collision operator becomes very small and can therefore

be neglected for such problems. This also means that such plasmas can exist far away from thermal equilibrium for relatively long times and moreover, eq. (1.6) then states that f_α is conserved along the particle trajectories in phase space, i.e. $\frac{\mathrm{d}f_\alpha}{\mathrm{d}t}(t, \mathbf{x}(t), \mathbf{v}(t)) = 0$. In this case the Boltzmann equation is called the *Vlasov* equation.

In order to get a self-consistent description of the plasma, the Boltzmann/Vlasov equation is coupled to Maxwell's equations

$$-\frac{1}{c^2}\frac{\partial \mathbf{E}}{\partial t} + \nabla \times \mathbf{B} = \mu_0 \mathbf{j}, \tag{1.7a}$$

$$\frac{\partial \mathbf{B}}{\partial t} + \nabla \times \mathbf{E} = 0, \tag{1.7b}$$

$$\nabla \cdot \mathbf{E} = \frac{\rho}{\epsilon_0}, \tag{1.7c}$$

$$\nabla \cdot \mathbf{B} = 0, \tag{1.7d}$$

which describe the generation and time evolution of the macroscopic electromagnetic fields $\mathbf{E}$ and $\mathbf{B}$. Here, ϵ_0 denotes the vacuum permittivity, μ_0 the vacuum permeability and c the speed of light which all satisfy $\mu_0 \epsilon_0 c^2 = 1$. The sources of the fields, which are the charge density ρ and the current density $\mathbf{j}$, are obtained by taking the first two moments of the distribution function in velocity space and summing over all species:

$$\rho(\mathbf{x}, t) = \sum_\alpha q_\alpha \int f_\alpha(\mathbf{x}, \mathbf{v}, t) \mathrm{d}^3\mathbf{v}, \tag{1.8a}$$

$$\mathbf{j}(\mathbf{x}, t) = \sum_\alpha q_\alpha \int \mathbf{v} f_\alpha(\mathbf{x}, \mathbf{v}, t) \mathrm{d}^3\mathbf{v}. \tag{1.8b}$$

The system of equations (1.6)-(1.8) is called the *Vlasov-Maxwell* system which is a closed system of coupled, nonlinear partial differential equations in seven dimensions (three in space, three in velocity space and one in time). Thus, compared to the previous model, the number of degree of freedom has been reduced from $6N$ to 6 (plus time).

3. **Fluid/macroscopic models**: A further simplification can be done by taking averages in velocity space in order to obtain fluid-like equations for the macroscopic plasma quantities. For this, we define the macroscopic quantities by

$$n_\alpha(\mathbf{x}, t) = \int f_\alpha(\mathbf{x}, \mathbf{v}, t)\, \mathrm{d}^3\mathbf{v}, \tag{1.9a}$$

$$n_\alpha(\mathbf{x}, t)\mathbf{u}_\alpha(\mathbf{x}, t) = \int \mathbf{v} f_\alpha(\mathbf{x}, \mathbf{v}, t)\, \mathrm{d}^3\mathbf{v}, \tag{1.9b}$$

$$n_\alpha(\mathbf{x}, t)T_\alpha(\mathbf{x}, t) = \frac{m_\alpha}{3} \int v^2 f_\alpha(\mathbf{x}, \mathbf{v}, t)\, \mathrm{d}^3\mathbf{v}, \tag{1.9c}$$

where n_α is the number density, $\mathbf{u}_\alpha$ the mean velocity and T_α the temperature (or the mean kinetic energy per particle) of the plasma species α. The time evolution

of these quantities is then obtained by taking the first three velocity moments of the Boltzmann equation which consists of multiplying successively by 1, $m_\alpha \mathbf{v}$, and $m_\alpha v^2/2$ and integrating over velocity space. However, after having done this, it is immediately clear that one dose not obtain a closed system of equations since the evolution equation for the p-th moment depends explicitly on the $(p+1)$-th moment of the distribution function. A simple closure of the equations can be obtained by neglecting collisions between different plasma species and by assuming a plasma which is in local thermal equilibrium. The latter means that the distribution function of every species α is close to a Maxwellian which, in the co-moving frame of $\mathbf{u}_\alpha$, reads

$$f_\alpha(\mathbf{x}, \mathbf{v}, t) = n_\alpha(\mathbf{x}, t) \left(\frac{m_\alpha}{2\pi T_\alpha(\mathbf{x}, t)} \right)^{3/2} \exp\left(-\frac{m_\alpha(\mathbf{v} - \mathbf{u}_\alpha(\mathbf{x}, t))^2}{2T_\alpha(\mathbf{x}, t)} \right). \tag{1.10}$$

Using this, as well as the fact that elastic collisions between particles of the same species conserve the number of particles, momentum and energy [16], one obtains, together with Maxwell's equations, the following closed set of evolution equations, which stand for the conservation of mass, momentum and energy, respectively:

$$\frac{\partial n_\alpha}{\partial t} + \nabla \cdot (n_\alpha \mathbf{u}_\alpha) = 0, \tag{1.11a}$$

$$\frac{\partial}{\partial t}(m_\alpha n_\alpha \mathbf{u}_\alpha) + \nabla \cdot (m_\alpha n_\alpha \mathbf{u}_\alpha \otimes \mathbf{u}_\alpha) + \nabla p_\alpha = q_\alpha n_\alpha (\mathbf{E} + \mathbf{u}_\alpha \times \mathbf{B}), \tag{1.11b}$$

$$\frac{\partial}{\partial t}(\frac{3}{2}p_\alpha + \frac{1}{2}m_\alpha n_\alpha \mathbf{u}_\alpha^2) + \nabla \cdot (\frac{5}{2}p_\alpha \mathbf{u}_\alpha + \frac{m_\alpha}{2}n_\alpha \mathbf{u}_\alpha^2 \mathbf{u}_\alpha) = q_\alpha n_\alpha \mathbf{E} \cdot \mathbf{u}_\alpha. \tag{1.11c}$$

Here, we have introduced the scalar pressure $p_\alpha(\mathbf{x}, t) = n_\alpha(\mathbf{x}, t)T_\alpha(\mathbf{x}, t)$.

As already indicated, the above description has the consequence that its validity is limited to plasmas which are in local thermal equilibrium. This has the consequence that particle effects like collision-less damping/heating caused by wave-particle interactions can not be described anymore. However, the advantage of this fluid approach is that the dimensionality has been further reduced to three in space plus one in time which enables nowadays performing large-scale simulations of fusion plasmas both in space and time (e.g. ref. [17]).

In this thesis, we shall use a combination of a kinetic model for energetic particles and a fluid model for a thermal background plasma. Such a model, that makes use of different plasma models at the same time, is called a *hybrid model*.

1.3   Computational aspects

Due to the fact that nonlinear partial differential equations can in general not be solved exactly, one needs to find approximate solutions for it. This procedure usually involves performing a *discretization* of the problem which consists of replacing some continuous mathematical object computers can not deal with by a corresponding discrete object which has a finite number of elements and can therefore be represented on a computer.

A simple example for this is the representation of the continuous three-dimensional space by a finite number of grid points at which approximate solutions are computed. This approach is done in the so-called *Finite Differences* method which consist of replacing the occurring derivatives in a PDE by a truncated Taylor series of arbitrary order. In contrast to that, the discretization in the so-called *Finite Element* method (FEM), which will be used in this thesis, consists of replacing continuous function spaces by finite-dimensional subspaces in which one looks for the approximate solution [18].

A numerical simulation is usually performed in the following way: One starts with an equilibrium state, slightly perturbs one or more quantities and then looks for the evolution of these perturbations in time. Such simulations can be split into two phases:

1. A *linear phase* where the perturbations either increase (unstable) or decrease (stable) exponentially in time and where the perturbations are much smaller than the corresponding equilibrium/background quantities. This has the consequence that only the interaction with the background quantities must be taken into account.

2. A subsequent *nonlinear phase* where the perturbations are of the order of the background quantities. Here, interactions between the perturbations themselves can not be neglected anymore.

Keeping certain conservation properties such as conservation of energy or momentum or laws arising in electrodynamics like the two Gauss laws (1.7c) and (1.7d) in particular in the nonlinear phase where complex nonlinear dynamics appear, is a challenging task for numerical algorithms. In order to trust the results of long simulations deep into the nonlinear phase, one would like to keep these fundamental physical conservation laws. Furthermore, it has been shown that the violation of conservation properties can lead to unstable algorithms meaning that, although having a consistent method, the numerical errors increase in time and therefore the simulations yields wrong results [2].

Modern numerical methods which use tools from the *finite-element-exterior calculus* (FEEC) are able to meet this requirement [1, 2]. This framework takes into account the geometric structure of a PDE in terms of differential geometry and the fact that different physical quantities are different objects therein (which is why we shall
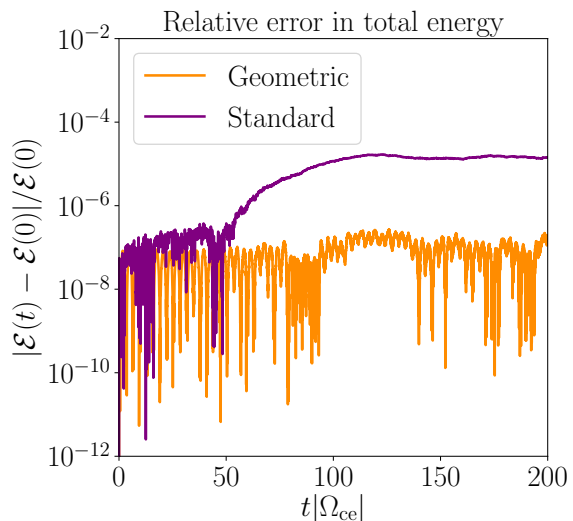
Figure 1.2: Comparison of the relative error in the conservation of the total energy $\mathcal{E}$ for a simulation performed with geometric and standard finite element methods (FEM). The difference between the linear and the nonlinear phase is only obvious for the standard FEM case. The time t is measured in units of the electron cyclotron frequency Ω_{ce} which will be defined later.

refer to these methods simply by *geometric methods*). Choosing different finite element spaces, which have certain relations to each other, for different physical quantities then leads to stable methods with very good conservation properties [3].

In ref. [19], this framework has been applied successfully on the Vlasov-Maxwell system (1.6)-(1.8). Kraus et al. could show that their discretization based on FEEC indeed conserves for instance the two aforementioned Gauss laws exactly on the fully discretized level (space and time).

The aim of this work is to apply this framework on an extended model which falls into the class of the above-mentioned hybrid kinetic/fluid models. In addition to that, another discretization with standard finite elements will be performed in order to demonstrate the similarities and differences of the two developed algorithms. In fig. 1.2 one can see the error in the conservation of energy we will end up with, and that the geometric methods indeed yield better results. However, before the numerics part, the physics content of the model is analyzed on the continuous level in order to judge whether the codes work properly.

This means that the outline of this work is as follows: First, the used hybrid model is introduced and analyzed on the continuous level. Second, the used numerical methods (particle-in-cell (PIC), standard finite elements, FEEC/geometric methods) are explained in a general sense followed by applying these methods on the hybrid model. Finally, simulation results obtained with the two developed algorithms are shown and compared.

2 Hybrid modeling

2.1 The model

2.1.1 Physics justification

The model which is investigated in this work in more detail is a high-frequency plasma model, i.e. wave frequencies ω are of the order of the electron cyclotron frequency $\Omega_{\mathrm{ce}} = q_{\mathrm{e}}|\mathbf{B}_0|/m_{\mathrm{e}}$, which is why the plasma ions (denoted by $\alpha = \mathrm{i}$) can not react on the fast fluctuations of the electromagnetic field and are therefore treated as a stationary, neutralizing background. Furthermore, we assume that the electron population consists mainly of cold electrons (denoted by $\alpha = \mathrm{c}$) which are in local thermal equilibrium and have negligible thermal effects (temperature $T_{\mathrm{c}} \approx 0$). In this case, the fluid equations introduced in the previous section are applicable and with the additional cold plasma assumption only the first two equations (1.11a) and (1.11b) are needed. Moreover, we assume that there is a small amount of energetic electrons (denoted by $\alpha = \mathrm{h}$) for which we shall use a kinetic description with negligible collisionality by assuming that the average collision times are much larger than the considered time scales. As already indicated, such an approach, which makes use of different plasmas models, is called a *hybrid model*.

From the full kinetic theory of plasma waves [15] one can show that the cold plasma approximation for an arbitrary species α is valid as long as

$$\frac{k_{\perp}^2 v_{\mathrm{th}\alpha}^2}{\Omega_{\mathrm{c}\alpha}^2} \ll 1, \qquad \left| \frac{\omega - n|\Omega_{\mathrm{c}\alpha}|}{k_{\parallel} v_{\mathrm{th}\alpha}} \right|^2 \gg 1, \tag{2.1}$$

for $n \in \mathbb{N}_0$. Here

$$k_{\parallel} = \frac{\mathbf{k} \cdot \mathbf{B}_0}{|\mathbf{B}_0|}, \qquad k_{\perp}^2 = k^2 - k_{\parallel}^2, \tag{2.2}$$

are the parallel and perpendicular components of the wave vector with respect to the background magnetic field $\mathbf{B}_0$ and $v_{\mathrm{th}\alpha} = \sqrt{2T_\alpha/m_\alpha}$ is the thermal velocity of species α.

The first inequality states that the Larmor radius $\rho_{\mathrm{th}\alpha} = v_{\mathrm{th}\alpha}/|\Omega_{\mathrm{c}\alpha}|$ of particles of the species α is much smaller than the perpendicular wavelength. This means that there is a negligible wave field variation due to the particles' perpendicular thermal motion. For $n = 0$, the second inequality states that the phase velocity $v_{\mathrm{ph}} = \omega/k$ of the wave is much larger than the thermal velocity of the particles which means that all particles essentially see the same wave fields without a significant Doppler shift. For $n > 0$, the inequality ensures that the wave is far from any harmonic of the particles' gyro motion which could lead to resonances and thus energy transfer between the wave and the particles [15].

The model which will be presented hereafter is for instance applicable to plasma dynamics in planetary magnetospheres and has been used successfully for the simulation of a special type of electromagnetic waves called *Chorus waves*. *Chorus waves* are electromagnetic emissions whose frequency-time-spectrograms show a series of discrete elements with rising frequencies with respect to time. An important condition for its excitation is the injection of energetic electrons with an anisotropic velocity distribution with respect to the earth's magnetic field into the magnetosphere. This is why *Chorus waves*

have been frequently observed in times with strong solar winds and the enhanced particle precipitation of particles in the earth's magnetosphere that comes along with it [13, 14].

Using the mass continuity and momentum balance equation for the cold electrons (1.11a) and (1.11b), the collision-less Boltzmann equation (1.6) (Vlasov equation) for the energetic electrons and Maxwell's equations (1.7) for the dynamics of the electromagnetic fields, the full set of equations in SI-units reads

$$\text{cold fluid electrons} \begin{cases} \dfrac{\partial n_\mathrm{c}}{\partial t} + \nabla \cdot (n_\mathrm{c} \mathbf{u}_\mathrm{c}) = 0, & \text{(2.3a)} \\[2mm] \dfrac{\partial \mathbf{u}_\mathrm{c}}{\partial t} + (\mathbf{u}_\mathrm{c} \cdot \nabla)\mathbf{u}_\mathrm{c} = \dfrac{q_\mathrm{e}}{m_\mathrm{e}}(\mathbf{E} + \mathbf{u}_\mathrm{c} \times \mathbf{B}), & \text{(2.3b)} \\[2mm] \mathbf{j}_\mathrm{c} = q_\mathrm{e} n_\mathrm{c} \mathbf{u}_\mathrm{c}, & \text{(2.3c)} \end{cases}$$

$$\text{hot kinetic electrons} \begin{cases} \dfrac{\partial f_\mathrm{h}}{\partial t} + \mathbf{v} \cdot \nabla f_\mathrm{h} + \dfrac{q_\mathrm{e}}{m_\mathrm{e}}(\mathbf{E} + \mathbf{v} \times \mathbf{B}) \cdot \nabla_\mathbf{v} f_\mathrm{h} = 0, & \text{(2.3d)} \\[2mm] \mathbf{j}_\mathrm{h} = q_\mathrm{e} \displaystyle\int f_\mathrm{h} \mathbf{v} \, \mathrm{d}^3 \mathbf{v}, & \text{(2.3e)} \\[2mm] n_\mathrm{h} = \displaystyle\int f_\mathrm{h} \, \mathrm{d}^3 \mathbf{v}, & \text{(2.3f)} \end{cases}$$

$$\text{Maxwell} \begin{cases} \dfrac{\partial \mathbf{B}}{\partial t} = -\nabla \times \mathbf{E}, & \text{(2.3g)} \\[2mm] \dfrac{1}{c^2} \dfrac{\partial \mathbf{E}}{\partial t} = \nabla \times \mathbf{B} - \mu_0 (\mathbf{j}_\mathrm{c} + \mathbf{j}_\mathrm{h}), & \text{(2.3h)} \\[2mm] \nabla \cdot \mathbf{E} = \dfrac{1}{\epsilon_0} \left[q_\mathrm{i} n_\mathrm{i} + q_\mathrm{e}(n_\mathrm{c} + n_\mathrm{h}) \right], & \text{(2.3i)} \\[2mm] \nabla \cdot \mathbf{B} = 0, & \text{(2.3j)} \end{cases}$$

where, as stated above, the ions shall form a stationary background. This implies a constant number density n_i in time, i.e. $\partial n_\mathrm{i}/\partial t = 0$, and a vanishing current $\mathbf{j}_\mathrm{i} = 0$ for all times.

2.1.2 Model reduction

The model (2.3) can be reduced to an equivalent set of equations for the evolution of the fields $\mathbf{u}_\mathrm{c}, \mathbf{E}$ and $\mathbf{B}$ and the distribution function f_h with the constraint that (2.3i) and (2.3j) must be satisfied at the initial time $t = 0$. The reduced model then takes the form

$$\frac{\partial \mathbf{u}_\mathrm{c}}{\partial t} + (\mathbf{u}_\mathrm{c} \cdot \nabla)\mathbf{u}_\mathrm{c} = \frac{q_\mathrm{e}}{m_\mathrm{e}}(\mathbf{E} + \mathbf{u}_\mathrm{c} \times \mathbf{B}), \tag{2.4a}$$

$$\frac{\partial f_\mathrm{h}}{\partial t} + \mathbf{v} \cdot \nabla f_\mathrm{h} + \frac{q_\mathrm{e}}{m_\mathrm{e}}(\mathbf{E} + \mathbf{v} \times \mathbf{B}) \cdot \nabla_\mathbf{v} f_\mathrm{h} = 0, \tag{2.4b}$$

$$\frac{\partial \mathbf{B}}{\partial t} = -\nabla \times \mathbf{E}, \tag{2.4c}$$

$$\frac{1}{c^2} \frac{\partial \mathbf{E}}{\partial t} = \nabla \times \mathbf{B} - \mu_0 (\mathbf{j}_\mathrm{c} + \mathbf{j}_\mathrm{h}), \tag{2.4d}$$

9

combined with the aforementioned constraints at $t = 0$ and the definitions of the currents (2.3c), (2.3e) and the hot electron number density (2.3f). In order to proof that the model (2.4) is indeed equivalent to the model (2.3), we first take the divergence of Faraday's law (2.4c),

$$\nabla \cdot \left(\frac{\partial \mathbf{B}}{\partial t} + \nabla \times \mathbf{E} \right) = \frac{\partial}{\partial t} \left(\nabla \cdot \mathbf{B} \right) \stackrel{!}{=} 0, \tag{2.5}$$

which means that the divergence constraint for the magnetic field (2.3j) remains satisfied for later times $t > 0$ provided that it was satisfied at the initial time $t = 0$. As a next step, assuming that we can reconstruct the cold electron number density n_c as

$$n_\mathrm{c} = \frac{1}{q_\mathrm{e}} \left(\epsilon_0 \nabla \cdot \mathbf{E} - q_\mathrm{i} n_\mathrm{i} - q_\mathrm{e} n_\mathrm{h} \right), \tag{2.6}$$

at any time $t \geq 0$ according to Gauss law (2.3i), we take the divergence of Ampére's law (2.4d),

$$
\begin{aligned}
\nabla \cdot \left[\frac{1}{c^2} \frac{\partial \mathbf{E}}{\partial t} - \nabla \times \mathbf{B} + \mu_0 \left(\mathbf{j}_\mathrm{c} + \mathbf{j}_\mathrm{h} \right) \right] &= \frac{1}{c^2} \frac{\partial}{\partial t} \left(\nabla \cdot \mathbf{E} \right) + \mu_0 \nabla \cdot \left(\mathbf{j}_\mathrm{c} + \mathbf{j}_\mathrm{h} \right) \\
&= \frac{q_\mathrm{e}}{c^2 \epsilon_0} \frac{\partial}{\partial t} \left(n_\mathrm{c} + n_\mathrm{h} \right) + \mu_0 \nabla \cdot \left(\mathbf{j}_\mathrm{c} + \mathbf{j}_\mathrm{h} \right) \\
&= q_\mathrm{e} \mu_0 \underbrace{\left[\frac{\partial n_\mathrm{c}}{\partial t} + \nabla \cdot \left(n_\mathrm{c} \mathbf{u}_\mathrm{c} \right) \right]}_{\text{cont. eq. (2.3a)}} + q_\mathrm{e} \mu_0 \left(\frac{\partial n_\mathrm{h}}{\partial t} + \nabla \cdot \mathbf{j}_\mathrm{h} \right) \stackrel{!}{=} 0,
\end{aligned}
\tag{2.7}
$$

where we used the fact that the divergence of the electric field can be expressed in terms of the densities according to Gauss' law (2.3i) at any time $t \geq 0$ and that the ion number density is constant in time. In the last line of (2.7) we recognize the continuity equation for the fluid electrons in the squared bracket. For the second part, we continue the calculation by using first the definitions of the number and current densities of the energetic electrons, (2.3e) and (2.3f) respectively, followed by the usage of the Vlasov equation (2.4b):

$$\frac{\partial n_\mathrm{h}}{\partial t} + \nabla \cdot \mathbf{j}_\mathrm{h} = \int \mathrm{d}^3 \mathbf{v} \left(\frac{\partial f_\mathrm{h}}{\partial t} + \mathbf{v} \cdot \nabla_\mathbf{v} f_\mathrm{h} \right) = -\frac{q_\mathrm{e}}{m_\mathrm{e}} \int \mathrm{d}^3 \mathbf{v} \left(\mathbf{E} + \mathbf{v} \times \mathbf{B} \right) \cdot \nabla_\mathbf{v} f_\mathrm{h} = 0. \tag{2.8}$$

The last step can be shown by partial integration, the application of the divergence theorem for integrals and noting that $f_\mathrm{h} \to 0$ for $v \to \infty$. Thus, (2.7) reduces to the mass continuity equation (2.3a) which is therefore satisfied automatically by Amperè's law. In summary, we have shown that solutions of the reduced model (2.4) with compatible initial conditions are indeed solutions of the full model (2.3).

The model can further be simplified by only considering small perturbations (denoted by tildes) around an time-independent equilibrium state (denoted with the subscript 0). In this case, the fluid quantities and electromagnetic fields are expressed as

$$n_\mathrm{c}(\mathbf{x}, t) = n_\mathrm{c0}(\mathbf{x}) + \tilde{n}_\mathrm{c}(\mathbf{x}, t), \tag{2.9a}$$

$$\mathbf{u}_\mathrm{c}(\mathbf{x}, t) = \tilde{\mathbf{u}}_\mathrm{c}(\mathbf{x}, t), \tag{2.9b}$$

$$\mathbf{B}(\mathbf{x}, t) = \mathbf{B}_0(\mathbf{x}) + \tilde{\mathbf{B}}(\mathbf{x}, t), \tag{2.9c}$$

$$\mathbf{E}(\mathbf{x}, t) = \tilde{\mathbf{E}}(\mathbf{x}, t), \tag{2.9d}$$

where we have assumed that there is no background electric field and no equilibrium plasma flow (which also means that there is no equilibrium current $\mathbf{j}_0$ and thus $\nabla \times \mathbf{B}_0 = 0$ must be satisfied). In what follows, nonlinear terms in the perturbations are neglected. E.g. the perturbed cold current density transfers to

$$\tilde{\mathbf{j}}_c = q_e \left(n_{c0} + \tilde{n}_c \right) \tilde{\mathbf{u}}_c \approx q_e n_{c0} \tilde{\mathbf{u}}_c, \tag{2.10}$$

which leads to a modified linearized momentum balance equation which is obtained by first linearizing eq. (2.4a) and subsequently expressing $\tilde{\mathbf{u}}_c$ in terms of $\tilde{\mathbf{j}}_c$ according to (2.10). Finally, this leads to the model

$$\frac{\partial \tilde{\mathbf{j}}_c}{\partial t} = \epsilon_0 \Omega_{pe}^2 \tilde{\mathbf{E}} + \tilde{\mathbf{j}}_c \times \mathbf{\Omega}_{ce}, \tag{2.11a}$$

$$\frac{\partial f_h}{\partial t} + \mathbf{v} \cdot \nabla f_h + \frac{q_e}{m_e} (\mathbf{E} + \mathbf{v} \times \mathbf{B}) \cdot \nabla_{\mathbf{v}} f_h = 0, \tag{2.11b}$$

$$\frac{\partial \tilde{\mathbf{B}}}{\partial t} = -\nabla \times \tilde{\mathbf{E}}, \tag{2.11c}$$

$$\frac{1}{c^2} \frac{\partial \tilde{\mathbf{E}}}{\partial t} = \nabla \times \tilde{\mathbf{B}} - \mu_0 (\tilde{\mathbf{j}}_c + \mathbf{j}_h), \tag{2.11d}$$

where $\Omega_{pe}^2(\mathbf{x}) = \frac{e^2}{\epsilon_0 m_e} n_{c0}(\mathbf{x})$ is the plasma frequency of the cold electrons and $\mathbf{\Omega}_{ce}(\mathbf{x}) = \frac{q_e}{m_e} \mathbf{B}_0(\mathbf{x})$ the signed electron cyclotron frequency. Note that nonlinearities for the Vlasov equation (2.11b) are kept in order to model nonlinear wave-particle interaction as well as to enable the application of the particle-in-cell method (later).

2.1.3 Energy theorem

An important property of the linearized model (2.11) is that its dynamics conserve the total energy

$$\epsilon := \frac{1}{2} \left[\epsilon_0 \int_\Omega \tilde{\mathbf{E}}^2 d^3\mathbf{x} + \frac{1}{\mu_0} \int_\Omega \tilde{\mathbf{B}}^2 d^3\mathbf{x} + \frac{1}{\epsilon_0} \int_\Omega \frac{1}{\Omega_{pe}^2} \tilde{\mathbf{j}}_c^2 d^3\mathbf{x} + m_e \int_\Omega \int v^2 f_h d^3\mathbf{v} d^3\mathbf{x} \right]$$
$$:= \epsilon_{em} + \epsilon_c + \epsilon_h, \tag{2.12}$$

in the domain $\Omega = \mathbb{R}^3$, which is the sum of the electromagnetic field energy ϵ_{em}, the kinetic energy of the fluid electrons ϵ_c and of the kinetic electrons ϵ_h, respectively. In order to proof this property, we compute the time derivative $\frac{d\epsilon}{dt} = 0$ and replace the occurring partial time derivatives by the dynamical equations (2.11). Let's start with the time derivative of the electromagnetic field energy:

$$\frac{d\epsilon_{em}}{dt} = \epsilon_0 \int_\Omega \tilde{\mathbf{E}} \cdot \frac{\partial \tilde{\mathbf{E}}}{\partial t} d^3\mathbf{x} + \frac{1}{\mu_0} \int_\Omega \tilde{\mathbf{B}} \cdot \frac{\partial \tilde{\mathbf{B}}}{\partial t} d^3\mathbf{x}$$
$$= \frac{1}{\mu_0} \int_\Omega \tilde{\mathbf{E}} \cdot (\nabla \times \tilde{\mathbf{B}} - \mu_0 (\tilde{\mathbf{j}}_c + \mathbf{j}_h)) d^3\mathbf{x} - \frac{1}{\mu_0} \int_\Omega \tilde{\mathbf{B}} \cdot (\nabla \times \tilde{\mathbf{E}}) d^3\mathbf{x}. \tag{2.13}$$

Using the vector calculus identity $\tilde{\mathbf{B}} \cdot (\nabla \times \tilde{\mathbf{E}}) - \tilde{\mathbf{E}} \cdot (\nabla \times \tilde{\mathbf{B}}) = \nabla \cdot (\tilde{\mathbf{E}} \times \tilde{\mathbf{B}})$, the subsequent application of the divergence theorem for integrals and noting that $\tilde{\mathbf{E}}, \tilde{\mathbf{B}} \to 0$ for $x \to \infty$ yields

$$\frac{\mathrm{d}\epsilon_{\mathrm{em}}}{\mathrm{d}t} = -\int_{\Omega} \tilde{\mathbf{E}} \cdot (\tilde{\mathbf{j}}_{\mathrm{c}} + \mathbf{j}_{\mathrm{h}}) \, \mathrm{d}^3\mathbf{x}. \tag{2.14}$$

As a next step, we compute the time derivative of the kinetic energy of the cold electrons ϵ_{c}. By using eq. (2.11a) and noting that $\tilde{\mathbf{j}}_{\mathrm{c}} \cdot \left(\tilde{\mathbf{j}}_{\mathrm{c}} \times \mathbf{\Omega}_{\mathrm{ce}} \right) = 0$, it is straightforward to show that

$$\frac{\mathrm{d}\epsilon_{\mathrm{c}}}{\mathrm{d}t} = \int_{\Omega} \tilde{\mathbf{E}} \cdot \tilde{\mathbf{j}}_{\mathrm{c}} \, \mathrm{d}^3\mathbf{x}, \tag{2.15}$$

which cancels the first term in eq. (2.14). The temporal change of the kinetic energy of hot electrons is given by

$$\begin{aligned}
\frac{\mathrm{d}\epsilon_{\mathrm{h}}}{\mathrm{d}t} &= \frac{m_{\mathrm{e}}}{2} \int_{\Omega} \int v^2 \partial_t f_{\mathrm{h}} \, \mathrm{d}^3\mathbf{v}\mathrm{d}^3\mathbf{x} \\
&= -\frac{m_{\mathrm{e}}}{2} \int_{\Omega} \int v^2 \left[\mathbf{v} \cdot \nabla f_{\mathrm{h}} + \frac{q_{\mathrm{e}}}{m_{\mathrm{e}}} (\mathbf{E} + \mathbf{v} \times \mathbf{B}) \cdot \nabla_{\mathbf{v}} f_{\mathrm{h}} \right] \mathrm{d}^3\mathbf{v} \, \mathrm{d}^3\mathbf{x} \\
&= -\frac{q_{\mathrm{e}}}{2} \int_{\Omega} \int \left[v^2 \mathbf{E} \cdot \nabla_v f_{\mathrm{h}} + v^2 (\mathbf{v} \times \mathbf{B}) \cdot \nabla_{\mathbf{v}} f_{\mathrm{h}} \right] \mathrm{d}^3\mathbf{v}\mathrm{d}^3\mathbf{x} \\
&= \frac{q_{\mathrm{e}}}{2} \left[\int_{\Omega} \int 2 f_{\mathrm{h}} \mathbf{v} \cdot \mathbf{E} \, \mathrm{d}^3\mathbf{v}\mathrm{d}^3\mathbf{x} + \int_{\Omega} \int f_{\mathrm{h}} \nabla_{\mathbf{v}} \cdot [v^2 (\mathbf{v} \times \mathbf{B})] \, \mathrm{d}^3\mathbf{v}\mathrm{d}^3\mathbf{x} \right],
\end{aligned} \tag{2.16}$$

where, from the second to the third line, we have performed an integration by parts in $\mathbf{x}$ for the convective term $\mathbf{v} \cdot \nabla f_{\mathrm{h}}$. Together with the fact that $\nabla \cdot \mathbf{v} = 0$, this term vanishes. From the third to the fourth line we have performed an integration by parts in $\mathbf{v}$ for the two force terms. Again, all surface integral vanish at infinity. In order to proceed the calculation we note that

$$\nabla_{\mathbf{v}}[v^2 (\mathbf{v} \times \mathbf{B})] = v^2 \nabla_{\mathbf{v}} \cdot (\mathbf{v} \times \mathbf{B}) + (\mathbf{v} \times \mathbf{B}) \cdot \nabla_{\mathbf{v}} v^2 = 2[(\mathbf{v} \times \mathbf{B}) \cdot \mathbf{v}] = 0, \tag{2.17}$$

which is why the second term in the last line of (2.16) vanishes. In the first term we recognize the definition of the current density since we can pull $\mathbf{E}$ out of the $\mathbf{v}$ integral. This finally means that

$$\frac{\mathrm{d}\epsilon_{\mathrm{h}}}{\mathrm{d}t} = \int_{\Omega} \mathbf{E} \cdot \mathbf{j}_{\mathrm{h}} \, \mathrm{d}^3\mathbf{x}, \tag{2.18}$$

which cancels the second term in (2.14) since $\mathbf{E} = \tilde{\mathbf{E}}$ by construction. In summary, we have proven that

$$\frac{\mathrm{d}\epsilon}{\mathrm{d}t} = \frac{\mathrm{d}}{\mathrm{d}t}(\epsilon_{\mathrm{em}} + \epsilon_{\mathrm{c}} + \epsilon_{\mathrm{h}}) = 0. \tag{2.19}$$

This energy conservation property will be used later as a criterion to judge whether the discretized version is a good approximation to the continuous model.

2.2 Linear dispersion relation

2.2.1 Derivation for a uniform plasma

In this section, the dispersion relation for the linearized model (2.11) is derived for the case of wave propagation parallel to a uniform background magnetic field $\mathbf{B}_0 = B_0\mathbf{e}_z$, i.e. the wave vector $\mathbf{k} \parallel \mathbf{B}_0 \parallel \mathbf{e}_z$. Furthermore, we assume a uniform cold plasma in the equilibrium state ($\Omega_{\mathrm{pe}}(\mathbf{x}) = \Omega_{\mathrm{pe}} = const.$). The parallel wave propagation makes the problem one-dimensional in space, which is why $\nabla = \mathbf{e}_z\partial_z$ in (2.11). In order to obtain a linear dispersion relation, the Vlasov equation (2.11b) is linearized around an equilibrium distribution function $f_{\mathrm{h}}^0 = f_{\mathrm{h}}^0(\mathbf{v})$, i.e. in analogy to (2.9), we write

$$f_{\mathrm{h}}(\mathbf{x}, \mathbf{v}, t) = f_{\mathrm{h}}^0(\mathbf{v}) + \tilde{f}_{\mathrm{h}}(\mathbf{x}, \mathbf{v}, t), \tag{2.20}$$

where $\tilde{f}_{\mathrm{h}} \ll f_{\mathrm{h}}^0$. Like the cold plasma, the equilibrium distribution function shall be uniform in space. This is equivalent to imposing a constant equilibrium electron number density

$$n_{\mathrm{h}0} = \int f_{\mathrm{h}}^0(\mathbf{v})\,\mathrm{d}^3\mathbf{v}, \tag{2.21}$$

which implies that f_{h}^0 must be normalized such that (2.21) is satisfied. Plugging (2.20), (2.9c) and (2.9d) into (2.11b), neglecting nonlinear terms in the perturbed quantities and relabeling for reasons of clarity (e.g. $\tilde{\mathbf{B}} \to \mathbf{B}$, $\tilde{f}_{\mathrm{h}} \to f_{\mathrm{h}}$, ...) yields the fully linearized model

$$\frac{\partial \mathbf{j}_{\mathrm{c}}}{\partial t} = \epsilon_0\Omega_{\mathrm{pe}}^2\mathbf{E} + \Omega_{\mathrm{ce}}\mathbf{j}_{\mathrm{c}} \times \mathbf{e}_z, \tag{2.22a}$$

$$\frac{\partial f_{\mathrm{h}}}{\partial t} + \mathbf{v} \cdot \nabla f_{\mathrm{h}} + \Omega_{\mathrm{ce}}(\mathbf{v} \times \mathbf{e}_z) \cdot \nabla_{\mathbf{v}}f_{\mathrm{h}} = -\frac{q_{\mathrm{e}}}{m_{\mathrm{e}}}(\mathbf{E} + \mathbf{v} \times \mathbf{B}) \cdot \nabla_{\mathbf{v}}f_{\mathrm{h}}^0, \tag{2.22b}$$

$$\frac{\partial \mathbf{B}}{\partial t} = -\nabla \times \mathbf{E}, \tag{2.22c}$$

$$\frac{1}{c^2}\frac{\partial \mathbf{E}}{\partial t} = \nabla \times \mathbf{B} - \mu_0(\mathbf{j}_{\mathrm{c}} + \mathbf{j}_{\mathrm{h}}). \tag{2.22d}$$

Note that $\Omega_{\mathrm{ce}} < 0$ for electrons ($q_{\mathrm{e}} = -e$). In order to verify an equilibrium state, f_{h}^0 must satisfy the steady state Vlasov equation for the background magnetic field $\mathbf{B}_0 = B_0\mathbf{e}_z$:

$$\Omega_{\mathrm{ce}}(\mathbf{v} \times \mathbf{e}_z) \cdot \nabla_{\mathbf{v}}f_{\mathrm{h}}^0 = 0. \tag{2.23}$$

Using cylindrical coordinates $(v_\perp, \phi, v_\parallel)$ and noting that $\mathbf{v} = (v_\perp\cos\phi, v_\perp\sin\phi, v_\parallel)$ therein, the above equation transfers to

$$-\Omega_{\mathrm{ce}}\frac{\partial f_{\mathrm{h}}^0}{\partial \phi} = 0. \tag{2.24}$$

This means that the equilibrium distribution function is rotationally symmetric around the static magnetic field and thus depends on $v_\perp$ and $v_\parallel$ only. By noting that the left-hand side of eq. (2.22b) is the total time derivative of the perturbed distribution function along

the unperturbed characteristics in the static magnetic field $\mathbf{B}_0$, (2.22b) can be integrated in the following manner (see [15]):

$$f_{\mathrm{h}}(\mathbf{x}, \mathbf{v}, t) = -\frac{q_{\mathrm{e}}}{m_{\mathrm{e}}} \int_{-\infty}^{t} \mathrm{d}t' \left[\mathbf{E}(\mathbf{x}'(t'), t') + \mathbf{v}' \times \mathbf{B}(\mathbf{x}'(t'), t') \right] \cdot \nabla_{\mathbf{v}'} f_{\mathrm{h}}^0. \qquad (2.25)$$

Here, we assumed that the perturbation vanishes in the limit $t \to -\infty$, i.e. $f_{\mathrm{h}}(\mathbf{x}, \mathbf{v}, t = -\infty) = 0$. The characteristics equations that reach the point $(\mathbf{x}, \mathbf{v})$ in phase space at time $t' = t$ are

$$\frac{\mathrm{d}\mathbf{x}'}{\mathrm{d}t'} = \mathbf{v}', \qquad \mathbf{x}'(t' = t) = \mathbf{x}, \qquad (2.26a)$$

$$\frac{\mathrm{d}\mathbf{v}'}{\mathrm{d}t'} = \Omega_{\mathrm{ce}}(\mathbf{v} \times \mathbf{e}_z), \quad \mathbf{v}'(t' = t) = \mathbf{v}. \qquad (2.26b)$$

In order to proceed with the evaluation of (2.25), explicit formulas for the characteristics equations (2.26) are needed. By using the fact that $v_\perp$ and $v_\parallel$ are constants of motion in a uniform magnetic field ($v_\perp' = v_\perp$ and $v_\parallel' = v_\parallel$), the solutions are given by

$$\begin{pmatrix} v_x' \\ v_y' \\ v_z' \end{pmatrix} = \begin{pmatrix} v_\perp \cos(\phi + \Omega_{\mathrm{ce}}(t - t')) \\ v_\perp \sin(\phi + \Omega_{\mathrm{ce}}(t - t')) \\ v_\parallel \end{pmatrix}, \qquad (2.27a)$$

$$\begin{pmatrix} x' \\ y' \\ z' \end{pmatrix} = \begin{pmatrix} x + \frac{v_\perp}{\Omega_{\mathrm{ce}}} \left[\sin \phi - \sin(\phi + \Omega_{\mathrm{ce}}(t - t')) \right] \\ y - \frac{v_\perp}{\Omega_{\mathrm{ce}}} \left[\cos \phi - \cos(\phi + \Omega_{\mathrm{ce}}(t - t')) \right] \\ z - v_\parallel(t - t') \end{pmatrix}. \qquad (2.27b)$$

As a next step, we express all quantities as plane waves propagating parallel to the static magnetic field ($\mathbf{k} = k\mathbf{e}_z$). For instance, we express the distribution function and the electric field as

$$f_{\mathrm{h}}(z, \mathbf{v}, t) = \hat{f}_{\mathrm{h}}(\mathbf{v}) \, \mathrm{e}^{i(kz - \omega t)}, \qquad (2.28a)$$

$$\mathbf{E}(z', t') = \hat{\mathbf{E}} \, \mathrm{e}^{i(kz' - \omega t')}, \qquad (2.28b)$$

and plug this in (2.25). In addition to that, the magnetic field is expressed in terms of the electric field according to Faraday's law (2.22c) by using the substitutions $\frac{\partial}{\partial t} \to -i\omega$ and $\nabla \to ik\mathbf{e}_z$ due to the plane wave ansatz. Thus, (2.25) becomes

$$\hat{f}_{\mathrm{h}}(k, \mathbf{v}, \omega) = -\frac{q_{\mathrm{e}}}{m_{\mathrm{e}}} \int_{-\infty}^{t} \mathrm{d}t' \mathrm{e}^{-i[k(z - z') - \omega(t - t')]} \left[\hat{\mathbf{E}} + \mathbf{v}' \times \frac{k}{\omega}(\mathbf{e}_z \times \hat{\mathbf{E}}) \right] \cdot \nabla_{\mathbf{v}'} f_{\mathrm{h}}^0. \qquad (2.29)$$

In order to proceed the calculation, the derivatives of the equilibrium distribution function need to be transformed in the following manner by noting that $v_\perp = \sqrt{v_x^2 + v_y^2}$ and $v_\parallel = v_z$ and again $v_\perp' = v_\perp$ and $v_\parallel' = v_\parallel$:

$$\frac{\partial f_{\mathrm{h}}^0}{\partial v_x'} = \frac{\partial f_{\mathrm{h}}^0}{\partial v_\perp'} \frac{\partial v_\perp'}{\partial v_x'} = \frac{v_x'}{v_\perp} \frac{\partial f_{\mathrm{h}}^0}{\partial v_\perp}, \qquad (2.30a)$$

$$\frac{\partial f_{\mathrm{h}}^0}{\partial v_y'} = \frac{\partial f_{\mathrm{h}}^0}{\partial v_\perp'} \frac{\partial v_\perp'}{\partial v_y'} = \frac{v_y'}{v_\perp} \frac{\partial f_{\mathrm{h}}^0}{\partial v_\perp}, \qquad (2.30b)$$

$$\frac{\partial f_{\mathrm{h}}^0}{\partial v_z'} = \frac{\partial f_{\mathrm{h}}^0}{\partial v_\parallel}. \qquad (2.30c)$$

Using these expressions together with the characteristics equations (2.27a) yields

$$-\frac{q_e}{m_e}\hat{f}_h(k,\mathbf{v},\omega) = \int_0^\infty d\tau\, e^{i\tau(\omega-kv_\parallel)}\left[\hat{\mathbf{E}} + \frac{k}{\omega}\begin{pmatrix} v_\perp\cos(\phi+\Omega_{ce}\tau) \\ v_\perp\sin(\phi+\Omega_{ce}\tau) \\ v_\parallel \end{pmatrix}\times\begin{pmatrix} -\hat{E}_y \\ \hat{E}_x \\ 0 \end{pmatrix}\right]\cdot\nabla_{\mathbf{v}'}f_h^0$$

$$= \int_0^\infty d\tau\, e^{i\tau(\omega-kv_\parallel)}\left[\hat{\mathbf{E}} + \frac{k}{\omega}\begin{pmatrix} -v_\parallel\hat{E}_x \\ -v_\parallel\hat{E}_y \\ v_\perp\hat{E}_x\cos(\phi+\Omega_{ce}\tau)+v_\perp\hat{E}_y\sin(\phi+\Omega_{ce}\tau)) \end{pmatrix}\right]$$
$$\cdot\begin{pmatrix} v_x'/v_\perp\cdot\partial_\perp f_h^0 \\ v_y'/v_\perp\cdot\partial_\perp f_h^0 \\ \partial_\parallel f_h^0 \end{pmatrix}$$

$$= \int_0^\infty d\tau\, e^{i\tau(\omega-kv_\parallel)}\left[\hat{E}_x\cos(\phi+\Omega_{ce}\tau)\hat{G}f_h^0 + \hat{E}_y\sin(\phi+\Omega_{ce}\tau)\hat{G}f_h^0 + \hat{E}_z\partial_\parallel f_h^0\right]$$

where we have used the substitution $\tau = t - t'$ and the notations $\frac{\partial}{\partial v_\parallel}\to\partial_\parallel$ and $\frac{\partial}{\partial v_\perp}\to\partial_\perp$ for reasons of clarity. Furthermore, we have introduced the differential operator

$$\hat{G} = \frac{\partial}{\partial v_\perp} + \frac{k}{\omega}\left(v_\perp\frac{\partial}{\partial v_\parallel} - v_\parallel\frac{\partial}{\partial v_\perp}\right). \tag{2.31}$$

The integration over τ can be performed easily by using the following integrals, which can be obtained by assuming that $\text{Im}(\omega) > 0$ (growing modes):

$$\int_0^\infty d\tau\, e^{i\tau(\omega-kv_\parallel)}\cos(\phi+\Omega_{ce}\tau) = \frac{i(\omega-kv_\parallel)\cos\phi+\Omega_{ce}\sin\phi}{\Omega_+\Omega_-}, \tag{2.32a}$$

$$\int_0^\infty d\tau\, e^{i\tau(\omega-kv_\parallel)}\sin(\phi+\Omega_{ce}\tau) = \frac{i(\omega-kv_\parallel)\sin\phi-\Omega_{ce}\cos\phi}{\Omega_+\Omega_-}, \tag{2.32b}$$

$$\int_0^\infty d\tau\, e^{i\tau(\omega-kv_\parallel)} = \frac{i}{\omega-kv_\parallel}. \tag{2.32c}$$

Here, we have used the abbreviations $\Omega_\pm = \omega - kv_\parallel \pm \Omega_{ce}$ for the frequencies of the resonant particles. With these integrals the perturbed distribution function finally reads

$$\hat{f}_h(k,\mathbf{v},\omega) = -\frac{q_e}{m_e}\hat{E}_x\frac{\hat{G}f_h^0}{\Omega_+\Omega_-}\left[i(\omega-kv_\parallel)\cos\phi+\Omega_{ce}\sin\phi\right]$$
$$-\frac{q_e}{m_e}\hat{E}_y\frac{\hat{G}f_h^0}{\Omega_+\Omega_-}\left[i(\omega-kv_\parallel)\sin\phi-\Omega_{ce}\cos\phi\right] \tag{2.33}$$
$$-\frac{q_e}{m_e}\hat{E}_z\frac{i\partial_\parallel f_h^0}{\omega-kv_\parallel}.$$

This can now be used to calculate the hot current density $\hat{\mathbf{j}}_h$ that is induced by the perturbed electric field:

$$\hat{\mathbf{j}}_h = q_e\int\mathbf{v}\hat{f}_h\, d^3\mathbf{v} = q_e\int_{-\infty}^\infty dv_\parallel\int_0^\infty dv_\perp v_\perp\int_0^{2\pi} d\phi\, \mathbf{v}\hat{f}_h := \sigma_h(k,\omega)\hat{\mathbf{E}}. \tag{2.34}$$

σ_{h} denotes the conductivity tensor that relates the current density of the hot electrons to the electric field. The integration over ϕ can be performed immediately, since the equilibrium distribution function does not depend on ϕ. This leads to a conductivity tensor of the form

$$\sigma_{\mathrm{h}} = \begin{pmatrix} \sigma_{\mathrm{h}xx} & \sigma_{\mathrm{h}xy} & 0 \\ \sigma_{\mathrm{h}yx} & \sigma_{\mathrm{h}yy} & 0 \\ 0 & 0 & \sigma_{\mathrm{h}zz} \end{pmatrix}, \tag{2.35}$$

where

$$\sigma_{\mathrm{h}xx} = -i \frac{q_{\mathrm{e}}^2}{m_{\mathrm{e}}} \int \mathrm{d}^3 \mathbf{v} \, \frac{v_\perp (\omega - k v_\parallel) \hat{G} f_{\mathrm{h}}^0}{2\Omega_+ \Omega_-} = \sigma_{\mathrm{h}yy}, \tag{2.36a}$$

$$\sigma_{\mathrm{h}xy} = \frac{q_{\mathrm{e}}^2}{m_{\mathrm{e}}} \Omega_{\mathrm{ce}} \int \mathrm{d}^3 \mathbf{v} \, \frac{v_\perp \hat{G} f_{\mathrm{h}}^0}{2\Omega_+ \Omega_-} = -\sigma_{\mathrm{h}yx}, \tag{2.36b}$$

$$\sigma_{\mathrm{h}zz} = -i \frac{q_{\mathrm{e}}^2}{m_{\mathrm{e}}} \int \mathrm{d}^3 \mathbf{v} \, \frac{v_\parallel \, \partial_\parallel f_{\mathrm{h}}^0}{\omega - k v_\parallel}. \tag{2.36c}$$

and $\mathrm{d}^3\mathbf{v} = \mathrm{d}v_\parallel \mathrm{d}v_\perp v_\perp 2\pi$. The structure of the conductivity tensor (2.35) immediately reveals the complete decoupling of perpendicular and parallel perturbations since parallel electric field components do not lead to a perpendicular current and vice versa. For the parallel case, (2.36c) corresponds to the standard Landau-damping case of electrostatic waves [15].

The same procedure can be done for the cold current density i.e. $\hat{\mathbf{j}}_{\mathrm{c}} = \sigma_{\mathrm{c}}(k, \omega) \hat{\mathbf{E}}$. For this, the momentum equation (2.22a) must be solved in the same way in Fourier space. We omit the detailed derivation and just give the result [5]:

$$\sigma_c = \begin{pmatrix} -\frac{i\epsilon_0 \omega \Omega_{\mathrm{pe}}^2}{\Omega_{\mathrm{ce}}^2 - \omega^2} & \frac{\epsilon_0 \Omega_{\mathrm{ce}} \Omega_{\mathrm{pe}}^2}{\Omega_{\mathrm{ce}}^2 - \omega^2} & 0 \\ -\frac{\epsilon_0 \Omega_{\mathrm{ce}} \Omega_{\mathrm{pe}}^2}{\Omega_{\mathrm{ce}}^2 - \omega^2} & -\frac{i\epsilon_0 \omega \Omega_{\mathrm{pe}}^2}{\Omega_{\mathrm{ce}}^2 - \omega^2} & 0 \\ 0 & 0 & \frac{i\epsilon_0 \Omega_{\mathrm{pe}}^2}{\omega} \end{pmatrix}. \tag{2.37}$$

In order to obtain the dispersion relation, we finally use Ampère's law (2.22d) and Faraday's law (2.22c) to derive an equation where only the perturbed electric field appears. As before, the ∇-operator can be replaced by $i\mathbf{k}$, where $\mathbf{k} = k\mathbf{e}_z$, and the time derivative can be replaced by $-i\omega$ due to the plane wave ansatz. This yields

$$-\frac{i\omega}{c^2}\hat{\mathbf{E}} = i\mathbf{k} \times \hat{\mathbf{B}} - \mu_0(\hat{\mathbf{j}}_{\mathrm{c}} + \hat{\mathbf{j}}_{\mathrm{h}}) \tag{2.38}$$

$$\Leftrightarrow \quad -\frac{i\omega}{c^2}\hat{\mathbf{E}} = i\mathbf{k} \times \frac{1}{\omega}(\mathbf{k} \times \hat{\mathbf{E}}) - \mu_0 (\sigma_{\mathrm{c}} + \sigma_{\mathrm{h}}) \hat{\mathbf{E}} \tag{2.39}$$

$$\Leftrightarrow \quad \hat{\mathbf{E}} - \frac{k^2 c^2}{\omega^2}\hat{E}_x \mathbf{e}_x - \frac{k^2 c^2}{\omega^2}\hat{E}_y \mathbf{e}_y + \frac{ic^2 \mu_0}{\omega} (\sigma_{\mathrm{c}} + \sigma_{\mathrm{h}}) \hat{\mathbf{E}} = 0, \tag{2.40}$$

which can be written as the linear system

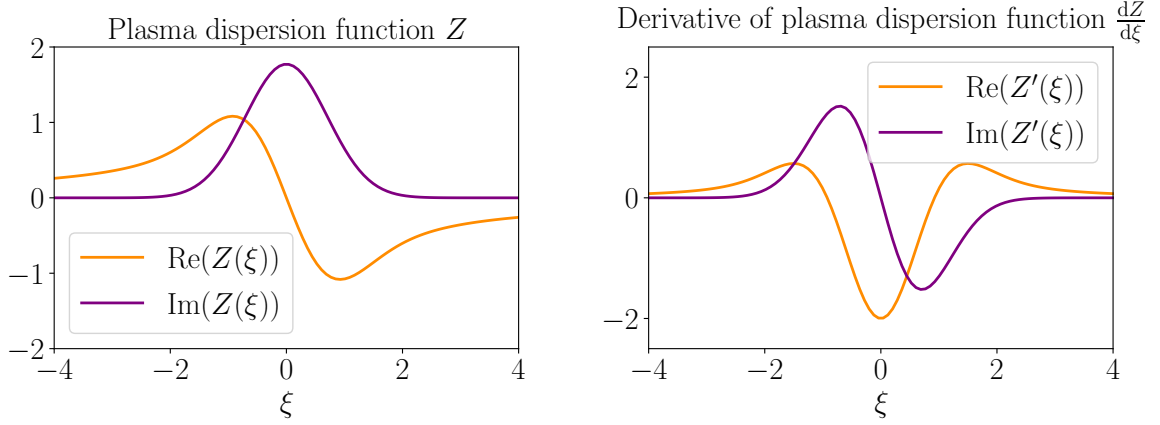$$\mathbb{D}(k, \omega)\hat{\mathbf{E}} = 0, \tag{2.41}$$

Figure 2.1: Left: *The real and imaginary part of the plasma dispersion function (2.47) for a real argument.* **Right**: *The real and imaginary part of the first derivative of the plasma dispersion function (2.47) for a real argument.*

where the matrix $\mathbb{D}$ is given by

$$\mathbb{D}(k,\omega) := \begin{pmatrix} 1 - \frac{k^2c^2}{\omega^2} + \frac{ic^2\mu_0}{\omega}\sigma_{xx} & \frac{ic^2\mu_0}{\omega}\sigma_{xy} & 0 \\ -\frac{ic^2\mu_0}{\omega}\sigma_{xy} & 1 - \frac{k^2c^2}{\omega^2} + \frac{ic^2\mu_0}{\omega}\sigma_{xx} & 0 \\ 0 & 0 & 1 + \frac{ic^2\mu_0}{\omega}\sigma_{zz}. \end{pmatrix} \tag{2.42}$$

Here, we have used that $\sigma_{\cdot,xx} = \sigma_{\cdot,yy}$ and $\sigma_{\cdot,xy} = -\sigma_{\cdot,yx}$ for both species and $\sigma = \sigma_c + \sigma_h$ denotes the total conductivity tensor. In order to get non-trivial solutions ($\hat{\mathbf{E}} \neq 0$) out of the linear system, the determinant of the matrix $\mathbb{D}$ must vanish, which means that the dispersion relation reads

$$\det \mathbb{D}(k,\omega) = 0. \tag{2.43}$$

By performing this calculation explicitly, one ends up with three types of solutions: One of these solutions corresponds to electrostatic waves which we do not consider further. The other two solutions correspond to R-waves (+) and L-waves (-) which are right-handed circularly and left-handed circularly polarized waves, respectively. The dispersion relation for these types of waves for an arbitrary hot electron equilibrium distribution function reads

$$D_{\mathrm{R/L}}(k,\omega) = 1 - \frac{c^2k^2}{\omega^2} - \frac{\Omega_{\mathrm{pe}}^2}{\omega(\omega \pm \Omega_{\mathrm{ce}})} + \nu_{\mathrm{h}}\frac{\Omega_{\mathrm{pe}}^2}{\omega}\int \mathrm{d}^3\mathbf{v}\frac{v_\perp}{2}\frac{\hat{G}F_{\mathrm{h}}^0}{\omega \pm \Omega_{\mathrm{ce}} - kv_\parallel} = 0, \tag{2.44}$$

where $\nu_{\mathrm{h}} = n_{\mathrm{h0}}/n_{\mathrm{c0}}$ is the ratio between hot and cold electron number densities and F_{h}^0 is the velocity part of the equilibrium distribution function, i.e. $f_{\mathrm{h}}^0(v_\parallel, v_\perp) = n_{\mathrm{h0}}F_{\mathrm{h}}^0(v_\parallel, v_\perp)$, which is normalized to one in velocity space. Note that this result is equivalent to the one obtained by Xiao et al. [20] for a fully kinetic plasma (where they split the total distribution function into $F_{\mathrm{c}}^0 + \nu_{\mathrm{h}}F_{\mathrm{h}}^0$ and represent the cold part by $F_{\mathrm{c}}^0 = \delta(v_\parallel)\delta(v_\perp)/2\pi v_\perp$), if one uses $\gamma_{\mathrm{L}} \to 1$ for the case of a non-relativistic plasma, which we consider here (γ_{L} is the well-known Lorentz factor).
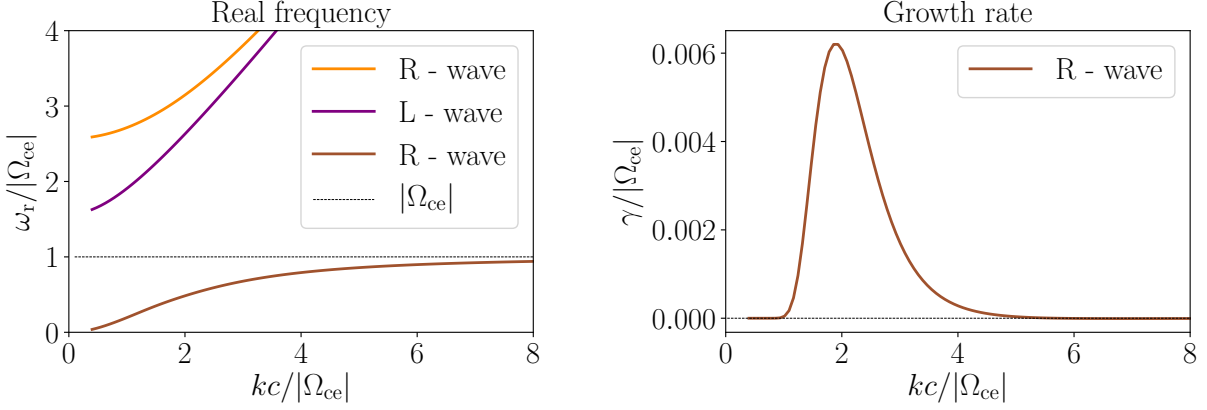
Figure 2.2: Left*: Numerical solutions of the dispersion relation (2.46) (real part) for* $\Omega_{pe} = 2|\Omega_{ce}|$, $\nu_h = 0.5\,\%$, $v_{th,\parallel} = 0.2\,c$ *and* $v_{th,\perp} = 0.6\,c$. ***Right****: Same for imaginary part. Here, only the solution for the R-wave below the electron cyclotron frequency* $|\Omega_{ce}|$ *is shown since the imaginary parts of the other two branches are close to zero.*

Let us consider the important example of an anisotropic Maxwellian with different thermal velocities in parallel and perpendicular direction with respect to the background magnetic field $\mathbf{B}_0 = B_0 \mathbf{e}_z$. As already indicated in the very beginning of this section, such a distribution can e.g. be found for fast electrons in the earth's magnetosphere [13, 14]:

$$F_{\mathrm{h}}^0(v_\parallel, v_\perp) = \frac{1}{(2\pi)^{3/2} v_{\mathrm{th},\parallel} v_{\mathrm{th},\perp}^2} \exp\left(-\frac{v_\parallel^2}{2 v_{\mathrm{th},\parallel}^2} - \frac{v_\perp^2}{2 v_{\mathrm{th},\perp}^2}.\right). \tag{2.45}$$

Plugging this in the general dispersion relation (2.44) and performing the integral over the perpendicular velocity one ends up with

$$\begin{aligned} D_{\mathrm{R/L}}(k,\omega) = 1 - \frac{k^2 c^2}{\omega^2} &- \frac{\Omega_{\mathrm{pe}}^2}{\omega(\omega \pm \Omega_{\mathrm{ce}})} \\ + \nu_{\mathrm{h}} \frac{\Omega_{\mathrm{pe}}^2}{\omega^2} &\left[\frac{\omega}{k\sqrt{2} v_{\mathrm{th},\parallel}} Z(\xi^\pm) - \left(1 - \frac{v_{\mathrm{th},\perp}^2}{v_{\mathrm{th},\parallel}^2}\right)\left(1 + \xi^\pm Z(\xi^\pm)\right) \right] = 0, \end{aligned} \tag{2.46}$$

where $\xi^\pm = (\omega \pm \Omega_{\mathrm{ce}})/(k\sqrt{2} v_{\mathrm{th},\parallel})$ and Z is the plasma dispersion function defined by

$$\begin{aligned} Z(\xi) &= \frac{1}{\sqrt{\pi}} \int_{-\infty}^{\infty} \frac{\mathrm{e}^{-u^2}}{u - \xi} \mathrm{d}u + i\sigma\sqrt{\pi}\mathrm{e}^{-\xi^2} = \sqrt{\pi}\mathrm{e}^{-\xi^2}(i - \mathrm{erfi}(\xi)), \\ \sigma &= \begin{cases} 0 & \text{for } \mathrm{Im}(\xi) > 0 \\ 1 & \text{for } \mathrm{Im}(\xi) = 0 \\ 2 & \text{for } \mathrm{Im}(\xi) < 0, \end{cases} \end{aligned} \tag{2.47}$$

where $\mathrm{erfi}(\xi) = \frac{2}{\sqrt{\pi}} \int_0^\xi \mathrm{e}^{t^2} \mathrm{d}t$ is the complex error function and the analytic continuation for $\mathrm{Im}(\omega) = \mathrm{Im}(\xi) \leq 0$ (damped modes) is obtained with the so-called Landau technique to
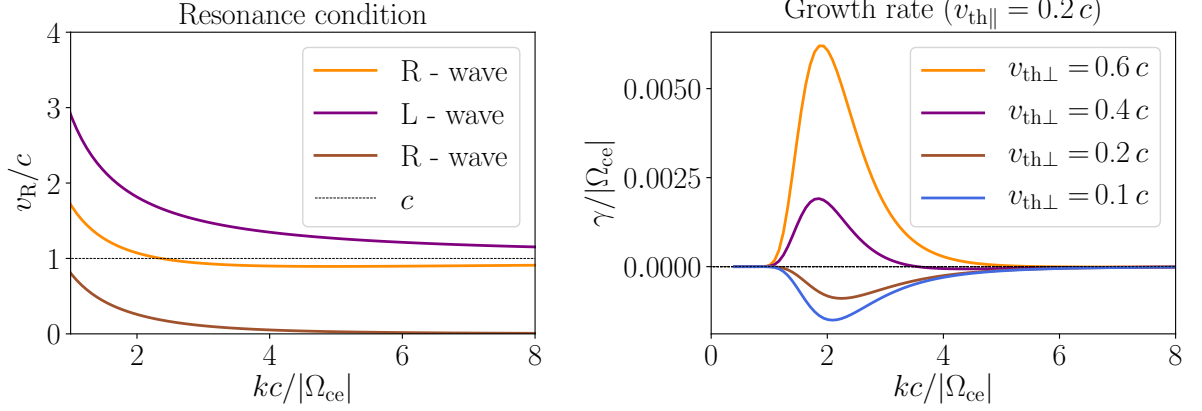
Figure 2.3: Left: *The resonant velocity of the three waves with respect to the wavenumber (parameters see caption of fig. 2.2).* **Right**: *Impact of temperature anisotropy on growth rates.*

treat the pole ($u = \xi$) in the denominator (not shown, see [15]). In fig. 2.1 the real and imaginary part of the plasma dispersion function as well as its first derivative is shown for a real argument.

In the absence of energetic electrons ($\nu_\mathrm{h} \to 0$), the dispersion relation (2.46) transfers to the well-known cold plasma dispersion relation for electron waves which does only provide solutions with real ω which means that there is no wave growth or damping. However, depending on the temperature anisotropy, eq. (2.46) provides solutions with an imaginary part $\gamma := \mathrm{Im}(\omega)$ which corresponds to wave growth or damping.

Numerical solutions of the dispersion relation obtained with Newton's method for finding roots of a nonlinear algebraic equation [21] are shown in fig. 2.2, where we plot the real frequency $\omega_\mathrm{r} := \mathrm{Re}(\omega)$ on the left-hand side and the growth rate γ on the right-hand side. One can see that there are two solutions for R-waves and one solution for L-waves which is well-known from the cold plasma theory [5]. However, due to the interaction of the wave with fast electrons that have velocities $v_\| = v_\mathrm{R}$ satisfying the resonance condition

$$\omega = k v_\mathrm{R} \mp \Omega_\mathrm{ce}, \tag{2.48}$$

the lower branch below the electron cyclotron frequency becomes unstable for a certain range of wavenumbers if the temperature anisotropy is sufficiently large. This means that energy is transferred from the electrons to the wave. In contrast to that, the two upper branches remain stable which is due to the fact that there are (almost) no fast electrons satisfying the above resonance condition. This can easily be understood by having a look at fig. 2.3 where we plot the resonant velocity with respect to the wavenumber for the same set of parameters as in fig. 2.2. One can see that (in this non-relativistic theory) the resonance condition can not be satisfied at all for the L-wave since the branch is entirely above the speed of light. For the upper R-wave branch and for $kc/|\Omega_\mathrm{ce}| \gtrsim 2.5$, very fast electrons close to the speed of light meet the condition, however, there are so few
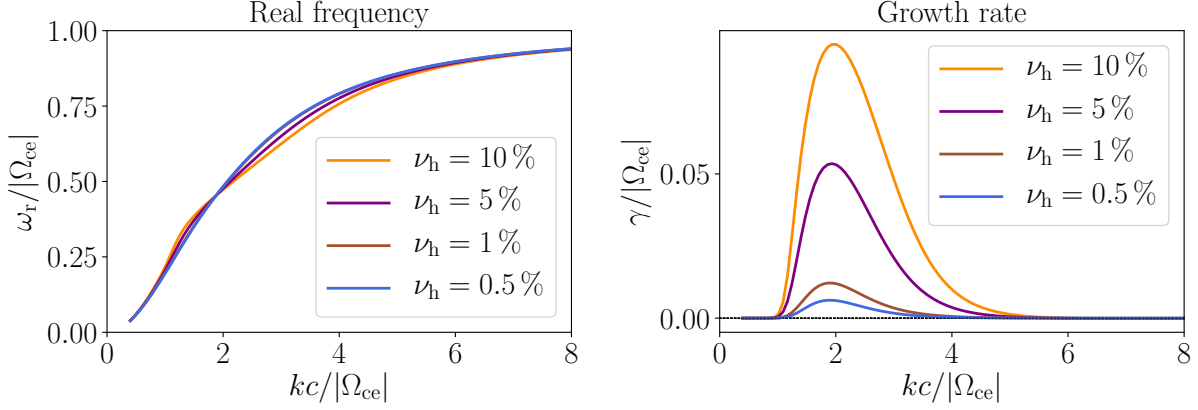
Figure 2.4: Left: *Real frequency for different amounts of fast electrons and* $\Omega_{pe} = 2|\Omega_{ce}|$, $v_{th,\parallel} = 0.2\,c$ *and* $v_{th,\perp} = 0.6\,c$). **Right**: *Same for growth rates.*

of them at the tail of the Maxwellian that they do not lead to significant wave-particle effects. Only the lower R-wave branch, which is well below the speed of light, has resonant velocities clearly within the Maxwellian.

By reducing the temperature anisotropy (fig. 2.3 on the right), we see that the growth rates become smaller and smaller until they become negative which corresponds to wave damping, i.e. energy is transferred from the wave to the electrons. Finally, we can also study the impact of different amounts of fast electrons, which is shown in fig. 2.4. We see that the real frequencies change very little whereas the growth rates become significantly larger for larger amounts of fast electrons.

2.2.2 Explicit solution for low fast electron densities

All results shown so far were obtained by solving the dispersion relation (2.46) numerically with the Newton's method for a fixed wavenumber k. This method needs on the one hand the knowledge of the derivative with respect to ω and on the other hand an initial guess of the solution ω for a fixed k. That means that an initial guess which is too far away from the true solution could possibly lead to a wrong solution or no solution at all if convergence is not achieved. Because of this, we want to compute an explicit expression for the growth rate γ for the case $\nu_h \ll 1$ since we assume that most of the plasma is already in a thermal state. For this case, we assume weak instability, i.e. $|\gamma| \ll |\omega_r|$ and expand the dispersion relation in the Taylor-series (we omit the subscripts R/L)

$$D(k, \omega_r + i\gamma) \approx D_r(k, \omega_r) + i\left(\gamma \frac{\partial}{\partial \omega_r} D_r(k, \omega_r) + D_i(k, \omega_r)\right) + \cdots = 0, \qquad (2.49)$$

where $D_{r/i}$ denotes the real/imaginary part of the dispersion relation [20]. In the expansion, we have neglected the term γD_i, since we assume that $\nu_h \ll 1$ ensures $D_i(k, \omega_r) \ll$

$D_\mathrm{r}(k, \omega_\mathrm{r})$. Indeed, writing the real and imaginary part explicitly yields

$$
\begin{aligned}
D_\mathrm{r}(k, \omega_\mathrm{r}) = \lim_{\gamma \to 0} D_\mathrm{r}(k, \omega_\mathrm{r} + i\gamma) = 1 &- \frac{k^2 c^2}{\omega_\mathrm{r}^2} - \frac{\Omega_\mathrm{pe}^2}{\omega_\mathrm{r}(\omega_\mathrm{r} \pm \Omega_\mathrm{ce})} \\
&+ \frac{\nu_\mathrm{h} \Omega_\mathrm{pe}^2}{\omega_\mathrm{r}^2} \left[-\frac{\sqrt{\pi}\omega_\mathrm{r}}{k\sqrt{2}v_\mathrm{th,\parallel}} \mathrm{erfi}(\xi_\mathrm{r}^\pm) + T_\mathrm{a}(\sqrt{\pi}\mathrm{erfi}(\xi_\mathrm{r}^\pm)\xi_\mathrm{r}^\pm - 1) \right],
\end{aligned}
\tag{2.50}
$$

and

$$
D_\mathrm{i}(k, \omega_\mathrm{r}) = \lim_{\gamma \to 0} D_\mathrm{r}(k, \omega_\mathrm{i} + i\gamma) = \frac{\nu_\mathrm{h}\sqrt{\pi}\Omega_\mathrm{pe}^2}{\omega_\mathrm{r}k\sqrt{2}v_\mathrm{th,\parallel}} \exp\left[-(\xi_\mathrm{r}^\pm)^2\right]\left(1 - T_\mathrm{a}\frac{\omega_\mathrm{r} \pm \Omega_\mathrm{ce}}{\omega_\mathrm{r}}\right), \tag{2.51}
$$

where $\xi_\mathrm{r}^\pm := (\omega_\mathrm{r} \pm \Omega_\mathrm{ce})/(k\sqrt{2}v_\mathrm{th,\parallel})$ and $T_\mathrm{a} := 1 - v_\mathrm{th,\perp}^2/v_\mathrm{th,\parallel}^2$ is a measure for the temperature anisotropy. Again, due to $\nu_\mathrm{h} \ll 1$, we neglect the squared bracket in the expression for D_r which is why the real oscillation frequency ω_r for a fixed k is simply determined from

$$
D_\mathrm{r}(k, \omega_\mathrm{r}) = 1 - \frac{k^2 c^2}{\omega_\mathrm{r}^2} - \frac{\Omega_\mathrm{pe}^2}{\omega_\mathrm{r}(\omega_\mathrm{r} \pm \Omega_\mathrm{ce})} = 0, \tag{2.52}
$$

since we set the two terms in (2.49) to zero, respectively. Since we have seen in fig. 2.4 that the fast electrons hardly have an impact on the real frequency, this result is reasonable. By setting the bracket in (2.49) to zero and using the above expression for the real part, the linear growth rate γ is obtained from

$$
\gamma = -\frac{D_\mathrm{i}(k, \omega_\mathrm{r})}{\frac{\partial}{\partial \omega_\mathrm{r}} D_\mathrm{r}(k, \omega_\mathrm{r})} = \frac{\nu_\mathrm{h}\sqrt{\pi}\Omega_\mathrm{pe}^2}{2\omega_\mathrm{r} \mp \frac{\Omega_\mathrm{pe}^2 \Omega_\mathrm{ce}}{(\omega_\mathrm{r} \pm \Omega_\mathrm{ce})^2}} \xi_\mathrm{r}^\pm \exp\left[-(\xi_\mathrm{r}^\pm)^2\right]\left(T_\mathrm{a} - \frac{\omega_\mathrm{r}}{\omega_\mathrm{r} \pm \Omega_\mathrm{ce}}\right). \tag{2.53}
$$

From this formula, we immediately see that the growth rate increases linearly with the amount of energetic electrons ν_h, which we have already seen in fig. 2.4.
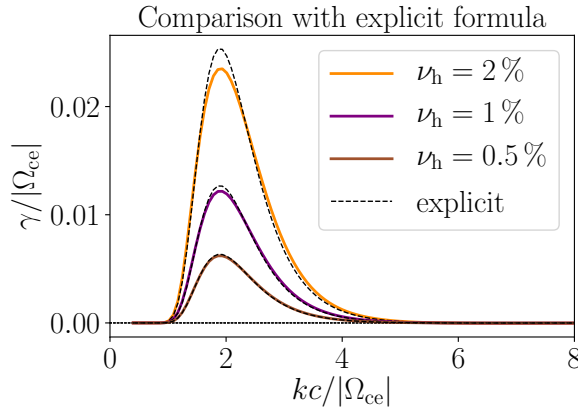
Figure 2.5: *Comparision of growth rates obtained numerically from the full disperson relation to the ones obtained with the analytical expression (2.53)*

In fig. 2.5 we compare the growth rates obtained by the explicit formula (2.53) with the numerical ones. We see the very good agreement for ratios up to $\nu_h \approx 1\,\%$. Above this threshold the solutions differ especially around the maximum value which is why the explicit formula should not be used for $\nu_h \gtrsim 1\,\%$.

3 Numerical methods

In this section, we introduce the numerical methods which will be used in order to solve numerically the electron hybrid model (2.11) which we have just discussed on the continuous level and for which we have calculated the dispersion relation. First, the three main classes of numerical methods we shall apply, namely the particle-in-cell method for solving the Vlasov equation and the finite element method for field equations (both standard and geometric) are introduced in a more general manner with some simple examples before applying them on our specific model.

3.1 Introduction

3.1.1 Particle-in-cell

We solve the Vlasov equation by means of the particle-in-cell method [22] which consists simply of tracking a large, but finite number of randomly drawn characteristics, the so-called *markers* or *particles*, in the continuous six-dimensional phase space. The distribution function at time t is then approximated by a sum of Dirac masses

$$f_{\mathrm{h}}(\mathbf{x}, \mathbf{v}, t) \approx \sum_{k=1}^{N_{\mathrm{p}}} w_k \delta(\mathbf{x} - \mathbf{x}_k(t)) \delta(\mathbf{v} - \mathbf{v}_k(t)), \tag{3.1}$$

where N_{p} is the number of particles and $w_k = w_k(t)$ its, in general, time dependent weights which we define later. $\mathbf{v}_k = \mathbf{v}_k(t)$ are the particles' velocities and $\mathbf{x}_k = \mathbf{x}_k(t)$ the particles' positions. By taking the total time derivative of the distribution function along a particle's trajectory in a Lagrangian frame,

$$\frac{\mathrm{d}}{\mathrm{d}t} f_{\mathrm{h}}(\mathbf{x}_k(t), \mathbf{v}_k(t), t) = \frac{\partial f_{\mathrm{h}}}{\partial t} + \frac{\mathrm{d}\mathbf{x}_k}{\mathrm{d}t} \nabla f_{\mathrm{h}} + \frac{\mathrm{d}\mathbf{v}_k}{\mathrm{d}t} \nabla_{\mathbf{v}} f_{\mathrm{h}} = 0, \tag{3.2}$$

and comparing with the Vlasov equation, we see that the particles must satisfy the following equations of motion

$$\frac{\mathrm{d}\mathbf{v}_k}{\mathrm{d}t} = \frac{q_{\mathrm{e}}}{m_{\mathrm{e}}} \left[\mathbf{E}(\mathbf{x}_k(t), t) + \mathbf{v}_k(t) \times \mathbf{B}(\mathbf{x}_k(t), t) \right], \qquad \mathbf{v}_k(0) = \mathbf{v}_k^0, \tag{3.3a}$$

$$\frac{\mathrm{d}\mathbf{x}_k}{\mathrm{d}t} = \mathbf{v}_k, \qquad \mathbf{x}_k(0) = \mathbf{x}_k^0, \tag{3.3b}$$

which are the same equations as for an electron in the macroscopic electromagnetic fields $\mathbf{E}$ and $\mathbf{B}$.

We solve this set of ODEs for the particles' trajectories (3.3) with the so-called *Boris method* which has shown to have a very good long-time accuracy which is the reason why it is a standard method for solving orbit equations in particle-in-cell codes [22]. Its main idea is to split the electric and magnetic forces and to use basic geometry to perform the pure rotation caused by the magnetic field. It can be shown that this splitting conserves the particle's phase space volume which is the reason for its good long-time properties, although it is not a symplectic integrator [23].
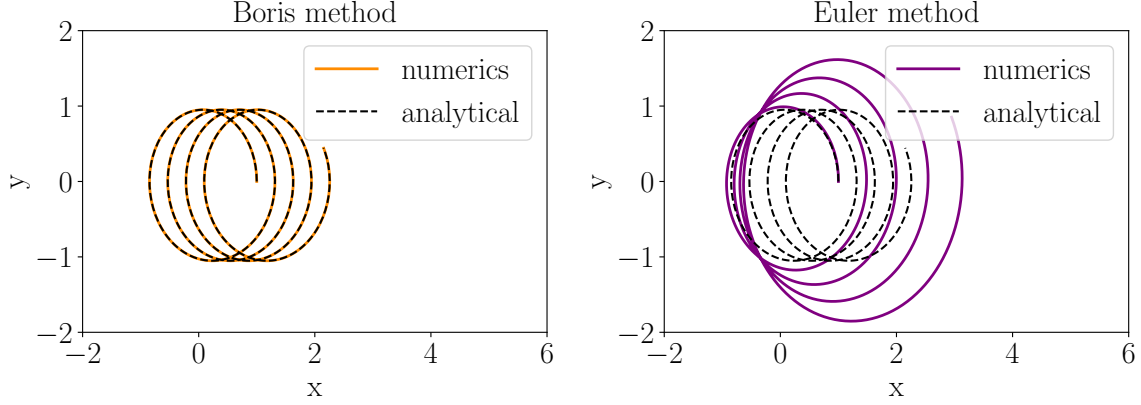
Figure 3.1: Left*: Numerical solution of the orbit of an electron in a static electro-magnetic field obtained with the Boris method (3.4) with initial conditions (3.5).* ***Right****: Numerical solution of the orbit of an electron in a static electromagnetic field obtained with the explicit Euler method (3.6) with initial conditions (3.5).*

The method which updates velocities and positions on a staggered time grid reads as follows: Starting from $\mathbf{v}^{n-1/2}$ and $\mathbf{x}^n$, do successively

$$\mathbf{v}^- = \mathbf{v}^{n-1/2} + \frac{q_{\mathrm{e}}\Delta t}{2m_{\mathrm{e}}}\mathbf{E}(\mathbf{x}^n, t^n), \tag{3.4a}$$

$$\mathbf{h} = \frac{q_{\mathrm{e}}\Delta t}{2m_{\mathrm{e}}}\mathbf{B}(\mathbf{x}^n, t^n), \tag{3.4b}$$

$$\mathbf{v}' = \mathbf{v}^- + \mathbf{v}^- \times \mathbf{h}, \tag{3.4c}$$

$$\mathbf{s} = \frac{2\mathbf{h}}{1+h^2}, \tag{3.4d}$$

$$\mathbf{v}^+ = \mathbf{v}^- + \mathbf{v}' \times \mathbf{s}, \tag{3.4e}$$

$$\mathbf{v}^{n+1/2} = \mathbf{v}^+ + \frac{q_{\mathrm{e}}\Delta t}{2m_{\mathrm{e}}}\mathbf{E}(\mathbf{x}^n, t^n), \tag{3.4f}$$

$$\mathbf{x}^{n+1} = \mathbf{x}^n + \Delta t \mathbf{v}^{n+1/2}, \tag{3.4g}$$

in order to update a particle's velocity and position by a time step Δt and n denotes the point in time, i.e. $t^n = n\Delta t$. In order to initialize the algorithm from some given $\mathbf{x}^0$ and $\mathbf{v}^0$, one can compute $\mathbf{v}^{-1/2}$ by using the same algorithm but with $\Delta t' = -\Delta t/2$. One then commits a small error since one does not use a staggered grid for this step, however, as this is done only one time in the very beginning the overall accuracy is not lost.

In fig. 3.1, an example is shown for a two-dimensional electron drift motion in the x-y-plane caused by a static electric field $\mathbf{E} = E\mathbf{e}_y$ and a static magnetic field $\mathbf{B} = B\mathbf{e}_z$. As initial conditions we choose

$$\mathbf{v}^0 = (0, v_y^0, 0)^\top, \tag{3.5a}$$

$$\mathbf{x}^0 = (r_{\mathrm{g}} = \frac{m_{\mathrm{e}}v_y^0}{|q_{\mathrm{e}}|B}, 0, 0)^\top, \tag{3.5b}$$

where r_g denotes the electron gyro radius. For this simple test case, the trajectory can be computed exactly which is why we can compare the numerical trajectory to the exact one. One can clearly see the good agreement in case of the Boris method. As a comparison we have performed the same test case for the explicit Euler method, which is probably the most intuitive way to solve an ODE numerically:

$$\mathbf{v}^{n+1} = \mathbf{v}^n + \Delta t \frac{q_\mathrm{e}}{m_\mathrm{e}} \left[\mathbf{E}(\mathbf{x}^n, t^n) + \mathbf{v}^n \times \mathbf{B}(\mathbf{x}^n, t^n) \right], \tag{3.6a}$$

$$\mathbf{x}^{n+1} = \mathbf{x}^n + \Delta t \mathbf{v}^n. \tag{3.6b}$$

One observes that the Euler method yields completely wrong results which is also well-known from the simulation of planetary motions. For the standard 4$^\mathrm{th}$-order Runge-Kutta method one would get a similar result as for the Euler method, however the deviation from the analytical result would be not as fast as for the Euler method [23].

The Boris method is a second-order method, meaning that the expected error is of the order Δt^2. In fig. 3.2 this is shown for the same test case as the one used in fig. 3.1, where we have computed the error of the numerical orbit to the exact orbit in the L^2-norm for different time steps.
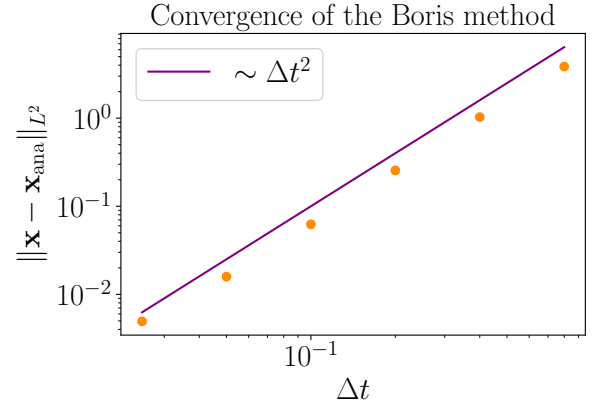

Figure 3.2: L^2-errors of the Boris method applied on the test case shown in fig. 3.1 for different time steps Δt. One can see that the convergence is of second order.

3.1.2 Standard finite elements

We shall apply the finite element method (FEM) for solving Maxwell's and fluid equations [9]. The main idea of the finite element method is to look for the approximate solution of a PDE in a finite-dimensional subspace of the function space where the original problem is posed. This is done by dividing the computational domain $\Omega \subset \mathbb{R}^d$ into a collection of small geometrically easy to handle pieces (squares, triangles, ...), the so-called *elements*, and then defining a set of *basis* functions, mostly polynomials, that span the subspace and have a compact support, meaning that a single basis function vanishes on most of the elements. This leads to sparse matrices in the final linear system for which quite efficient algorithms are available. The approximate solution in the basis of the subspace is expressed as

$$\Phi_h(\mathbf{x}) = \sum_{j=0}^{N-1} \phi_j \varphi_j(\mathbf{x}), \tag{3.7}$$

where N is the number of basis functions and the subscript h denotes the approximation compared to the exact solution Φ (*trial* function). The unknowns which need be found are thus the coefficients $\phi_0, \ldots, \phi_{N-1}$. In the FEM this is done with the *method of weighted*

residuals [9] which consists of demanding that the residual R of a PDE does not have to vanish in a local sense (which would be the exact solution) but in a global sense. Mathematically speaking: For a general PDE with the differential operator $\mathcal{L}$ and right-hand side f,

$$\mathcal{L}\Phi = f \quad \text{in } \Omega, \tag{3.8}$$

we define the residual R by

$$R := \mathcal{L}\Phi - f, \tag{3.9}$$

and demand its vanishing in a a global sense:

$$\int_\Omega R \mathrm{d}\Omega = 0. \tag{3.10}$$

Furthermore, we introduce a *test* function w in order to get a spatially different weighting of this vanishing:

$$\int_\Omega w R \mathrm{d}\Omega = 0 \Leftrightarrow \int_\Omega w \mathcal{L}\Phi \mathrm{d}\Omega = \int_\Omega w f \mathrm{d}\Omega. \tag{3.11}$$

Let us apply this formulation on one of the simplest examples, namely the Poisson equation in one dimension with periodic boundary conditions, i.e. $\Omega \subset \mathbb{R} = (a, b)$, with a and b being the domain boundaries, and $\mathcal{L} = \partial^2/\partial z^2$:

$$-\frac{\partial^2 \Phi}{\partial z^2} = f \quad \text{in } \Omega, \tag{3.12a}$$

$$\Phi(a) = \Phi(b). \tag{3.12b}$$

In this strong formulation of the problem Φ must be twice continuously differentiable. Applying the formulation of weighted residuals yields

$$-\int_a^b w \frac{\partial^2 \Phi}{\partial z^2} \mathrm{d}z = \int_a^b w f \mathrm{d}z, \tag{3.13}$$

which means that the second derivative of Φ must be square integrable which is a less demanding requirement than twice differentiability. For this, let us define the spaces $L^2(\Omega)$ of square integrable functions, $H^1(\Omega)$ of square integrable functions including its first derivative and its respective norms:

$$L^2(\Omega) = \{u, \int_\Omega u^2 \mathrm{d}\Omega < \infty\}, \qquad \|u\|_{L^2}^2 = \int_\Omega u^2 \mathrm{d}\Omega, \tag{3.14a}$$

$$H^1(\Omega) = \{u \in L^2(\Omega), \nabla u \in (L^2(\Omega))^d\}, \qquad \|u\|_{H^1}^2 = \int_\Omega u^2 \mathrm{d}\Omega + \int_\Omega \nabla u^2 \mathrm{d}\Omega. \tag{3.14b}$$

The weak formulation of (3.13) is obtained by partial integration

$$-\int_a^b w \frac{\partial^2 \Phi}{\partial z^2} \mathrm{d}z = \underbrace{\left[w \frac{\partial \Phi}{\partial z}\right]_a^b}_{=0} + \int_a^b \frac{\partial w}{\partial z} \frac{\partial \Phi}{\partial z} \mathrm{d}z = \int_a^b w f \mathrm{d}z, \tag{3.15}$$

where the boundary term vanishes since we impose periodic boundary conditions as well for the test function w. In this formulation $\Phi \in H^1$ and $w \in H^1$, which means that a weaker requirement is imposed to the trail function Φ compared to (3.13). Finally, the total weak formulation of the problem reads: find $\Phi \in H^1$ such that

$$\int_a^b \frac{\partial w}{\partial z} \frac{\partial \Phi}{\partial z} \mathrm{d}z = \int_a^b wf \mathrm{d}z \quad \forall w \in H^1. \tag{3.16}$$

As a next step, the domain Ω is discretized into N_{el} elements with the characteristic length h and the continuous space H^1 is replaced by a finite-dimensional subspace $\mathcal{S}_h \subset H^1(\Omega)$ for the trial function and $\mathcal{V}_h \subset H^1(\Omega)$ for the test function. If the two spaces are the same, the method is called *(Bubnov-) Galerkin-method* otherwise *Petrov-Galerkin-method*. Since we will exclusively use the former one, we immediately set $\mathcal{S}_h = \mathcal{V}_h$. The discrete version of (3.16) then reads: find $\Phi \in \mathcal{S}_h$ such that

$$\int_a^b \frac{\partial w_h}{\partial z} \frac{\partial \Phi_h}{\partial z} \mathrm{d}z = \int_a^b w_h f \mathrm{d}z \quad \forall w \in \mathcal{S}_h. \tag{3.17}$$

As already indicated, we denote the dimension of $\mathcal{S}_h$ and thus the number of basis functions by N. Expanding trial and test function as

$$\Phi_h(z) = \sum_{j=0}^{N-1} \phi_j \varphi(z), \quad w_h(z) = \sum_{i=0}^{N-1} w_i \varphi(z), \tag{3.18}$$

and plugging this in the Galerkin-formulation (3.17) yields

$$\sum_{i,j=0}^{N-1} w_i \phi_j \int_a^b \varphi_i'(z) \varphi_j'(z) \mathrm{d}z = \sum_{i=0}^{N-1} w_i \int_a^b f \varphi_i(z) \mathrm{d}z. \tag{3.19}$$

In order to obtain a matrix formulation, we define the stiffness matrix $\mathbb{K}$ as well as the mass matrix $\mathbb{M}$ and the advection matrix $\mathbb{C}$. The latter two we will need later for the hybrid model:

$$\mathbb{K} := \left(\int_a^b \varphi_i'(z) \varphi_j'(z) \mathrm{d}z \right)_{i,j=0,\dots,N-1}, \tag{3.20a}$$

$$\mathbb{M} := \left(\int_a^b \varphi_i(z) \varphi_j(z) \mathrm{d}z \right)_{i,j=0,\dots,N-1}, \quad \mathbb{C} := \left(\int_a^b \varphi_i(z) \varphi_j'(z) \mathrm{d}z \right)_{i,j=0,\dots,N-1}. \tag{3.20b}$$

Furthermore, we introduce vectors for the coefficients and the right-hand side, i.e. $\boldsymbol{\phi} = (\phi_0, \dots, \phi_{N-1})^\top$, $\mathbf{w} = (w_0, \dots, w_{N-1})^\top$ and

$$\bar{\mathbf{f}} := \left(\int_a^b f(z) \varphi_0(z) \mathrm{d}z, \dots, \int_a^b f(z) \varphi_{N-1}(z) \mathrm{d}z \right)^\top. \tag{3.21}$$

This finally leads to the matrix formulation:

$$\mathbf{w}^\top \mathbb{K} \boldsymbol{\phi} = \mathbf{w}^\top \bar{\mathbf{f}} \tag{3.22a}$$

$$\Leftrightarrow \quad \mathbb{K} \boldsymbol{\phi} = \bar{\mathbf{f}}, \tag{3.22b}$$

where the last step is due to the fact that we want this to be true for all $\mathbf{w}$. Solving the linear system (3.22b) then yields the unknown coefficients $\boldsymbol{\phi}$.

Let us now construct the basis of the finite-dimensional space $\mathcal{S}_h$ with $\dim \mathcal{S}_h = N$. Throughout this work, whenever we will work with standard finite elements, we shall do this with so-called B-splines, which are piecewise polynomials of degree p [24, 25]. The set of basis functions is fully determined by a sequence of $m + 1$ points (or knots) $a = z_0 \leq z_1 \leq \ldots \leq z_m = b$ which define a knot vector $T = (z_0, z_1, \ldots, z_m)$. For degree $p = 0$ the basis functions $(\varphi_i^{p=0}(z))_{i=0,\ldots,m-1}$ are defined by

$$\varphi_i^0(z) = \begin{cases} 1 & z \in [z_i,\, z_{i+1}) \\ 0 & \text{else.} \end{cases} \tag{3.23}$$

Higher degrees are defined by the following recursion formula:

$$\varphi_i^p(z) = w_i^p(z)\varphi_i^{p-1}(z) + (1 - w_{i+1}^p)\varphi_{i+1}^{p-1}(z), \qquad w_i^p(z) = \frac{z - z_i}{z_{i+p} - z_i}. \tag{3.24}$$

If the knot vector T contains r repeated knots one says that this knot has multiplicity r. Using multiple knots at the interval boundaries a and b enables the application of Dirichlet boundary conditions by enforcing all the interior splines to vanish at the boundaries and setting the first and last spline there to one. This can be achieved by using $r = p+1$ equal knots for the left and right boundary, respectively. In this case $\dim \mathcal{S}_h = m - p$. However, since we are using periodic boundary conditions, we need a periodic basis. This can be achieved by extending the knot vector over the boundaries by p additional points. The result is shown in fig. 3.3 for generic degrees $p = 1$ and $p = 2$. In this case $\dim \mathcal{S}_h = m - 2p$. Note in fig. 3.3 that B-splines which leave the domain at one boundary come back at the other boundary which can be seen by the respective color codings.

The elements of the discretized domain are now naturally related to the knot sequence by simply using all interior knots together with the boundaries of the domain as the element boundaries which we shall denote by $(c_k)_{k=0,\ldots,N_{\text{el}}}$, where N_{el} is the total number of elements and $c_0 = a$ and $c_{N_{\text{el}}} = b$.

Let us summarize some important properties of a B-spline basis:

- B-splines are piecewise polynomials of degree p,

- B-splines are non-negative,

- local support: there are exactly $p + 1$ non-vanishing B-splines in each element and the support of the B-spline φ_i^p is located in $[z_i, \ldots, z_{i+p+1}]$,

- B-splines form a partition of unity: $\sum_{i=0}^{N-1} \varphi_i^p(z) = 1, \quad \forall z \in \mathbb{R}$.

Since B-splines are piecewise polynomials, all matrices can be computed exactly by using for instance a quadrature rule [21]. Here we shall use a Gauss-Legendre quadrature formula with $p + 1$ quadrature points which allows us to integrate exactly polynomials of an order up to $2p + 1$. This choice for the number of quadrature points is due to the
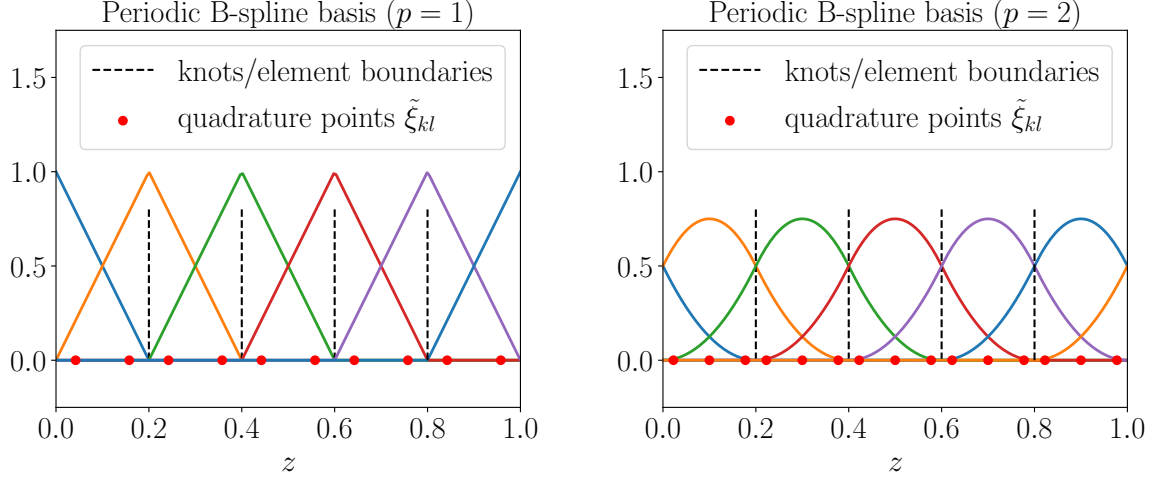
Figure 3.3: Left: *Example for a periodic B-spline basis of degree $p = 1$ on the domain $a = 0$ to $b = 1.0$ discretized by $N_{el} = 5$ elements. The corresponding knot vector $T = (-0.2, 0, 0.2, 0.4, 0.6, 0.8, 1.0, 1.2)$. The red dots denote the corresponding quadrature grid that results from (3.26). The points ξ_l and weights w_l on the reference interval are $\xi_1 = -\sqrt{1/3}$, $\xi_2 = \sqrt{1/3}$, $w_1 = 1$ and $w_2 = 1$. **Right**: Same for $p = 2$. The knot vector in this case $T = (-0.4, -0.2, 0, 0.2, 0.4, 0.6, 0.8, 1.0, 1.2, 1.4)$.*

fact that for the mass matrix we have to integrate in each element a multiplication of polynomials of order p which yields a polynomial of order $2p$ for the integrand. For the stiffness matrix p points would be sufficient but we do not want to restrict ourselves to this matrix. For instance, the computation of the mass matrix is done in the following way:

$$
\begin{aligned}
\int_a^b \varphi_i(z)\varphi_j(z)\mathrm{d}z &= \sum_{k=0}^{N_{el}-1} \int_{c_k}^{c_{k+1}} \varphi_i(z)\varphi_j(z)\mathrm{d}z \\
&= \sum_{k=0}^{N_{el}-1} \frac{c_{k+1} - c_k}{2} \sum_{l=1}^{p+1} w_l \varphi_i\left(\frac{c_{k+1} - c_k}{2}\xi_l + \frac{c_{k+1} + c_k}{2}\right)\varphi_j\left(\frac{c_{k+1} - c_k}{2}\xi_l + \frac{c_{k+1} + c_k}{2}\right),
\end{aligned}
\tag{3.25}
$$

Here, ξ_l and w_l are the $p + 1$ Gauss-Legendre quadrature points and weights on the reference interval $I = [-1, 1]$ where quadrature rules are usually defined. The last step is just the transformation of the integral over the element to the reference interval and the coefficients are can be found e.g. in textbooks [21] or on the Internet. However, what is useful in practice in order to simplify the implementation is to define a "quadrature grid" on the physical domain (see fig. 3.3) defined by

$$
\tilde{w}_{kl} = \frac{c_{k+1} - c_k}{2} w_l,
\tag{3.26a}
$$

$$
\tilde{\xi}_{kl} = \frac{c_{k+1} - c_k}{2}\xi_l + \frac{c_{k+1} + c_k}{2},
\tag{3.26b}
$$

where $k = 0, \ldots, N_{el} - 1$ denotes again the element and $l = 1, \ldots, p + 1$ the quadrature
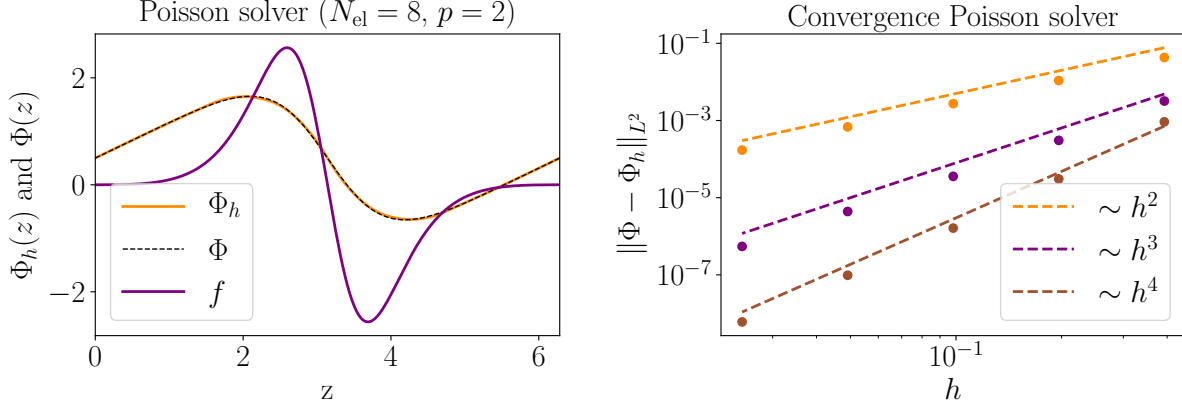
Figure 3.4: Left: *Approximate solution* Φ_h *(orange line) of the Poisson equation together with the exact one with const. = 0.5 (black dashed line) obtained with $N_{el} = 8$ elements and B-splines of degree $p = 2$.* **Right**: *L^2-errors of the approximate solution for different element sizes h and polynomial degrees (dots) and expected convergence rates (dashed lines).*

points/weights on the reference interval. With this (3.25) simply becomes

$$\int_a^b \varphi_i(z)\varphi_j(z)\mathrm{d}z = \sum_{kl} \tilde{w}_{kl}\varphi_i(\tilde{\xi}_{kl})\varphi_j(\tilde{\xi}_{kl}). \tag{3.27}$$

For the stiffness and advection matrix one can use the same formula, however, the first derivative of the B-splines is needed. With the recursion formula one can show that it is given by

$$\frac{\mathrm{d}}{\mathrm{d}z}\varphi_i^p(z) = p\left(\frac{\varphi_i^{p-1}(z)}{z_{i+p} - z_i} - \frac{\varphi_{i+1}^{p-1}(z)}{z_{i+p+1} - z_{i+1}}\right). \tag{3.28}$$

Let us come back to the Poisson example and use these formulas to assemble the stiffness matrix. For the right-hand side $\bar{\mathbf{f}}$ we always use the same quadrature rule as for the matrices, however, here we commit a numerical error since the function f is in general of course not a polynomial of small enough order. In order to check the implementation we use the so-called *method of manufactured solutions* [26] which consists of taking an arbitrary function Φ and computing the right-hand side f such that the exact solution if available. As an example we take

$$\Phi(z) = \frac{\sin(z)}{\frac{1}{2}\cos(z) + 1} + const. \quad \text{in } \Omega = (0, 2\pi), \tag{3.29}$$

where the *const.* appears due to the fact that periodicity does not result in a unique solution for the Poisson equation. We do not want to go too much into detail because we will not need this for the hybrid model but obtaining a unique solution can e.g. be achieved by fixing the average of the desired solution which, in the linear system, consists
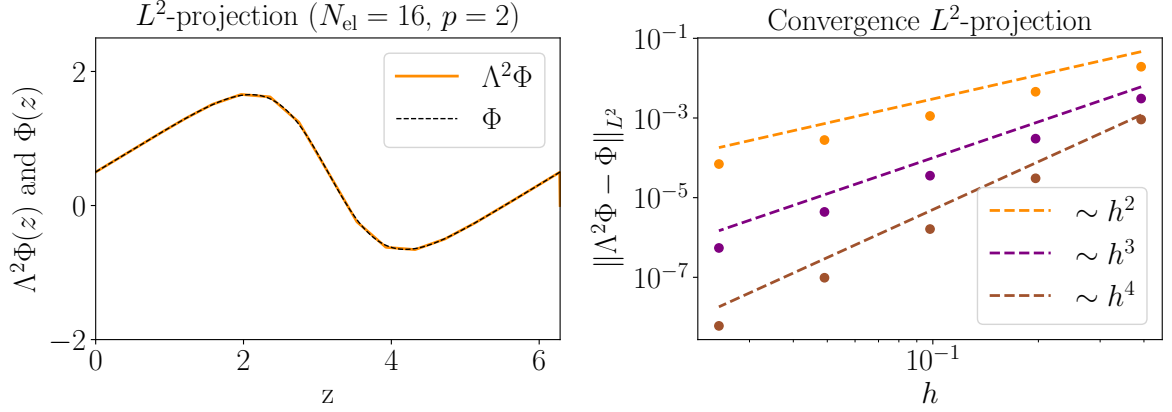
Figure 3.5: Left: *L^2-projection of the function (3.29) obtained with $N_{el} = 16$ elements and B-splines of degree $p = 2$.* ***Right:*** *L^2-errors of the projected function for different element sizes h and polynomial degrees (dots) and expected convergence rates (dashed lines).*

of replacing one line of the stiffness matrix by ones and replacing the corresponding value of the right-hand side $\bar{\mathbf{f}}$ with a specific value that takes into account the normalization of every B-spline of the basis.

In fig. 3.4, the approximate solution Φ_h for $N_{\text{el}} = 8$ and $p = 2$ is shown together with the exact solution (3.29) and the right-hand side f. One can see the qualitatively good agreement even for this rather coarse grid and low polynomial degree.

Finally, we check the convergence of the method by computing the deviation of the approximate solution from the exact one in the L^2-norm. One can show that the expected error is

$$\|\Phi - \Phi_h\|_{L^2} \leq Ch^{p+1}, \tag{3.30}$$

where C is a constant independent of the element size h. The results for the same example are shown in fig. 3.4 on the right-hand side and we clearly see the enhanced convergence rate for higher polynomial degrees.

L2-projection The L2-projection denoted by $\Lambda^2 : L^2 \to \mathcal{S}_h$ is a simple method to project an arbitrary function $\Phi \in L^2$ on a finite element space $\mathcal{S}_h$ [27]. We will use this method to project the initial, continuous fields of the hybrid model on the space $\mathcal{S}_h \subset H^1 \subset L^2$. The method consist of minimizing the L^2-error of the projected function denoted by $\Lambda^2\Phi$ which is equivalent to demanding

$$\int_a^b (\Lambda^2\Phi - \Phi)\varphi_i \mathrm{d}z = 0, \quad \forall \varphi_i \in \mathcal{S}_h. \tag{3.31}$$

Expressing the projected function $\Lambda^2\Phi$ as usual in the finite element basis as

$$(\Lambda^2\Phi)(z) = \sum_{j=0}^{N-1} \phi_j \varphi_j(z) \tag{3.32}$$

and plugging this in the definition (3.31) yields

$$\sum_{j=0}^{N-1} \phi_j \int_a^b \varphi_i(z)\varphi_j(z)\mathrm{d}z = \int_a^b \Phi(z)\varphi_i(z)\mathrm{d}z, \quad \forall \varphi_i \in \mathcal{S}_h, \tag{3.33a}$$

$$\Leftrightarrow \quad \mathbb{M}\boldsymbol{\phi} = \bar{\bar{\boldsymbol{\Phi}}}, \tag{3.33b}$$

where $\mathbb{M}$ is the mass matrix, $\boldsymbol{\phi}$ the vector containing the coefficients of (3.32) and $\bar{\bar{\boldsymbol{\Phi}}}$ the right-hand side vector defined above. The numerical error here is once more due to the fact that $\bar{\bar{\boldsymbol{\Phi}}}$ can, in general, not be computed exactly. In fig. 3.5 we have performed the L^2-projection for the function (3.29) with $N_{\mathrm{el}} = 16$ elements and quadratic B-splines ($p = 2$). On the right-hand side one can see that the convergence rates follow the same estimation (3.30) as for the Poisson equation.

3.1.3 Finite element exterior calculus

The finite element exterior calculus (FEEC) [1] is a more advanced method that uses tools from differential geometry and the fact that certain physical quantities are different objects therein and should therefore be discretized in different ways in order to keep the underlying geometric structure of the considered model. As already indicated in the beginning of this thesis, this is needed to preserve certain invariants like energy or the two Gauss laws in Maxwell's equations which is indispensable to guarantee stability for long simulations [1].

As an example one can have a look

Figure 3.6: *De Rham sequence in one spatial dimension. The upper line represents the continuous spaces and the lower line the discrete finite-dimensional spaces.*

at the relation of the electric and magnetic field in three dimensions which is given by Faraday's law whose integral form is

$$\oint_{\partial S} \mathbf{E} \cdot \mathrm{d}\mathbf{l} = -\int_S \frac{\partial \mathbf{B}}{\partial t} \cdot \mathrm{d}\mathbf{S}, \tag{3.34}$$

where we have used Stoke's theorem on the left-hand side and S is some surface with fringe ∂S. One can see that this relates a line integral to a surface integral which is due to the fact that $\mathbf{E}$ and $\mathbf{B}$ are different objects in terms of differential geometry. With its notions, $\mathbf{E}$ is a 1-form and wants to be integrated along a curve whereas $\mathbf{B}$ is a 2-form and wants to be integrated over a surface. In one spatial dimension, in which we exclusively work, this means that if we have point values for the electric field, the appropriate object to discretize the magnetic field is its integral between the two points.

In order to preserve a geometric structure and to get stable discretizations, the discrete Finite Element spaces must be related to the continuous spaces by a so-called de Rham sequence with a commuting diagram [1, 2]. In one spatial dimension, where the
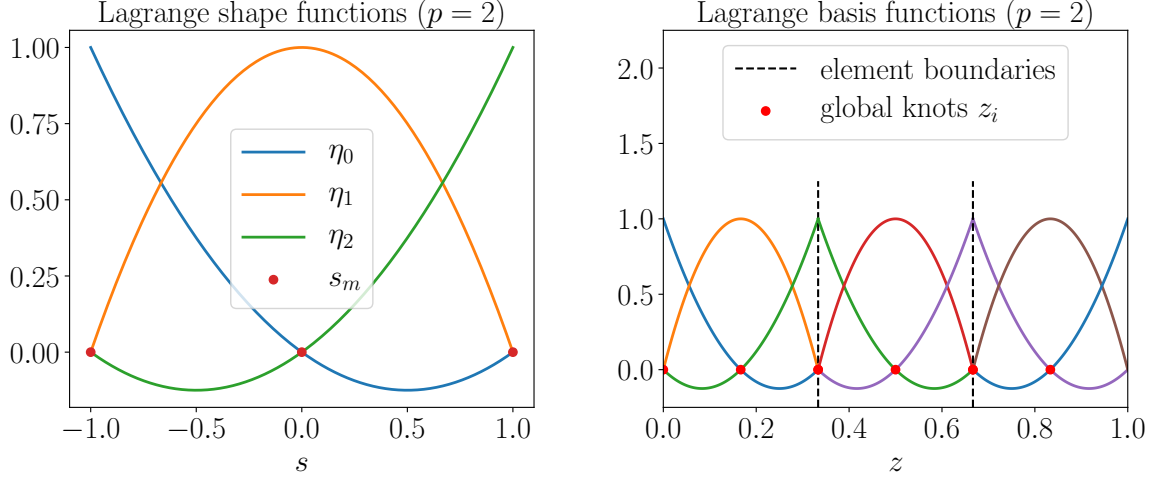
Figure 3.7: Left: *Lagrange shape functions of degree $p = 2$ on the reference interval $I = [-1, 1]$ and the corresponding knot sequence s_m (red dots).* **Right**: *Lagrange basis functions on the physical domain discretized by $N_{el} = 3$ elements. Note that there are three basis functions that have a support of one element and three basis functions that have a support of two elements (green, purple and blue).*

only first order differential operator we have to deal with is the standard derivative $\partial/\partial z$ (compared to grad, curl and div in three dimensions), the diagram takes the simple form depicted in fig. 3.6, where the upper line represents the sequence of infinite dimensional function spaces involved in Maxwell's equations in one dimension and the lower line the finite dimensional subspaces V_0 and V_1 which are related to the continuous ones via the projectors Π_0 and Π_1.

Let us construct a basis for each of the two subspaces that satisfy the commuting diagram property and subsequently apply this on the Poisson equation to introduce the basic notions and definitions needed for the application on the hybrid model. For the space $V_0 \subset H^1$ with $\dim V_0 = N_0$, i.e. N_0 is the number of basis functions denoted by $(\varphi_i^0(z))_{i=0,\ldots,N_0-1}$, we choose Lagrange polynomials (LPs) of degree p. These functions are most easily defined directly in an element $\Omega_k = [c_k, c_{k+1}]$, where $k = 0, \ldots, N_{el} - 1$, which has been mapped on the reference element $I = [-1, 1]$. The functions in this reference element are then called Lagrange *shape* functions which are later transferred back on the global domain in order to construct the *basis* functions. This, as well as the other direction, is done with the mapping $F_k : I \to \Omega_k$, $s \in I \mapsto \Omega_k$ and its inverse F_k^{-1} defined by

$$z = F_k(s) := c_k + \frac{s+1}{2}(c_{k+1} - c_k), \tag{3.35a}$$

$$s = F_k^{-1}(z) := \frac{2(z - c_k)}{c_{k+1} - c_k} - 1. \tag{3.35b}$$

The Lagrange shape functions $(\eta_n(s))_{n=0,\dots,p}$ of degree p on the reference element I are created from a sequence of knots $s_0 = -1 < \dots < s_p = 1$ and are defined by

$$\eta_n(s_m) = \delta_{n,m}, \quad n,m = 0,\dots,p, \tag{3.36}$$

which leads to the formula

$$\eta_n(s) = \prod_{m \neq n} \frac{s - s_m}{s_n - s_m}. \tag{3.37}$$

On the left of fig. 3.7 one can see as an example the Lagrange shape functions of degree $p = 2$ on the reference element I. On the right, the corresponding set of basis functions is shown on the physical domain. It is important to note that the shape functions whose knots correspond to the boundaries of I form a mutual basis function. In our case of periodic boundary conditions, this also means that the first and last shape function on the physical domain form one basis function which can again be seen in fig. 3.7 by the color coding. This leads to a total number of $N_0 = p N_{\mathrm{el}}$ basis functions which is thus the dimension of the first space V_0. Note that we can use the same quadrature formula (3.27) as for the B-spline basis for the computation of the mass matrix.

The corresponding projector Π_0 on this basis acting on some continuous function $E \in H^1$ is defined as follows:

$$\begin{aligned} \Pi_0 &: H^1 \longrightarrow V_0, \\ (\Pi_0 E)(z_i) &= E(z_i) \quad \forall i \in \{0,\dots,N_0-1\}. \end{aligned} \tag{3.38}$$

Here, z_i denotes the global knot sequence on the physical domain (see fig. 3.7) that satisfies $\varphi_i^0(z_j) = \delta_{ij}$. Denoting the approximate function by $\Pi_0 E := E_h$ we thus have

$$E(z_i) \underset{\substack{\uparrow \\ \text{by def. (3.38)}}}{=} E_h(z_i) = \sum_{j=0}^{N_0-1} e_j \varphi_j^0(z_i) = e_j, \tag{3.39}$$

which means that the coefficients are the values of the function at the knot sequence z_i (in contrast to a B-spline basis).

As a next step, we consider the space $V_1 \subset L^2$ with $\dim V_1 = N_1$ and basis functions $(\varphi_{i+1/2}^1(z))_{i=0,\dots,N_1-1}$. Here, we choose Lagrange histopolation polynomials (LHPs) $(\chi_{n+1/2}(s))_{n=0,\dots,p-1}$ on the reference element I defined by

$$\int_{s_m}^{s_{m+1}} \chi_{n+1/2}(s)\mathrm{d}s = \delta_{n,m}, \quad n,m = 0,\dots,p-1, \tag{3.40}$$

where $s_0 = -1 < \dots < s_p = 1$ is the same local knot sequence as for the LPs. Some simple consideration yield that the solution of these equations is given by linear combinations of first order derivatives of the Lagrange shape functions η_n,

$$\chi_{n+1/2}(s) = \sum_{m=n+1}^{p} \frac{\mathrm{d}}{\mathrm{d}s}\eta_m(s), \quad n = 0,\dots,p-1, \tag{3.41}$$
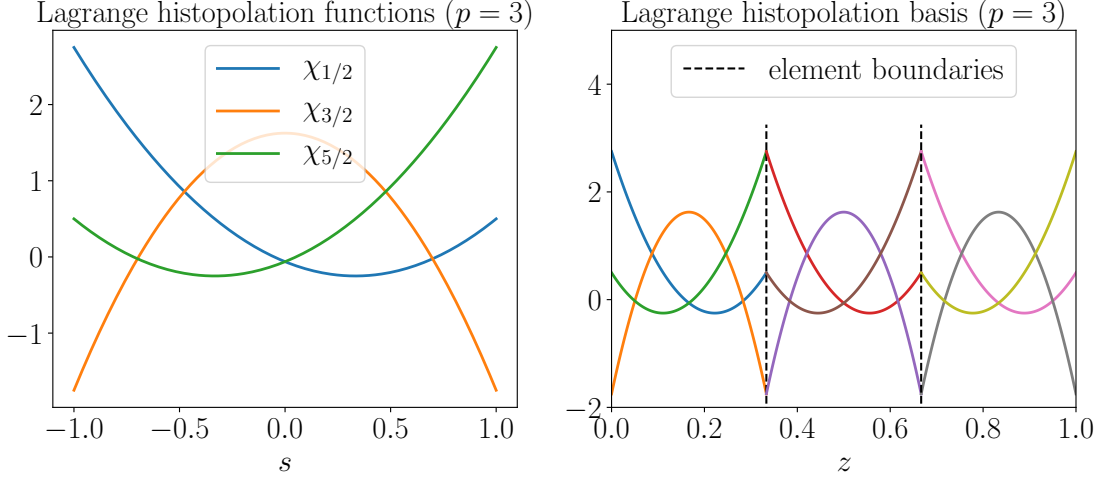
Figure 3.8: Left: *Lagrange histopolation shape functions of degree $p = 3$ on the reference interval $I = [-1, 1]$. **Right**: Lagrange histopolation basis functions of the physical domain discretized by $N_{el} = 3$ elements. Unlike LPs every basis function has a support of only one element.*

which can easily be verified by plugging this into the definition and using the definition of the LPs. In fig. 3.8 the respective shape and basis functions are shown for generic $p = 3$. Note that, in contrast to LPs, there are no shared degrees of freedom, i.e. the shape functions on the reference element are just put next to each other on the physical domain and therefore no boundary conditions must be taken into account. It also means that the total number of basis functions is again $N_1 = pN_{\mathrm{el}}$. However, in contrast to the LPs, there are p non-vanishing basis functions per element (in contrast to $p + 1$ for LPs) which is due to the fact that there are not shared degrees of freedom.

Coming once more back to the commuting diagram, we define the second projector Π_1 as follows:

$$\Pi_1 : L^2 \longrightarrow V_1,$$
$$\int_{z_i}^{z_{i+1}} (\Pi_1 B)(z)\mathrm{d}z = \int_{z_i}^{z_{i+1}} B(z)\mathrm{d}z \quad \forall i \in \{0, \dots, N_0 - 1\}. \tag{3.42}$$

Here, z_{N_0} (which does actually not exist due to periodic boundary conditions) is just the right end of the domain, i.e. $z_{N_0} = b$. Denoting the approximate function by $(\Pi_1 B) := B_h$, we have

$$\int_{z_i}^{z_{i+1}} B(z)\mathrm{d}z \underset{\substack{\uparrow \\ \text{by def. (3.42)}}}{=} \int_{z_i}^{z_{i+1}} B_h(z)\mathrm{d}z$$
$$= \sum_{j=0}^{N_1-1} b_{j+1/2} \int_{z_i}^{z_{i+1}} \varphi_{j+1/2}^1(z)\mathrm{d}z = \frac{c_{k+1} - c_k}{2} b_{i+1/2}, \tag{3.43}$$

where we have transferred the integral on the reference element and used the the definition of the LHPs in the last step.

Commuting diagram property   Let us now proof that this choice for the projectors indeed satisfies the commuting diagram property shown in fig. 3.6. For this, we first take the derivative of an arbitrary function $E \in H^1$ that has been projected on the space V_0 with the projector Π_0:

$$\frac{\partial}{\partial z}(\Pi_0 E) = \sum_{j=0}^{N_0-1} e_j \frac{\partial}{\partial z}\varphi_j^0(z). \tag{3.44}$$

On the other hand, according to the diagram, we know that the function now lives in the space V_1, which means that we can expand the function in the corresponding basis with some modified coefficients $e'_{j+1/2}$:

$$\frac{\partial}{\partial z}(\Pi_0 E) = \sum_{j=0}^{N_1-1} e'_{j+1/2}\varphi_{j+1/2}^1(z). \tag{3.45}$$

The new coefficients are uniquely determined by applying formula (3.43):

$$
\begin{aligned}
e'_{j+1/2} &= \frac{2}{c_{k+1}-c_k}\int_{z_j}^{z_{j+1}} \frac{\partial}{\partial z}(\Pi_0 E)\mathrm{d}z = \frac{2}{c_{k+1}-c_k}\sum_{i=0}^{N_0-1} e_i \int_{z_j}^{z_{j+1}} \frac{\partial}{\partial z}\varphi_i^0(z)\mathrm{d}z \\
&= \frac{2}{c_{k+1}-c_k}\sum_{i=0}^{N_0-1} e_i[\varphi_i^0(z_{j+1}) - \varphi_i^0(z_j)] = \frac{2}{c_{k+1}-c_k}(e_{j+1}-e_j).
\end{aligned}
\tag{3.46}
$$

Note that we have $e_{N_0} = e_0$ for periodic boundary conditions. As a next step, we go the other way and project the function $\partial E/\partial z \in L^2$ on the space V_1 with the projector Π_1:

$$\Pi_1 \frac{\partial E}{\partial z} = \sum_{j=0}^{N_1-1} e''_{j+1/2}\varphi_{j+1/2}^1(z). \tag{3.47}$$

We again use formula (3.43) in order to obtain the coefficients $e''_{j+1/2}$:

$$
\begin{aligned}
e''_{j+1/2} &= \frac{2}{c_{k+1}-c_k}\int_{z_j}^{z_{j+1}} \Pi_1\frac{\partial E}{\partial z}\mathrm{d}z = \frac{2}{c_{k+1}-c_k}\int_{z_j}^{z_{j+1}} \frac{\partial E}{\partial z}(z)\mathrm{d}z \\
&= \frac{2}{c_{k+1}-c_k}[E(z_{j+1}) - E(z_1)] = \frac{2}{c_{k+1}-c_k}(e_{j+1}-e_j).
\end{aligned}
\tag{3.48}
$$

In the last step we have used the property (3.39) of the projector Π_0. We see that this leads to the same coefficients in the final space V_1 as for the other way, i.e.

$$\frac{\partial}{\partial z}(\Pi_0 E) = \Pi_1 \frac{\partial}{\partial z}E \tag{3.49}$$

and hence the diagram is commuting.

To demonstrate how this framework can be applied in practice, we once more take a look at the Poisson equation in one dimension with periodic boundary conditions. Since this framework is applicable on first order partial differential equations only, we first have to rewrite the Poisson equation as a system of coupled first order PDEs [2]:

$$\begin{cases} \sigma = -\frac{\partial \Phi}{\partial z}, \\ \frac{\partial \sigma}{\partial z} = f. \end{cases} \tag{3.50}$$

We shall solve the first equation in a weak sense and the second equation in a strong sense which means that we only integrate by parts in the first equation in order to shift the derivative from the trail to the test function. This yields the following weak formulation: find $\sigma \in H^1$ and $\Phi \in L^2$ such that

$$\int_a^b \sigma \tau \mathrm{d}z = \int_a^b \Phi \frac{\partial \tau}{\partial z} \mathrm{d}z \quad \forall \tau \in H^1, \tag{3.51a}$$

$$\int_a^b \frac{\partial \sigma}{\partial z} v \mathrm{d}z = \int_a^b f v \mathrm{d}z \quad \forall v \in L^2. \tag{3.51b}$$

The corresponding discrete version is obtained by the projectors Π_0 and Π_1, respectively: find $\sigma_h := \Pi_0 \sigma \in V_0$, $\Phi_h := \Pi_1 \Phi \in V_1$ such that

$$\int_a^b \sigma_h \tau_h \mathrm{d}z = \int_a^b \Phi_h \frac{\partial \tau_h}{\partial z} \mathrm{d}z \quad \forall \tau_h := \Pi_0 \tau \in V_0, \tag{3.52a}$$

$$\int_a^b \frac{\partial \sigma_h}{\partial z} v_h \mathrm{d}z = \int_a^b f v_h \mathrm{d}z \quad \forall v_h := \Pi_1 v \in V_1. \tag{3.52b}$$

Next, as usual, all functions are expressed in their respective basis, however, since we take the derivative of $\tau_h \in V_0$ and $\sigma_h \in V_0$ in the above formulation, these functions now live in the space V_1. For a uniform mesh, i.e. $c_{k+1} - c_k = h \; \forall k$, this means that

$$\frac{\partial \tau_h}{\partial z}(z) = \frac{2}{h} \sum_{j=0}^{N_1-1} (\tau_{j+1} - \tau_j) \varphi_{j+1/2}^1(z), \tag{3.53}$$

where we have used formula (3.46) and the same is true for σ_h. Plugging this in the weak formulation yields

$$\sum_{i,j=0}^{N_0-1} \sigma_j \tau_i \int_a^b \varphi_i^0(z) \varphi_i^0(z) \mathrm{d}z = \sum_{i,j=0}^{N_1-1} \phi_j \frac{2}{h} (\tau_{i+1} - \tau_i) \int_a^b \varphi_{i+1/2}^1(z) \varphi_{j+1/2}^1(z) \mathrm{d}z, \tag{3.54a}$$

$$\sum_{i,j=0}^{N_1-1} \frac{2}{h} (\sigma_{j+1} - \sigma_j) v_i \int_a^b \varphi_{i+1/2}^1(z) \varphi_{j+1/2}^1(z) \mathrm{d}z = \sum_{i=0}^{N_1-1} v_i \int_a^b f \varphi_{i+1/2}^1(z) \mathrm{d}z. \tag{3.54b}$$

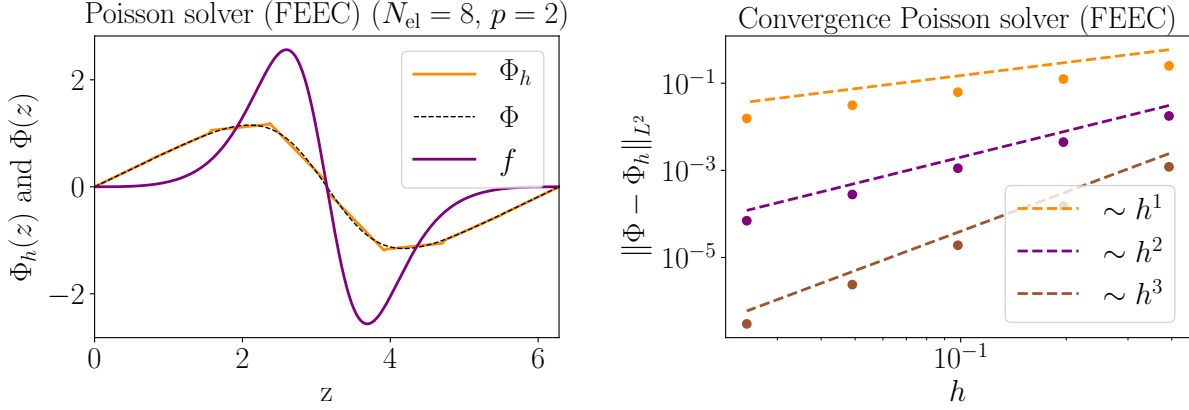In order to obtain a matrix formulation, we introduce the discrete gradient matrix $\mathbb{G} \in$

Figure 3.9: Left: *Approximate solution Φ_h (orange line) of the Poisson equation together with the exact one for const. $= 0.5$ (black dashed line) obtained with functions spaces satisfying the commuting diagram 3.6, $N_{el} = 8$ elements and LPs of degree $p = 2$ (and thus the degree of the LHPs $p = 1$). **Right**: L^2-errors of the approximate solution for different element sizes h and polynomial degrees (dots) and expected convergence rates (dashed lines).*

$\mathbb{R}^{N_1 \times N_0}$ which can be seen as the discrete version of the first order derivative:

$$\mathbb{G} := \frac{2}{h} \begin{pmatrix} -1 & 1 & & & \\ & -1 & 1 & & \\ & & \ddots & \ddots & \\ & & & -1 & 1 \\ 1 & & & & -1 \end{pmatrix} \in \mathbb{R}^{N_1 \times N_0}. \tag{3.55}$$

Note that the 1 in the lower left corner and $N_0 = N_1$ is again due to periodic boundary conditions. Furthermore, in (3.54), we recognize the mass matrix in the space V_0 which we denote by $\mathbb{M}^0$ and the mass matrix in the space V_1 which we denote by $\mathbf{M}^1$. The integral on the right-hand side of (3.54b) is performed in V_1 which is why we denote this vector by $\bar{\mathbf{f}}^1$. In summary, we get

$$\begin{cases} \boldsymbol{\tau}^\top \mathbb{M}^0 \boldsymbol{\sigma} = (\mathbb{G}\boldsymbol{\tau})^\top \mathbb{M}^1 \boldsymbol{\Phi} \\ \mathbf{v}^\top \mathbb{M}^1 \mathbb{G} \boldsymbol{\sigma} = \mathbf{v}^\top \bar{\mathbf{f}}^1 \end{cases} \tag{3.56}$$

$$\Leftrightarrow \begin{cases} \mathbb{M}^0 \boldsymbol{\sigma} = \mathbb{G}^\top \mathbb{M}^1 \boldsymbol{\Phi} \\ \mathbb{M}^1 \mathbb{G} \boldsymbol{\sigma} = \bar{\mathbf{f}}^1 \end{cases} \tag{3.57}$$

since we want this to be true for all $\boldsymbol{\tau}$ and $\mathbf{v}$. This system can also be written in the block matrix form

$$\begin{pmatrix} \mathbb{M}^0 & -\mathbb{G}^\top \mathbb{M}^1 \\ \mathbb{M}^1 \mathbb{G} & 0 \end{pmatrix} \begin{pmatrix} \boldsymbol{\sigma} \\ \boldsymbol{\Phi} \end{pmatrix} = \begin{pmatrix} 0 \\ \bar{\mathbf{f}}^1 \end{pmatrix}, \tag{3.58}$$

which is not solvable without additional information about the solution $\boldsymbol{\Phi}$. Like it was done in the previous section, getting a unique solution can easily be achieved by fixing

the average of the solution by replacing the correct entries of the system matrix and the right-hand side by the imposed additional condition (see previous section).

In fig. 3.9 on the left the result for the usual example (3.29) is shown for the case $N_{\mathrm{el}} = 8$ elements and LPs of degree $p = 2$. Thus the degree of the LHPs is $p = 1$. Note that the integrals involved in both mass matrices can be evaluated with the quadrature rule introduced in the previous section. On the right we observe convergence rates $\sim h^p$ for different element sizes which is different to standard FEM where we had $\sim h^{p+1}$.

3.2 Application on hybrid model

3.2.1 Standard finite elements

Let us now apply the methods introduced in the previous sections on the hybrid model (2.11) with constant electron plasma frequency Ω_{pe} and constant electron cyclotron frequency Ω_{ce} for which we have derived the dispersion relation (2.44). In this section, we choose standard B-spline finite elements of degree p for the fields $\tilde{\mathbf{E}}, \tilde{\mathbf{B}}$ and $\tilde{\mathbf{j}}_{\mathrm{c}}$ and the particle-in-cell method for solving the Vlasov equation for the energetic electrons. As a first step, we write equations (2.11a), (2.11c) and (2.11d) in the compact form

$$\frac{\partial \mathbf{U}}{\partial t} + A_1 \frac{\partial \mathbf{U}}{\partial z} + A_2 \mathbf{U} = \mathbf{S}, \tag{3.59a}$$

$$\mathbf{U}(0, t) = \mathbf{U}(L, t), \tag{3.59b}$$

for the vector of unknowns $\mathbf{U} = (\tilde{E}_x, \tilde{E}_y, \tilde{B}_x, \tilde{B}_y, \tilde{j}_{\mathrm{c},x}, \tilde{j}_{\mathrm{c},y})^2$ and impose periodic boundary conditions on the domain $\Omega = (0, L)$, where L is the length of the domain. The constant matrices A_1, A_2 and the source term $\mathbf{S}$ are

$$A_1 = \begin{pmatrix} 0 & 0 & 0 & c^2 & 0 & 0 \\ 0 & 0 & -c^2 & 0 & 0 & 0 \\ 0 & -1 & 0 & 0 & 0 & 0 \\ 1 & 0 & 0 & 0 & 0 & 0 \\ 0 & 0 & 0 & 0 & 0 & 0 \\ 0 & 0 & 0 & 0 & 0 & 0 \end{pmatrix}, \tag{3.60a}$$

$$A_2 = \begin{pmatrix} 0 & 0 & 0 & 0 & \mu_0 c^2 & 0 \\ 0 & 0 & 0 & 0 & 0 & \mu_0 c^2 \\ 0 & 0 & 0 & 0 & 0 & 0 \\ 0 & 0 & 0 & 0 & 0 & 0 \\ -\epsilon_0 \Omega_{\mathrm{pe}}^2 & 0 & 0 & 0 & 0 & -\Omega_{\mathrm{ce}} \\ 0 & -\epsilon_0 \Omega_{\mathrm{pe}}^2 & 0 & 0 & \Omega_{\mathrm{ce}} & 0 \end{pmatrix}, \tag{3.60b}$$

---

[2] We shall restrict ourselves on perpendicular perturbations since they are completely decoupled from the parallel ones. This is why the z-components are not taken into account here.

$$\mathbf{S} = \begin{pmatrix} -\mu_0 c^2 j_{\mathrm{h},x} \\ -\mu_0 c^2 j_{\mathrm{h},y} \\ 0 \\ 0 \\ 0 \\ 0 \end{pmatrix}. \tag{3.60c}$$

Following the methods introduced in section 3.1.2, the corresponding weak formulation of eq. (3.59) is obtained by multiplying the equation with a test function $V \in H^1$ and integrating over the domain Ω. The problem then reads: Find $\mathbf{U} \in \underbrace{H^1 \times \cdots \times H^1}_{6 \text{ times}}$ such that

$$\int_0^L \frac{\partial \mathbf{U}}{\partial t} V \, \mathrm{d}z + A_1 \int_0^L \frac{\partial \mathbf{U}}{\partial z} V \, \mathrm{d}z + A_2 \int_0^L \mathbf{U} V \, \mathrm{d}z = \int_0^L \mathbf{S} V \, \mathrm{d}z \quad \forall V \in H^1. \tag{3.61}$$

Note that we have not integrated by parts this time since this would just shift the derivative from the trial to the test function. As we use the same spaces for both functions, this would not change the formulation.

As a next step, the vector space H^1 is replaced by the finite-dimensional subspace $\mathcal{S}_h \subset H^1$ in which we shall look for the approximate solution $\mathbf{U}_{\mathrm{h}}$ of the problem (3.59). Again, following the methods of section 3.1.2, we choose a B-spline basis to span the subspace $\mathcal{S}_h$. Expanding trail and test functions as

$$\mathbf{U}_h(z,t) = \sum_{j=0}^{N-1} \mathbf{u}_j(t)\varphi_j(z), \qquad V_h(z) = \sum_{j=0}^{N-1} v_j \varphi_j(z), \tag{3.62}$$

where we put the time dependency into the coefficients, and plugging these expressions in the (discrete) weak formulation (3.61) yields

$$\sum_{i,j=0}^{N-1} v_i \frac{\mathrm{d}\mathbf{u}_j}{\mathrm{d}t} \int_0^L \varphi_i(z)\varphi_j(z)\mathrm{d}z + A_1 \sum_{i,j=0}^{N-1} v_i \mathbf{u}_j \int_0^L \varphi_i(z)\varphi'_j(z)\mathrm{d}z$$

$$+ A_2 \sum_{i,j=0}^{N-1} v_i \mathbf{u}_j \int_0^L \varphi_i(z)\varphi_j(z)\mathrm{d}z = \sum_{i=0}^{N-1} v_i \int_0^L \mathbf{S}\varphi_i(z) \, \mathrm{d}z. \tag{3.63}$$

This can be expressed equivalently in the following semi-discrete block matrix form:

$$\mathbb{V}\mathbb{M}_{\mathrm{b}} \frac{\mathrm{d}\mathbf{u}}{\mathrm{d}t} + \mathbb{V}\tilde{\mathbb{C}}\mathbf{u} + \mathbb{V}\tilde{\mathbb{M}}\mathbf{u} = \mathbb{V}\mathbb{S}. \tag{3.64}$$

In this matrix formulation, the vector $\mathbf{u}$ contains all the unknown finite element coefficients of the expansion (3.62), i.e. $\mathbf{u} = (\mathbf{u}_0, \mathbf{u}_1, ..., \mathbf{u}_{N-1})^\top$ and every $\mathbf{u}_j$ contains the respective coefficients of all six physical quantities which makes $\mathbf{u}$ a vector of total length $6N$. The block matrix $\mathbb{V}$ for the coefficients of the test function V_h is

$$\mathbb{V} = \begin{pmatrix} v_0 I_6 & 0 & \cdots & 0 \\ 0 & v_1 I_6 & \cdots & 0 \\ \vdots & \vdots & \ddots & \vdots \\ 0 & 0 & \cdots & v_{N-1} I_6 \end{pmatrix} \in \mathbb{R}^{6N \times 6N}, \tag{3.65}$$

where I_6 denotes the 6×6 identity matrix. Furthermore, the block matrices $\tilde{\mathbb{M}}$ and $\tilde{\mathbb{C}}$ are given by

$$\tilde{\mathbb{M}} = \begin{pmatrix} m_{0,0}A_1 & m_{0,1}A_1 & \cdots & m_{0,N-1}A_1 \\ m_{1,0}A_1 & m_{1,1}A_1 & \cdots & m_{1,N-1}A_1 \\ \vdots & \vdots & \ddots & \vdots \\ m_{N-1,0}A_1 & m_{N-1,1}A_1 & \cdots & m_{N-1,N-1}A_1 \end{pmatrix} \in \mathbb{R}^{6N \times 6N}, \qquad (3.66a)$$

$$\tilde{\mathbb{C}} = \begin{pmatrix} c_{0,0}A_2 & c_{0,1}A_2 & \cdots & c_{0,N-1}A_2 \\ c_{1,0}A_2 & c_{1,1}A_2 & \cdots & c_{1,N-1}A_2 \\ \vdots & \vdots & \ddots & \vdots \\ c_{N-1,0}A_2 & c_{N-1,1}A_2 & \cdots & c_{N-1,N-1}A_2 \end{pmatrix} \in \mathbb{R}^{6N \times 6N}, \qquad (3.66b)$$

where m_{ij} and c_{ij} are the entries of the mass and advection matrix (3.20b), respectively. The missing matrix $\mathbb{M}_{\mathrm{b}}$ and the vector $\mathbb{S}$ are

$$\mathbb{M}_{\mathrm{b}} = \begin{pmatrix} m_{0,0}I_6 & m_{0,1}I_6 & \cdots & m_{0,N-1}I_6 \\ m_{1,0}I_6 & m_{1,1}I_6 & \cdots & m_{1,N-1}I_6 \\ \vdots & \vdots & \ddots & \vdots \\ m_{N-1,0}I_6 & m_{N-1,1}I_6 & \cdots & m_{N-1,N-1}I_6 \end{pmatrix} \in \mathbb{R}^{6N \times 6N}, \qquad (3.67)$$

and

$$\mathbb{S} = \begin{pmatrix} \int_0^L \mathbf{S}\varphi_0(z)\mathrm{d}z \\ \vdots \\ \int_0^L \mathbf{S}\varphi_{N-1}(z)\mathrm{d}z \end{pmatrix} \in \mathbb{R}^{6N}. \qquad (3.68)$$

As usual, we want (3.64) to be true for all $\mathbb{V}$ which is why we finally end up with the semi-discrete system

$$\mathbb{M}_{\mathrm{b}}\frac{\mathrm{d}\mathbf{u}}{\mathrm{d}t} = -\tilde{\mathbb{C}}\mathbf{u} - \tilde{\mathbb{M}}\mathbf{u} + \mathbb{S} \qquad (3.69)$$

for the time evolution of all finite element coefficients $\mathbf{u} \in \mathbb{R}^{6N}$.

Having done the the spatial discretization, the next step is to apply a time stepping scheme on the semi-discrete system (3.69). Here, we use a second-order Crank-Nicolson scheme [28] which consist of applying a mid-point rule on the quantities on the right-hand side of above equation. Denoting the time step by n, i.e. $t_n = n\Delta t$, the fully discrete matrix formulation for $\mathbf{u}^n \to \mathbf{u}^{n+1}$ then reads

$$(\mathbb{M}_{\mathrm{b}} + \frac{1}{2}\Delta t\tilde{\mathbb{C}} + \frac{1}{2}\Delta t\tilde{\mathbb{M}})\mathbf{u}^{n+1} = (\mathbb{M}_{\mathrm{b}} - \frac{1}{2}\Delta t\tilde{\mathbb{C}} - \frac{1}{2}\Delta t\tilde{\mathbb{M}})\mathbf{u}^n + \frac{1}{2}\Delta t\left(\mathbb{S}^{n+1} + \mathbb{S}^n\right). \quad (3.70)$$

We immediately see that this time stepping method is implicit, since it needs the computation of the inverse of the matrix appearing on the left-hand. However, since this needs to be done only one time in the very beginning of a simulation, this is not considered to be a problem.

What remains is the question how to treat the integrals appearing in (3.68) which contains the current contribution of the energetic electrons. Since we are using a particle-in-cell solver for the time evolution of the distribution function, the evaluation of the

integrals in phase space can be achieved by a using a Monte Carlo interpretation [29]. For this, we introduce a probability density g_h

$$g_h = g_h(z, \mathbf{v}, t), \quad g_h^0(z, \mathbf{v}) := g_h(z, \mathbf{v}, 0), \tag{3.71}$$

which satisfies the Vlasov equation for the initial state g_h^0 and is normalized to one in phase space:

$$\int_0^L \int g_h(z, \mathbf{v}, t) \mathrm{d}^3\mathbf{v}\mathrm{d}z = 1 \quad \forall t. \tag{3.72}$$

In addition to that, we use a variance reduction technique called *control variate* which means that we only simulate the deviation of the distribution function from some known distribution $\mathcal{M}_0 = \mathcal{M}_0(\mathbf{v})$ as we assume that the distribution function will always be close to an equilibrium [29].

   Mathematically speaking, we write the non-zero components of the vector (3.68) for some basis function φ_i in the following way (we omit the constant in the definition of (3.60c) for reasons of clarity):

$$\int_0^L j_{h,x/y}\, \varphi_i(z)\mathrm{d}z \underset{\substack{\uparrow \\ \text{see def. (2.3f)}}}{=} q_e \int_0^L \int v_{x/y} f_h \varphi_i(z)\mathrm{d}^3\mathbf{v}\mathrm{d}z$$

$$= q_e \int_0^L \int v_{x/y}(f_h - \mathcal{M}_0)\varphi_i(z)\mathrm{d}^3\mathbf{v}\mathrm{d}z + \underbrace{q_e \int_0^L \int v_{x/y}\mathcal{M}_0\varphi_i(z)\mathrm{d}^3\mathbf{v}\mathrm{d}z}_{:=\tilde{j}_{h,x/y}^0}. \tag{3.73}$$

If one chooses for $\mathcal{M}_0$ a known equilibrium distribution function which depends on velocity only, the velocity and space integrals in the second term can be computed separately and preferably analytically. Whenever we use this technique, we shall use for $\mathcal{M}_0$ the same function as we use for the equilibrium hot electron distribution function $f_h^0 = n_{h0} \cdot (2.45)$, i.e.

$$\mathcal{M}_0(\mathbf{v}) = f_h^0(\mathbf{v}) \quad \Rightarrow \quad \tilde{j}_{h,x/y}^0 = q_e \int_0^L \int v_{x/y}\mathcal{M}_0(\mathbf{v})\varphi_i(z)\mathrm{d}^3\mathbf{v}\mathrm{d}z = 0, \tag{3.74}$$

since non-shifted Maxwellians do not result in currents. As a next step, we expand everything with the probability density g_h. This yields

$$\int_0^L j_{h,x/y}\, \varphi_i(z)\mathrm{d}z = q_e \int_0^L \int v_{x/y}(f_h - \mathcal{M}_0)\varphi_i(z)\mathrm{d}^3\mathbf{v}\mathrm{d}z$$

$$= q_e \int_0^L \int v_{x/y}\underbrace{\frac{f_h - \mathcal{M}_0}{g_h}\varphi_i(z)}_{:=\mathcal{R}}\, g_h\mathrm{d}^3\mathbf{v}\mathrm{d}z, \tag{3.75}$$

which means that we can interpret the integral as the expectation value of the random variable $\mathcal{R}$ distributed according to the probability density g_h in phase space. This enables us to write down a Monte Carlo estimate for a finite number of N_p realizations of the

random variable $\mathcal{R}$ by evaluating the random variable at the positions and velocities of the particles introduced in section 3.1.1. Thus, we have

$$
\int_0^L j_{\mathrm{h,x/y}}\,\varphi_i(z)\mathrm{d}z
$$
$$
\approx \frac{q_{\mathrm{e}}}{N_{\mathrm{p}}} \sum_{k=1}^{N_{\mathrm{p}}} \left\{ v_{k,x/y}(t) \left[\frac{f_{\mathrm{h}}(z_k(t),\mathbf{v}_k(t),t)}{g_{\mathrm{h}}(z_k(t),\mathbf{v}_k(t),t)} - \frac{\mathcal{M}_0(\mathbf{v}_k(t))}{g_{\mathrm{h}}(z_k(t),\mathbf{v}_k(t),t)} \right] \varphi_i(z_k(t)) \right\}, \tag{3.76}
$$

where $\mathbf{v}_k(t)$ and $z_k(t)$ are the solutions of the orbit equations (3.3). Furthermore, since the Vlasov equation states that the distribution function f_{h} is constant along the particle trajectories and since we have imposed that the same is true for the probability density g_{h}, this is equivalent to

$$
q_{\mathrm{e}} \sum_{k=1}^{N_{\mathrm{p}}} \left\{ v_{k,x/y}(t) \frac{1}{N_{\mathrm{p}}} \left[\frac{f_{\mathrm{h}}^0(z_k^0,\mathbf{v}_k^0)}{g_{\mathrm{h}}^0(z_k^0,\mathbf{v}_k^0)} - \frac{\mathcal{M}_0(\mathbf{v}_k(t))}{g_{\mathrm{h}}^0(z_k^0,\mathbf{v}_k^0)} \right] \varphi_i(z_k(t)) \right\}, \tag{3.77}
$$

where $\mathbf{v}_k^0$ and z_k^0 are the initial velocities and positions drawn from the initial probability density g_{h}^0. The first term in the squared bracket, which we denote by w_k^0, is a constant since it only depends on the initial configuration of the particles in phase space. In contrast to that, the second term varies in time as the velocities of the particles change. Thus, we define the particle weights by

$$
w_k(t) := \frac{1}{N_{\mathrm{p}}} \left[\frac{f_{\mathrm{h}}^0(z_k^0,\mathbf{v}_k^0)}{g_{\mathrm{h}}^0(z_k^0,\mathbf{v}_k^0)} - \frac{\mathcal{M}_0(\mathbf{v}_k(t))}{g_{\mathrm{h}}^0(z_k^0,\mathbf{v}_k^0)} \right] := w_k^0 - \frac{1}{N_{\mathrm{p}}} \frac{\mathcal{M}_0(\mathbf{v}_k(t))}{g_{\mathrm{h}}^0(z_k^0,\mathbf{v}_k^0)}. \tag{3.78}
$$

Note that this definition is independent of the particular velocity moment of the distribution function one is interested in, i.e. the same weights can be used for computations of the number density (0th moment) or the kinetic energy (2nd moment). However, one needs to take into account that the equilibrium part does not vanish in general like it was the case in (3.74).

In what follows, we shall entirely use the initial sampling distribution

$$
g_{\mathrm{h}}^0(z, v_x, v_y, v_z) = \frac{1}{L} \frac{1}{(2\pi)^{3/2} v_{\mathrm{th},\parallel} v_{\mathrm{th},\perp}^2} \exp\left(-\frac{v_z^2}{2v_{\mathrm{th},\parallel}^2} - \frac{v_x^2 + v_y^2}{2v_{\mathrm{th},\perp}^2}. \right), \tag{3.79}
$$

which means that we sample uniformly in space and normally in velocity space using standard random number generators. With this particular choice

$$
w_k^0 = \frac{n_{\mathrm{h}0}L}{N_{\mathrm{p}}}, \tag{3.80a}
$$

$$
w_k(0) = 0, \tag{3.80b}
$$

for the anisotropic Maxwellian $f_{\mathrm{h}}^0 = n_{\mathrm{h}0} \cdot (2.45)$. From this we can already see the impact of the control variate method since zero initial weights imply that we start from

a configuration with zero hot electron current and thus the source term $\mathbb{S}(t = 0) = 0$. This is exactly what is expected from the non-current carrying distribution function $f_{\mathrm{h}}^0 = n_{\mathrm{h}0} \cdot (2.45)$.

The control variate technique can easily be switched off by setting $\mathcal{M}_0(\mathbf{v}) = 0$. Then all particles have the same weights (3.80a) which do not change in time. Then, however, $\mathbb{S}(t = 0) \neq 0$ due to noise which comes from the finite Monte Carlo estimate of the original integral which is of the order $\sim 1/\sqrt{N_{\mathrm{p}}}$ [29]. We will perform simulations with and without control variate in order to check its impact on the results.

Since the Boris method (3.4) computes positions at integer time steps and velocities at interleaved time steps, we need to approximate the average of the source term appearing on the right-hand side of (3.70) in the following manner:

$$
\begin{aligned}
&- \frac{\mu_0 c^2 q_{\mathrm{e}} \Delta t}{2} \sum_{k=1}^{N_{\mathrm{p}}} \left[w_k^n v_{k,x/y}^n \varphi_i(z_k^n) + w_k^{n+1} v_{k,x/y}^{n+1} \varphi_i(z_k^{n+1}) \right] \\
&\approx - \frac{\mu_0 c^2 q_{\mathrm{e}} \Delta t}{2} \sum_{k=1}^{N_{\mathrm{p}}} w_k^{n+1/2} v_{k,x/y}^{n+1/2} \varphi_i(z_k^{n+1/2}),
\end{aligned}
\tag{3.81}
$$

where $z_k^{n+1/2} = \frac{1}{2}\left(z_k^n + z_k^{n+1}\right)$.

Now we have everything to write down the algorithm for numerically solving the model (2.11) with perpendicular perturbations only:

1. Create a periodic B-spline basis of degree p on a domain of length L discretized by N_{el} elements using (3.23)-(3.24).

2. Compute the global quadrature points and the corresponding quadrature weights using (3.26).

3. Assemble the mass matrix $\mathbb{M}$ and advection matrix $\mathbb{C}$ (3.20b) by applying formula (3.27) and assemble the block matrices $\mathbb{M}_{\mathrm{b}}$ (3.66a), $\tilde{\mathbb{C}}$ (3.66b) and $\tilde{\mathbb{M}}$ (3.67).

4. Load the initial fields $\mathbf{U}(z, t = 0)$ and perform a L^2-projection according to (3.33) in order to get the $6N$ initial coefficients $\mathbf{u}^0$.

5. Sample the initial positions $(z_k^0)_{k=1,\dots,N_{\mathrm{p}}}$ and velocities $(v_{k,x}^0, v_{k,y}^0, v_{k,z}^0)_{k=1,\dots,N_{\mathrm{p}}}$ of N_{p} particles according to the sampling distribution (3.79) by using a random number generator.

6. Compute the electric and magnetic field at the particle positions by noting that

$$
B_{x/y}(z_k(t^n), t^n) = \tilde{B}_{h,x/y}(z_k(t^n), t^n) = \sum_{j=0}^{N-1} b_{x/y,j}^n \varphi_j(z_k(t^n)),
\tag{3.82a}
$$

$$
B_z(z_k(t^n), t^n) = B_0,
\tag{3.82b}
$$

$$
E_{x/y}(z_k(t^n), t^n) = \tilde{E}_{h,x/y}(z_k(t^n), t^n) = \sum_{j=0}^{N-1} e_{x/y,j}^n \varphi_j(z_k(t^n)),
\tag{3.82c}
$$

$$
E_z(z_k(t^n), t^n) = 0, \quad \forall k \in \{1, \dots, N_{\mathrm{p}}\}.
\tag{3.82d}
$$

7. Compute the particle velocities $(v_{k,x}^{-1/2}, v_{k,y}^{-1/2}, v_{k,z}^{-1/2})_{k=1,\dots,N_{\mathrm{p}}}$ by applying the Boris algorithm (3.4) with the time step $\tilde{\Delta}t = -\Delta t/2$.

8. Compute the weights $(w_k^{-1/2})_{k=1,\dots,N_{\mathrm{p}}}$ according to (3.78) for the distribution function $f_{\mathrm{h}}^0(\mathbf{v}) = n_{\mathrm{h0}} \cdot (2.45)$ and **either** $\mathcal{M}_0(\mathbf{v}) = f_{\mathrm{h}}^0(\mathbf{v})$ (with control variate) **or** $\mathcal{M}_0(\mathbf{v}) = 0$ (without control variate) from the velocities $\mathbf{v}_k^{-1/2}$.

9. Start the time loop:

    a) Update the particle positions $(z_k^n \to z_k^{n+1})$ and velocities $(\mathbf{v}_k^{n-1/2} \to \mathbf{v}_k^{n+1/2})$ by applying the Boris algorithm (3.4) with the time step Δt.

    b) Update the weights $(w_k^{n-1/2} \to w_k^{n+1/2})$ according to (3.78).

    c) Assemble the source term $\frac{\Delta t}{2}(\mathbb{S}^n + \mathbb{S}^{n+1})$ in the scheme (3.70) according to formula (3.81)

    d) Update the finite element coefficients $(\mathbf{u}^n \to \mathbf{u}^{n+1})$ according to the scheme (3.70) with the time step Δt.

    e) Compute the new fields at the particle positions by using formulas (3.82).

    f) Go to a).

This algorithm has been implemented in Python. Results will be shown in section 4.1.

3.2.2 Geometric methods

In this section, we apply the methods introduced in section 3.1.3. In contrast to standard finite elements, this means that we look for the approximate solutions in different subspaces which are related to the continuous spaces according to the commuting diagram 3.6. Again, we assume the domain to be $\Omega = (0, L)$ and impose periodic boundary conditions on all quantities. In order to obtain a weak formulation, we multiply by (this time different) test functions $F_x, F_y, C_x, C_y, O_x, O_y$ and integrate over Ω. This yields

$$\int_0^L \frac{\partial \tilde{E}_x}{\partial t} F_x \mathrm{d}z + c^2 \int_0^L \frac{\partial \tilde{B}_y}{\partial z} F_x \mathrm{d}z + \mu_0 c^2 \int_0^L \tilde{j}_{\mathrm{c},x} F_x \mathrm{d}z = -\mu_0 c^2 \int_0^L j_{\mathrm{h},x} F_x \mathrm{d}z, \qquad (3.83\mathrm{a})$$

$$\int_0^L \frac{\partial \tilde{E}_y}{\partial t} F_y \mathrm{d}z - c^2 \int_0^L \frac{\partial \tilde{B}_x}{\partial z} F_y \mathrm{d}z + \mu_0 c^2 \int_0^L \tilde{j}_{\mathrm{c},y} F_y \mathrm{d}z = -\mu_0 c^2 \int_0^L j_{\mathrm{h},y} F_y \mathrm{d}z, \qquad (3.83\mathrm{b})$$

$$\int_0^L \frac{\partial \tilde{B}_x}{\partial t} C_x \mathrm{d}z - \int_0^L \frac{\partial \tilde{E}_y}{\partial z} C_x \mathrm{d}z = 0, \qquad (3.83\mathrm{c})$$

$$\int_0^L \frac{\partial \tilde{B}_y}{\partial t} C_y \mathrm{d}z + \int_0^L \frac{\partial \tilde{E}_x}{\partial z} C_y \mathrm{d}z = 0, \qquad (3.83\mathrm{d})$$

$$\int_0^L \frac{\partial \tilde{j}_{\mathrm{c},x}}{\partial t} O_x \mathrm{d}z - \epsilon_0 \Omega_{\mathrm{pe}}^2 \int_0^L \tilde{E}_x O_x \mathrm{d}z - \Omega_{\mathrm{ce}} \int_0^L \tilde{j}_{\mathrm{c},y} O_x \mathrm{d}z = 0, \qquad (3.83\mathrm{e})$$

$$\int_0^L \frac{\partial \tilde{j}_{\mathrm{c},y}}{\partial t} O_y \mathrm{d}z - \epsilon_0 \Omega_{\mathrm{pe}}^2 \int_0^L \tilde{E}_y O_y \mathrm{d}z + \Omega_{\mathrm{ce}} \int_0^L \tilde{j}_{\mathrm{c},x} O_y \mathrm{d}z = 0. \qquad (3.83\mathrm{f})$$

Note that this procedure is actually not necessary for the last two equations since these equations do not involve spatial derivatives and are thus ODEs in time. However, for reasons of clarity, we continue with the above formulation. We will see later that all matrices due to the spatial discretization cancel out.

If we have a closer look at the structure of the equations, we see that we should look for $\tilde{\mathbf{E}}$ and $\tilde{\mathbf{j}}_c$ in the same space since they are never connected via a spatial derivative in the same equation. The opposite is true for the magnetic field, i.e. in the first four (Maxwell's) equations $\tilde{\mathbf{B}}$ is connected with the other two quantities via a spatial derivative. This means that there are in principle two options: Either, we choose $\tilde{\mathbf{B}} \in H^1$ and $\tilde{\mathbf{E}}, \tilde{\mathbf{j}}_c \in L^2$ or vice versa. This influences where we have to integrate by parts. We follow [19] and choose the latter option. This leads to the following weak formulation: find $(\tilde{E}_x, \tilde{E}_y, \tilde{B}_x, \tilde{B}_y, \tilde{j}_{c,x}, \tilde{j}_{c,y}) \in H^1 \times H^1 \times L^2 \times L^2 \times H^1 \times H^1$ such that

$$\int_0^L \frac{\partial \tilde{E}_x}{\partial t} F_x \mathrm{d}z - c^2 \int_0^L \tilde{B}_y \frac{\partial F_x}{\partial z} \mathrm{d}z + \mu_0 c^2 \int_0^L \tilde{j}_{c,x} F_x \mathrm{d}z$$
$$= -\mu_0 c^2 \int_0^L j_{h,x} F_x \mathrm{d}z \quad \forall F_x \in H^1, \tag{3.84a}$$

$$\int_0^L \frac{\partial \tilde{E}_y}{\partial t} F_y \mathrm{d}z + c^2 \int_0^L \tilde{B}_x \frac{\partial F_y}{\partial z} \mathrm{d}z + \mu_0 c^2 \int_0^L \tilde{j}_{c,y} F_y \mathrm{d}z$$
$$= -\mu_0 c^2 \int_0^L j_{h,y} F_y \mathrm{d}z \quad \forall F_y \in H^1, \tag{3.84b}$$

$$\int_0^L \frac{\partial \tilde{B}_x}{\partial t} C_x \mathrm{d}z - \int_0^L \frac{\partial \tilde{E}_y}{\partial z} C_x \mathrm{d}z = 0 \quad \forall C_x \in L^2, \tag{3.84c}$$

$$\int_0^L \frac{\partial \tilde{B}_y}{\partial t} C_y \mathrm{d}z + \int_0^L \frac{\partial \tilde{E}_x}{\partial z} C_y \mathrm{d}z = 0 \quad \forall C_y \in L^2, \tag{3.84d}$$

$$\int_0^L \frac{\partial \tilde{j}_{c,x}}{\partial t} O_x \mathrm{d}z - \epsilon_0 \Omega_{\mathrm{pe}}^2 \int_0^L \tilde{E}_x O_x \mathrm{d}z - \Omega_{\mathrm{ce}} \int_0^L \tilde{j}_{c,y} O_x \mathrm{d}z = 0 \qquad \forall O_x \in H^1, \tag{3.84e}$$

$$\int_0^L \frac{\partial \tilde{j}_{c,y}}{\partial t} O_y \mathrm{d}z - \epsilon_0 \Omega_{\mathrm{pe}}^2 \int_0^L \tilde{E}_y O_y \mathrm{d}z + \Omega_{\mathrm{ce}} \int_0^L \tilde{j}_{c,x} O_y \mathrm{d}z = 0 \qquad \forall O_y \in H^1. \tag{3.84f}$$

Due to this particular choice, we have integrated the terms involving the magnetic field in the first two equations by parts in order to shift the derivative from $\tilde{\mathbf{B}}$ to the test functions $F_{x/y}$ (this changes the sign). This means that we will solve these equations in a weak sense whereas we will solve the other equations in a strong sense. As a next step, the spaces H^1 and L^2 are replaced by their finite-dimensional counterparts $V_0 \subset H^1$ and $V_1 \subset L^2$ with $\dim V_0 = N_0 < \infty$ and $\dim V_1 = N_1 < \infty$. In analogy to section 3.1.3, the basis functions will be denoted by $(\varphi_i^0)_{i=0,\ldots,N_0-1}$ and $(\varphi_{i+1/2}^1)_{i=0,\ldots,N_1-1}$, where $N_0 = N_1$ in our case due to periodic boundary conditions. The discrete version then reads: find

$(\tilde{E}_{h,x}, \tilde{E}_{h,y}, \tilde{B}_{h,x}, \tilde{B}_{h,y}, \tilde{j}_{c,x}^h, \tilde{j}_{c,y}^h) \in V_0 \times V_0 \times V_1 \times V_1 \times V_0 \times V_0$ such that

$$\int_0^L \frac{\partial \tilde{E}_{h,x}}{\partial t} F_{h,x}\mathrm{d}z - c^2 \int_0^L \tilde{B}_{h,y}\frac{\partial F_{h,x}}{\partial z}\mathrm{d}z + \mu_0 c^2 \int_0^L \tilde{j}_{c,x}^h F_{h,x}\mathrm{d}z$$

$$= -\mu_0 c^2 \int_0^L j_{h,x} F_{h,x}\mathrm{d}z \quad \forall F_{h,x} \in V_0, \tag{3.85a}$$

$$\int_0^L \frac{\partial \tilde{E}_{h,y}}{\partial t} F_{h,y}\mathrm{d}z + c^2 \int_0^L \tilde{B}_{h,x}\frac{\partial F_{h,y}}{\partial z}\mathrm{d}z + \mu_0 c^2 \int_0^L \tilde{j}_{c,y}^h F_{h,y}\mathrm{d}z$$

$$= -\mu_0 c^2 \int_0^L j_{h,y} F_{h,y}\mathrm{d}z \quad \forall F_{h,y} \in V_0, \tag{3.85b}$$

$$\int_0^L \frac{\partial \tilde{B}_{h,x}}{\partial t} C_{h,x}\mathrm{d}z - \int_0^L \frac{\partial \tilde{E}_{h,y}}{\partial z} C_{h,x}\mathrm{d}z = 0 \quad \forall C_{h,x} \in V_1, \tag{3.85c}$$

$$\int_0^L \frac{\partial \tilde{B}_{h,y}}{\partial t} C_{h,y}\mathrm{d}z + \int_0^L \frac{\partial \tilde{E}_{h,x}}{\partial z} C_{h,y}\mathrm{d}z = 0 \quad \forall C_{h,y} \in V_1, \tag{3.85d}$$

$$\int_0^L \frac{\partial \tilde{j}_{c,x}^h}{\partial t} O_{h,x}\mathrm{d}z - \epsilon_0 \Omega_{\mathrm{pe}}^2 \int_0^L \tilde{E}_{h,x}O_{h,x}\mathrm{d}z - \Omega_{\mathrm{ce}} \int_0^L \tilde{j}_{c,y}^h O_{h,x}\mathrm{d}z = 0 \quad \forall O_{h,x} \in V_0, \tag{3.85e}$$

$$\int_0^L \frac{\partial \tilde{j}_{c,y}^h}{\partial t} O_{h,y}\mathrm{d}z - \epsilon_0 \Omega_{\mathrm{pe}}^2 \int_0^L \tilde{E}_{h,y}O_{h,y}\mathrm{d}z + \Omega_{\mathrm{ce}} \int_0^L \tilde{j}_{c,x}^h O_{h,y}\mathrm{d}z = 0 \quad \forall O_{h,y} \in V_0. \tag{3.85f}$$

As a next step, we derive the matrix formulation by expanding all quantities in their respective spaces. To keep things simple, we use a uniform mesh, i.e. the same element size $c_{k+1} - c_k = h \; \forall k \in \{0, \dots, N_{\mathrm{el}} - 1\}$. Since $\tilde{E}_{h,x/y}, \tilde{j}_{c,x/y}^h \in V_0$ and the magnetic field $\tilde{B}_{h,x/y} \in V_1$, we can write

$$\tilde{E}_{h,x/y}(z,t) = \sum_{j=0}^{N_0-1} e_{x/y,j}(t)\varphi_j^0(z), \tag{3.86a}$$

$$\tilde{j}_{c,x/y}^h(z,t) = \sum_{j=0}^{N_0-1} y_{x/y,j}(t)\varphi_j^0(z), \tag{3.86b}$$

$$\tilde{B}_{h,x/y}(t,z) = \sum_{j=0}^{N_1-1} b_{x/y,j+1/2}(t)\varphi_{j+1/2}^1(z), \tag{3.86c}$$

and plug this in the above weak formulation. The same is done for the test functions $F_{h,x/y}, O_{h,x/y} \in V_0$ and $C_{h,x/y} \in V_1$.

Let us start with the weak formulation of the x-component of Faraday's law (3.85c): Following the methods introduced in section 3.1.3, we use the fact that the appearing spatial derivative of the y-component of the electric field lives in the space V_1 and can thus be written as

$$\frac{\partial \tilde{E}_{h,y}}{\partial z}(z,t) = \frac{2}{h} \sum_{j=0}^{N_1-1} [e_{y,j+1}(t) - e_{y,j}(t)]\varphi_{j+1/2}^1(z). \tag{3.87}$$

This results in

$$
\sum_{i,j=0}^{N_1-1} \frac{\mathrm{d}b_{x,j+1/2}}{\mathrm{d}t} c_{x,i+1/2} \underbrace{\int_0^L \varphi_{i+1/2}^1 \varphi_{j+1/2}^1 \mathrm{d}z}_{=M_{ij}^1}
$$
$$
- \frac{2}{h} \sum_{i,j=0}^{N_1-1} [e_{y,j+1} - e_{y,j}] c_{x,i+1/2} \underbrace{\int_0^L \varphi_{i+1/2}^1 \varphi_{j+1/2}^1 \mathrm{d}z}_{=M_{ij}^1} = 0.
\tag{3.88}
$$

Introducing coefficient vectors $\mathbf{e}_y = (e_{y,0}, \ldots, e_{y,N_0-1})^\top$, $\mathbf{b}_x = (b_{x,0}, \ldots, b_{x,N_1-1})^\top$ and $\mathbf{c}_x = (c_{x,0}, \ldots, c_{x,N_1-1})^\top$ as well as using the mass matrix $\mathbb{M}^1$ and the discrete gradient matrix $\mathbb{G}$ defined by (3.55) yields the matrix formulation

$$
\mathbf{c}_x^\top \mathbb{M}^1 \frac{\mathrm{d}\mathbf{b}_x}{\mathrm{d}t} - \mathbf{c}_x^\top \mathbb{M}^1 \mathbb{G} \mathbf{e}_y = 0 \tag{3.89a}
$$
$$
\Leftrightarrow \quad \frac{\mathrm{d}\mathbf{b}_x}{\mathrm{d}t} = \mathbb{G}\mathbf{e}_y, \tag{3.89b}
$$

since this must be true for arbitrary $\mathbf{c}_x$. The same calculation for the y-component leads to

$$
\frac{\mathrm{d}\mathbf{b}_y}{\mathrm{d}t} = -\mathbb{G}\mathbf{e}_x. \tag{3.90}
$$

As a next step, we consider the x-component of Ampéres law (3.85a), where the spatial derivative in the second terms acts this time on the test function $F_{h,x}$ since we have integrated by parts. Hence we get

$$
\sum_{i,j=0}^{N_0-1} \frac{\mathrm{d}e_{x,j}}{\mathrm{d}t} f_{x,i} \underbrace{\int_0^L \varphi_i^0 \varphi_j^0 \mathrm{d}z}_{=M_{ij}^0} - c^2 \frac{2}{h} \sum_{i,j=0}^{N_1-1} b_{y,j+1/2}[f_{x,i+1} - f_{x,i}] \underbrace{\int_0^L \varphi_{i+1/2}^1 \varphi_{j+1/2}^1 \mathrm{d}z}_{=M_{ij}^1}
$$
$$
+ \mu_0 c^2 \sum_{i,j=0}^{N_0-1} y_{x,j} f_{x,i} \underbrace{\int_0^L \varphi_i^0 \varphi_j^0 \mathrm{d}z}_{=M_{ij}^0} = -\mu_0 c^2 \sum_{i=0}^{N_0-1} f_{x,i} \int_0^L j_{\mathrm{h},x} \varphi_i^0 \mathrm{d}z.
\tag{3.91}
$$

The integral on the right-hand side over the current density of the hot electrons is the coupling to the particle-in-cell part of the algorithm and will be treated in the exact same way as for the standard finite elements algorithm (see (3.73)-(3.80)). Thus, we introduce the vector

$$
\bar{j}_{\mathrm{h},x,i} := \int_0^L j_{\mathrm{h},x} \varphi_i^0 \mathrm{d}z \quad \Rightarrow \quad \bar{\mathbf{j}}_{\mathrm{h},x} = (\bar{j}_{\mathrm{h},x,0}, \ldots, \bar{j}_{\mathrm{h},x,N_0-1})^\top, \tag{3.92}
$$

which leads to the matrix formulation

$$\mathbf{f}_x^\top \mathbb{M}^0 \frac{\mathrm{d}\mathbf{e}_x}{\mathrm{d}t} - c^2 (\mathbb{G}\mathbf{f}_x)^\top \mathbb{M}^1 \mathbf{b}_y + \mu_0 c^2 \mathbf{f}_x^\top \mathbb{M}^0 \mathbf{y}_x = -\mu_0 c^2 \mathbf{f}_x^\top \tilde{\mathbf{j}}_{\mathrm{h},x} \tag{3.93a}$$

$$\Leftrightarrow \quad \mathbb{M}^0 \frac{\mathrm{d}\mathbf{e}_x}{\mathrm{d}t} - c^2 \mathbb{G}^\top \mathbb{M}^1 \mathbf{b}_y + \mu_0 c^2 \mathbb{M}^0 \mathbf{y}_x = -\mu_0 c^2 \tilde{\mathbf{j}}_{\mathrm{h},x}. \tag{3.93b}$$

In order to evaluate the vector $\bar{\mathbf{j}}_{\mathrm{h},x}$ (same for the y-component) in terms of matrix-vector multiplications of the particle positions $\mathbf{Z} = (z_1, \ldots, z_{N_\mathrm{p}})^\top$ and velocities $\mathbf{V}_{x/y/z} = (v_{1,x/y/z}, \ldots, v_{N_\mathrm{p},x/y/z})^\top$, we define the following matrices:

$$\mathbb{Q}^0(\mathbf{Z}) := (\varphi_i^0(z_k))_{i=0,\ldots,N_0-1,\, k=1,\ldots,N_\mathrm{p}} \qquad \in \mathbb{R}^{N_0 \times N_\mathrm{p}}, \tag{3.94}$$

$$\mathbb{W}(\mathbf{V}) := \mathrm{diag}(w_0, \ldots, w_{N_\mathrm{p}}) \qquad \in \mathbb{R}^{N_\mathrm{p} \times N_\mathrm{p}}. \tag{3.95}$$

Again, if we do not use a control variate, i.e. $\mathcal{M}_0(\mathbf{v}) = 0$, the diagonal matrix $\mathbb{W}$ **does not change in time**. The missing subscript in the velocity dependency of $\mathbb{W}$ is supposed to indicate that it depends on all three velocity components. With these matrices we obtain

$$\bar{\mathbf{j}}_{\mathrm{h},x} = q_\mathrm{e} \mathbb{Q}^0(\mathbf{Z}) \mathbb{W}(\mathbf{V}) \mathbf{V}_x, \tag{3.96a}$$

$$\bar{\mathbf{j}}_{\mathrm{h},y} = q_\mathrm{e} \mathbb{Q}^0(\mathbf{Z}) \mathbb{W}(\mathbf{V}) \mathbf{V}_y. \tag{3.96b}$$

This finally yields the semi-discrete equation

$$\mathbb{M}^0 \frac{\mathrm{d}\mathbf{e}_x}{\mathrm{d}t} - c^2 \mathbb{G}^\top \mathbb{M}^1 \mathbf{b}_y + \mu_0 c^2 \mathbb{M}^0 \mathbf{y}_x = -\mu_0 c^2 q_\mathrm{e} \mathbb{Q}^0 \mathbb{W} \mathbf{V}_x. \tag{3.97}$$

for the x-component of Ampere's law (3.85a) and the the same procedure for the y-component leads to

$$\mathbb{M}^0 \frac{\mathrm{d}\mathbf{e}_y}{\mathrm{d}t} + c^2 \mathbb{G}^\top \mathbb{M}^1 \mathbf{b}_x + \mu_0 c^2 \mathbb{M}^0 \mathbf{y}_y = -\mu_0 c^2 q_\mathrm{e} \mathbb{Q}^0 \mathbb{W} \mathbf{V}_y. \tag{3.98}$$

What remains are the two momentum balance equations for the cold current density. Since here only functions within the same space appear, the equations (3.85e)-(3.85f) immediately transfer to

$$\frac{\mathrm{d}\mathbf{y}_x}{\mathrm{d}t} - \epsilon_0 \Omega_{\mathrm{pe}}^2 \mathbf{e}_x - \Omega_{\mathrm{ce}} \mathbf{y}_y = 0, \tag{3.99a}$$

$$\frac{\mathrm{d}\mathbf{y}_y}{\mathrm{d}t} - \epsilon_0 \Omega_{\mathrm{pe}}^2 \mathbf{e}_y + \Omega_{\mathrm{ce}} \mathbf{y}_x = 0. \tag{3.99b}$$

Writing the equations of motion (3.3) for the particles in a compact matrix form (not shown), we finally end up with the following semi-discrete system for the ten variables

$\mathbf{u} = (\mathbf{e}_x, \mathbf{e}_y, \mathbf{b}_x, \mathbf{b}_y, \mathbf{y}_x, \mathbf{y}_y, \mathbf{Z}, \mathbf{V}_x, \mathbf{V}_y, \mathbf{V}_z)^\top \in \mathbb{R}^{4N_0 + 2N_1 + 4N_P}$:

$$\frac{d\mathbf{e}_x}{dt} = c^2 (\mathbb{M}^0)^{-1} \mathbb{G}^\top \mathbb{M}^1 \mathbf{b}_y - \mu_0 c^2 \mathbf{y}_x - \mu_0 c^2 q_e (\mathbb{M}^0)^{-1} \mathbb{Q}^0 \mathbb{W} \mathbf{V}_x, \qquad (3.100a)$$

$$\frac{d\mathbf{e}_y}{dt} = -c^2 (\mathbb{M}^0)^{-1} \mathbb{G}^\top \mathbb{M}^1 \mathbf{b}_x - \mu_0 c^2 \mathbf{y}_y - \mu_0 c^2 q_e (\mathbb{M}^0)^{-1} \mathbb{Q}^0 \mathbb{W} \mathbf{V}_y, \qquad (3.100b)$$

$$\frac{d\mathbf{b}_x}{dt} = \mathbb{G} \mathbf{e}_y, \qquad (3.100c)$$

$$\frac{d\mathbf{b}_y}{dt} = -\mathbb{G} \mathbf{e}_x, \qquad (3.100d)$$

$$\frac{d\mathbf{y}_x}{dt} = \epsilon_0 \Omega_{pe}^2 \mathbf{e}_x + \Omega_{ce} \mathbf{y}_y, \qquad (3.100e)$$

$$\frac{d\mathbf{y}_y}{dt} = \epsilon_0 \Omega_{pe}^2 \mathbf{e}_y - \Omega_{ce} \mathbf{y}_x, \qquad (3.100f)$$

$$\frac{d\mathbf{Z}}{dt} = \mathbf{V}_z, \qquad (3.100g)$$

$$\frac{d\mathbf{V}_x}{dt} = \frac{q_e}{m_e} [(\mathbb{Q}^0)^\top \mathbf{e}_x - \mathbb{B}_y \mathbf{V}_z + B_0 \mathbf{V}_y], \qquad (3.100h)$$

$$\frac{d\mathbf{V}_y}{dt} = \frac{q_e}{m_e} [(\mathbb{Q}^0)^\top \mathbf{e}_y + \mathbb{B}_x \mathbf{V}_z - B_0 \mathbf{V}_x], \qquad (3.100i)$$

$$\frac{d\mathbf{V}_z}{dt} = \frac{q_e}{m_e} [\mathbb{B}_y \mathbf{V}_x - \mathbb{B}_x \mathbf{V}_y], , \qquad (3.100j)$$

where we have introduced the matrices $\mathbb{Q}^1 = \mathbb{Q}^1(\mathbf{Z})$ and $\mathbb{B}_{x/y} = \mathbb{B}_{x/y}(\mathbf{Z}, \mathbf{b}_{x/y})$ defined by

$$\mathbb{Q}^1(\mathbf{Z}) := (\varphi_i^0(z_k))_{i=0,\dots,N_0-1,\, k=1,\dots,N_P} \qquad \in \mathbb{R}^{N_0 \times N_P}, \qquad (3.101)$$

$$\mathbb{B}_{x/y}(\mathbf{Z}, \mathbf{b}_{x/y}) = \mathrm{diag}[(\mathbb{Q}^1)^\top (\mathbf{Z}) \mathbf{b}_{x/y}] \qquad \in \mathbb{R}^{N_P \times N_P}, \qquad (3.102)$$

which arise naturally after writing the equations of motion for the particles in matrix-vector form and noting that the discrete electric and magnetic field can be expanded in their respective bases (like it was done in (3.82)).

For the further analysis of the above semi-discrete system, let us compute the total energy of the system (see 2.12). This energy we call the system's Hamiltonian $H : \mathbb{R}^n \mapsto \mathbb{R}$, where $n = 4N_0 + 2N_1 + 4N_P$:

$$
\begin{aligned}
H :&= \frac{1}{2} \left[\epsilon_0 \int_0^L \mathbf{E}_h^2 dz + \frac{1}{\mu_0} \int_0^L \mathbf{B}_h^2 dz + \frac{1}{\epsilon_0 \Omega_{pe}^2} \int_0^L (\mathbf{j}_c^h)^2 dz + m_e \int_0^L \int f_h v^2 \, d^3\mathbf{v} dz \right] \\
&= \frac{\epsilon_0}{2} (\mathbf{e}_x^\top \mathbb{M}^0 \mathbf{e}_x + \mathbf{e}_y^\top \mathbb{M}^0 \mathbf{e}_y) + \frac{1}{2\mu_0} (\mathbf{b}_x^\top \mathbb{M}^1 \mathbf{b}_x + \mathbf{b}_y^\top \mathbb{M}^1 \mathbf{b}_y) \\
&\quad + \frac{1}{2\epsilon_0 \Omega_{pe}^2} (\mathbf{y}_x^\top \mathbb{M}^0 \mathbf{y}_x + \mathbf{y}_y^\top \mathbb{M}^0 \mathbf{y}_y) + \frac{m_e}{2} \mathbf{V}_x^\top \mathbb{W} \mathbf{V}_x + \frac{m_e}{2} \mathbf{V}_y^\top \mathbb{W} \mathbf{V}_y + \frac{m_e}{2} \mathbf{V}_z^\top \mathbb{W} \mathbf{V}_z \\
&:= H_E + H_B + H_Y + H_x + H_y + H_z.
\end{aligned}
\qquad (3.103)
$$

With this discrete Hamiltonian, the system (3.100) can be written in a non-canonical Hamiltonian structure for the combined variables $\mathbf{u} = \mathbf{u}(t)$, if we suppose a constant

weight matrix $\mathbb{W}(\mathbf{V}(t)) = \mathbb{W}$, i.e. **no control variate**:

$$\frac{\mathrm{d}\mathbf{u}}{\mathrm{d}t} = \mathbb{J}(\mathbf{u})\nabla_{\mathbf{u}}H(\mathbf{u}). \tag{3.104}$$

Here

$$\frac{\mathrm{d}\mathbf{u}}{\mathrm{d}t} = \frac{\mathrm{d}}{\mathrm{d}t}\begin{pmatrix} \mathbf{e}_x \\ \mathbf{e}_y \\ \mathbf{b}_x \\ \mathbf{b}_y \\ \mathbf{y}_x \\ \mathbf{y}_y \\ \mathbf{Z} \\ \mathbf{V}_x \\ \mathbf{V}_y \\ \mathbf{V}_z \end{pmatrix}, \quad \nabla_{\mathbf{u}}H = \begin{pmatrix} \epsilon_0\mathbb{M}^0\mathbf{e}_x \\ \epsilon_0\mathbb{M}^0\mathbf{e}_y \\ 1/\mu_0\mathbb{M}^1\mathbf{b}_x \\ 1/\mu_0\mathbb{M}^1\mathbf{b}_y \\ 1/(\epsilon_0\Omega_{\mathrm{pe}}^2)\mathbb{M}^0\mathbf{y}_x \\ 1/(\epsilon_0\Omega_{\mathrm{pe}}^2)\mathbb{M}^0\mathbf{y}_y \\ 0 \\ \mathbb{W}\mathbf{V}_x \\ \mathbb{W}\mathbf{V}_y \\ \mathbb{W}\mathbf{V}_z \end{pmatrix} \tag{3.105}$$

and $\mathbb{J}(\mathbf{u}) \overset{3}{=}$

$$\mathbb{J}(\mathbf{u}) = \begin{pmatrix}
 & & & -\tfrac{1}{\epsilon_0}\mathbb{G}\mathbb{M}_0^{-1} & \Omega_{pe}^2\mathbb{M}_0^{-1} & & \tfrac{q_e}{\epsilon_0 m_e}\mathbb{Q}_0^\top\mathbb{M}_0^{-1} & \\[4pt]
 & & \tfrac{1}{\epsilon_0}\mathbb{G}\mathbb{M}_0^{-1} & & & \Omega_{pe}^2\mathbb{M}_0^{-1} & & \tfrac{q_e}{\epsilon_0 m_e}\mathbb{Q}_0^\top\mathbb{M}_0^{-1} \\[4pt]
 & -\tfrac{1}{\epsilon_0}\mathbb{M}_0^{-1}\mathbb{G}^\top & & -\epsilon_0\Omega_{pe}^2\Omega_{ce}\mathbb{M}_0^{-1} & & & & \\[4pt]
 \tfrac{1}{\epsilon_0}\mathbb{M}_0^{-1}\mathbb{G}^\top & & \epsilon_0\Omega_{pe}^2\Omega_{ce}\mathbb{M}_0^{-1} & & & & & \\[4pt]
 -\Omega_{pe}^2\mathbb{M}_0^{-1} & & & & & \Omega_{ce}\mathbb{W}^{-1} & & -\tfrac{q_e}{m_e}\mathbb{B}_y\mathbb{W}^{-1} \\[4pt]
 & -\Omega_{pe}^2\mathbb{M}_0^{-1} & & & -\Omega_{ce}\mathbb{W}^{-1} & & \tfrac{q_e}{m_e}\mathbb{B}_x\mathbb{W}^{-1} & \\[4pt]
 -\tfrac{q_e}{\epsilon_0 m_e}\mathbb{M}_0^{-1}\mathbb{Q}_0 & & & & & -\tfrac{q_e}{m_e}\mathbb{B}_x\mathbb{W}^{-1} & & \mathbb{W}^{-1} \\[4pt]
 & -\tfrac{q_e}{\epsilon_0 m_e}\mathbb{M}_0^{-1}\mathbb{Q}_0 & & & \tfrac{q_e}{m_e}\mathbb{B}_y\mathbb{W}^{-1} & & -\mathbb{W}^{-1} &
\end{pmatrix}$$

(3.106)

---

[3] Here, we write $\mathbb{M}_0$, $\mathbb{M}_1$ and $\mathbb{Q}_0$ instead of $\mathbb{M}^0$, $\mathbb{M}^1$ and $\mathbb{Q}^0$.

The dynamical system (3.104) is called *non-canonical* since the matrix $\mathbb{J} = \mathbb{J}(\mathbf{u})$ depends on $\mathbf{u}$. Furthermore, in order to be a Hamiltonian system, the matrix $\mathbb{J}$ needs to define a Poisson bracket which is well-known from classical Lagrangian and Hamiltonian mechanics [3].

An operation $\{\cdot, \cdot\}$ on functionals $F, G, K : \mathbb{R}^n \to \mathbb{R}$ is called a Poisson bracket if the following holds:

1. Bilinearity
   $\{aF + bG, K\} = a\{F, K\} + b\{G, K\}, \quad a, b \in \mathbb{R}$

2. Anti-commutativity
   $\{F, G\} = -\{G, F\} \Rightarrow \{F, F\} = 0$

3. Leibniz's rule
   $\{FG, K\} = F\{G, K\} + G\{F, K\}$

4. Jacobi identity
   $\{F, \{G, K\}\} + \{G, \{K, F\}\} + \{K, \{F, G\}\} = 0$

If we define the Poisson bracket of the system (3.104) for two functionals $F, G : \mathbb{R}^n \to \mathbb{R}$, $\mathbf{u} \mapsto F, G(\mathbf{u})$ of the dynamical variables $\mathbf{u}$ by

$$\{F, G\} := \nabla_\mathbf{u} F^\top \mathbb{J}(\mathbf{u}) \nabla_\mathbf{u} G, \tag{3.107}$$

(see [3, 19]) we immediately see that conditions 1 and 3 are satisfied since the nabla operator is a linear operator satisfying the standard product rule of calculus. The matrix $\mathbb{J}$ is then called the Poisson matrix of the system. However, the other two conditions are not obvious and depend on the particular structure of the Poisson matrix $\mathbb{J}$. With the definition 3.107, the anti-commutativity condition 2 imposes skew-symmetry on $\mathbb{J}$, i.e. $\mathbb{J}^\top = -\mathbb{J}$. Indeed, under the assumption that $\mathbb{J}$ is skew symmetric, we have

$$\begin{aligned}
\{F, G\} = \nabla_\mathbf{u} F^\top \mathbb{J}(\mathbf{u}) \nabla_\mathbf{u} G &= \nabla_\mathbf{u} G^\top (\nabla_\mathbf{u} F^\top \mathbb{J}(\mathbf{u}))^\top \\
&= -\nabla_\mathbf{u} G^\top \mathbb{J}(\mathbf{u}) \nabla_\mathbf{u} F = -\{G, F\}.
\end{aligned} \tag{3.108}$$

By having a closer look at the compact block matrix form (3.106) we see that this is true in our the case since the mass matrices $\mathbb{M}^0$ and $\mathbb{M}^1$ are symmetric and the weight matrix $\mathbb{W}$ and the matrices $\mathbb{B}_{x/y}$ are diagonal. This is already enough for exact conservation of the Hamiltonian which can be seen by noting that the time evolution of an arbitrary functional F is given by

$$\frac{\mathrm{d}}{\mathrm{d}t} F(\mathbf{u}(t)) = \nabla_\mathbf{u} F^\top \frac{\mathrm{d}\mathbf{u}}{\mathrm{d}t} = \nabla_\mathbf{u} F^\top \mathbb{J}(\mathbf{u}) \nabla_\mathbf{u} H = \{F, H\}, \tag{3.109}$$

and taking $F = H$ yields

$$\frac{\mathrm{d}}{\mathrm{d}t} H(\mathbf{u}(t)) = \{H, H\} = -\{H, H\} = 0. \tag{3.110}$$

This means that the particular choice of finite element spaces satisfying the commuting diagram 3.6 leads to the preservation of the energy theorem on the continuous level shown in section 2.1.3 even on the semi-discrete level.

What would remain is to proof the Jacobi identity 4. However, we skip this and just assume that this condition is satisfied by our Poisson matrix (see [19] how this is done for the Vlasov-Maxwell system). It is important to note though that the Jacobi identity enables the construction of new conserved quantities from two other ones, i.e. if F and G are conserved, $\{F, G\}$ is conserved as well which can easily be seen by computing $\{\{F, G\}, H\}$ and using the Jacobi identity 4.

Time discretization   Since it is not obvious if the ODE system (3.104) can be solved analytically, we have to perform another discretization in time. Common methods for Hamiltonian systems are so-called splitting methods which consist of splitting the right-hand side of the ODE system into a sum of simpler problems which can then ideally be solved analytically [4]. In the case of a Hamiltonian system of the form (3.104), this means that one can either split the Poisson matrix $\mathbb{J}$ or the Hamiltonian H. The former leads to exact conservation of the Hamiltonian if one performs the splitting such that each sub-matrix is still skew-symmetric (see (3.110)) and the sub-systems are solved with a discrete gradient method (not shown). The latter, which consist of keeping the full Poisson matrix and thus also the Poisson bracket, leads to the preservation of the so-called Casimirs C of a Hamiltonian system. These are conserved quantities that Poisson-commute with every other one including the Hamiltonian H, i.e. $\{C, F\} = 0 \ \forall F$.

In practice, the latter option should be preferred as ensuring exact conservation of the Casimirs (for instance Gauss's law 2.3i of the divergence constraint for the magnetic field (2.3j), see [19] for full 6D Vlasov-Maxwell) is important to obtain stable algorithms [2]. Furthermore, it is also important to note that splitting the Hamiltonian and keeping the full Poisson structure yields so-called Poisson time integrators (if the sub-systems can be solved analytically) which still have good properties regarding the conservation of the Hamiltonian.

This means that we apply the Hamiltonian splitting and split the Hamiltonian in

$$H = H_E + H_B + H_Y + H_x + H_y + H_z, \tag{3.111}$$

and keep the full Poisson matrix (3.106). This leads to the six sub-problems listed in the Appendix 6 for advancing $\mathbf{u}$ by a time step Δt. Indeed, we find that each of the sub-steps can be integrated analytically, however, the two integrals in the sixth integrator over the basis functions of the space V_1 involve some additional work, especially from a programming point of view. In summary, we obtain a set of six integrators denoted by $\Phi_{\Delta t}^E$, $\Phi_{\Delta t}^B$, $\Phi_{\Delta t}^Y$, $\Phi_{\Delta t}^x$, $\Phi_{\Delta t}^y$ and $\Phi_{\Delta t}^z$, which can be applied successively in a specific order.

The easiest composition is the Lie-Trotter splitting [30] which consist of simply applying each integrator one after the other:

$$\Phi_{\Delta t}^L := \Phi_{\Delta t}^z \circ \Phi_{\Delta t}^y \circ \Phi_{\Delta t}^x \circ \Phi_{\Delta t}^Y \circ \Phi_{\Delta t}^B \circ \Phi_{\Delta t}^E. \tag{3.112}$$

Here, it is important to note that the input to each integrator must be the output of the previous integrator, i.e. this means that if the magnetic field changes, for instance, the

matrices $\mathbb{B}_{x/y} = \mathbb{B}_{x/y}(\mathbf{Z}, \mathbf{b}_{x/y})$ need to be updated. However, this splitting is not time reversible meaning that the same integrator applied to the final state by a time step $-\Delta t$ does not yield the original state. This can be achieved with the second order symmetric Strang splitting [31]

$$
\begin{aligned}
\Phi_{\Delta t}^S := {} & \Phi_{\Delta t/2}^z \circ \Phi_{\Delta t/2}^y \circ \Phi_{\Delta t/2}^x \circ \Phi_{\Delta t/2}^Y \circ \Phi_{\Delta t/2}^B \circ \Phi_{\Delta t/2}^E \\
& \circ \Phi_{\Delta t/2}^E \circ \Phi_{\Delta t/2}^B \circ \Phi_{\Delta t/2}^Y \circ \Phi_{\Delta t/2}^x \circ \Phi_{\Delta t/2}^y \circ \Phi_{\Delta t/2}^z.
\end{aligned}
\tag{3.113}
$$

We shall only use these two splitting schemes, but note that higher-oder splitting schemes exist [4].

Like it was done in the previous section, we want to summarize the algorithm to numerically solve the hybrid model with perpendicular perturbations only:

1. Create a periodic basis of Lagrange polynomials $(\varphi_i^0(z))_{i=0,\ldots,N_0-1}$ of degree p on a domain L discretized by N_{el} elements using the definition of the shape functions (3.37) on the reference interval $I = [-1, 1]$ and the formulas (3.35) for transformations on the physical domain. This results in $N_0 = pN_{\mathrm{el}}$.

2. Create the corresponding basis of Lagrange histopolation polynomials $(\varphi_{i+1/2}^1(z))_{i=0,\ldots,N_1-1}$ of degree $p-1$ using the definition of the shape functions (3.41) on the reference interval $I = [-1, 1]$ and the formulas (3.35) for transformations on the physical domain. This results in $N_1 = pN_{\mathrm{el}}$.

3. Compute the global quadrature points and the corresponding quadrature weights using (3.26).

4. Assemble the global mass matrices $\mathbb{M}^0$ and $\mathbb{M}^1$ by applying formula (3.27).

5. Load the initial fields $E_x(z, t = 0)$, $E_y(z, t = 0)$, $B_x(z, t = 0)$, $B_y(z, t = 0)$, $j_{\mathrm{c},x}(z, t = 0)$, $j_{\mathrm{c},y}(z, t = 0)$ and use the projectors Π_0 (3.38)-(3.39) and Π_1 (3.42)-(3.43) in order to get the initial finite element coefficients $\mathbf{e}_x^0$, $\mathbf{e}_y^0$, $\mathbf{b}_x^0$, $\mathbf{b}_y^0$, $\mathbf{y}_x^0$, $\mathbf{y}_y^0$.

6. Sample the initial positions $(z_k^0)_{k=1,\ldots,N_{\mathrm{p}}}$ and velocities $(v_{k,x}^0, v_{k,y}^0, v_{k,z}^0)_{k=1,\ldots,N_{\mathrm{p}}}$ of N_{p} particles according to the sampling distribution (3.79) by using a random number generator in order to get the initial vectors $\mathbf{Z}^0$, $\mathbf{V}_x^0$, $\mathbf{V}_y^0$ and $\mathbf{V}_z^0$.

7. Assemble the matrices $\mathbb{G}$ (3.55), $\mathbb{Q}^0(\mathbf{Z}^0)$ (3.94), $\mathbb{Q}^1(\mathbf{Z}^0)$ (3.101), $\mathbb{B}_x(\mathbf{Z}^0, \mathbf{b}_x^0)$ (3.102) and $\mathbb{B}_y(\mathbf{Z}^0, \mathbf{b}_y^0)$ (3.102).

8. Assemble the weight matrix $\mathbb{W}(\mathbf{V}^0)$ (3.95) with weights according to (3.78) for the distribution function $f_{\mathrm{h}}^0(\mathbf{v}) = n_{\mathrm{h}0} \cdot$ (2.45) and **either** $\mathcal{M}_0(\mathbf{v}) = f_{\mathrm{h}}^0(\mathbf{v})$ (with control variate) **or** $\mathcal{M}_0(\mathbf{v}) = 0$ (without control variate) from the velocities $\mathbf{V}_x^0$, $\mathbf{V}_y^0$ and $\mathbf{V}_z^0$.

9. Start the time loop:

a) Apply one of the time integrators (3.112) (Lie-Trotter) or (3.113) (Strang) for a time step Δt in order to update $\mathbf{e}_x^n$, $\mathbf{e}_y^n$, $\mathbf{b}_x^n$, $\mathbf{b}_y^n$, $\mathbf{y}_x^n$, $\mathbf{y}_y^n$, $\mathbf{Z}^n$, $\mathbf{V}_x^n$, $\mathbf{V}_y^n$, $\mathbf{V}_z^n$ $\rightarrow \mathbf{e}_x^{n+1}$, $\mathbf{e}_y^{n+1}$, $\mathbf{b}_x^{n+1}$, $\mathbf{b}_y^{n+1}$, $\mathbf{y}_x^{n+1}$, $\mathbf{y}_y^{n+1}$, $\mathbf{Z}^{n+1}$, $\mathbf{V}_x^{n+1}$, $\mathbf{V}_y^{n+1}$, $\mathbf{V}_z^{n+1}$. The single integrators are listed in the Appendix 6.

b) Go to a)

Like the algorithm introduced in the previous section, this algorithm has been implemented in Python and results will be shown in the next section.

4   Numerical results and discussions

In this section, we present a collection of results obtained with the two developed algorithms explained in sections 3.2.1 and 3.2.2. First, physics results and verification tests for the standard FEM code are presented, followed by results obtained with the geometric methods with a special focus on long-term energy conservation.

4.1   Standard finite elements

As a first test run, we initialize the code as follows: We choose an anisotropic Maxwellian for the fast electrons with parameters given in the caption of fig. 4.1 and perturb the x-component of the magnetic field by

$$\tilde{B}_x(z, t = 0) = a \sin(kz), \tag{4.1}$$

in order to seed the instability for one particular k-mode. The amplitude $a = 1 \cdot 10^{-4} \, B_0$ is chosen with respect to the background field B_0 such that it is small enough to start in the linear phase, but large enough to reach the nonlinear phase within a reasonable simulation time. All other field quantities are initially zero, i.e. there is no electric field and cold plasma current at $t = 0$. Other simulation parameters are listed in the figure caption. With the chosen wavenumber of $k = 2 \, |\Omega_{\mathrm{ce}}|/c$, the numerical solution of the dispersion relation (2.46) yields an expected growth rate of $\gamma \approx 0.0447 |\Omega_{\mathrm{ce}}|$ and a real frequency of $\omega_{\mathrm{r}} \approx 0.4742 |\Omega_{\mathrm{ce}}|$. In fig. 4.1 we plot the resulting time evolution of all the energies involved in the system normalized to the initial total energy (which is (3.103), however, with the same mass matrix $\mathbb{M}$ for $\mathbf{e}$, $\mathbf{b}$ and $\mathbf{j}_{\mathrm{c}}$ since we are using standard B-spline finite elements). $\mathcal{E}_{\tilde{B}}$ denotes the magnetic field energy, $\mathcal{E}_{\tilde{E}}$ the electric field energy, $\mathcal{E}_{\mathrm{c}}$ the kinetic energy of the cold plasma and $\mathcal{E}_{\mathrm{h}}$ the kinetic energy of the fast electrons. With our choice of parameters, most of the energy in the system is carried by the fast electrons (blue line).
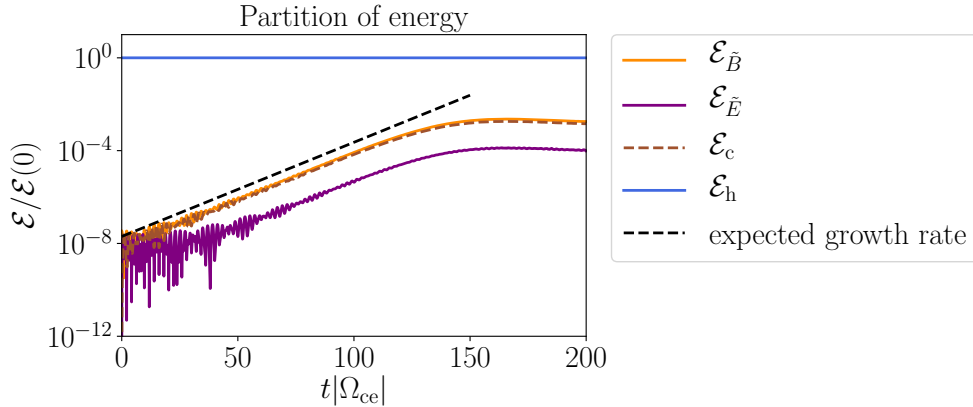

Partition of energy

Figure 4.1: Standard FEM with control variate (Run 1): Time evolution of all the energies involved in the system for a run with parameters $v_{th,\parallel} = 0.2 \, c$, $v_{th,\perp} = 0.53 \, c$, $\nu_h = 0.06$, $\Omega_{pe} = 2|\Omega_{ce}|$, $k = 2 \, |\Omega_{ce}|/c$, $L = 2\pi/k$, $N_{el} = 32$, $p = 1$, $N_p = 1 \cdot 10^5$ and $\Delta t = 0.0125 \, |\Omega_{ce}|$ together with the expected growth rate (black dashed line).

We clearly see the linear growth of all quantities up to $t \approx 140 \, |\Omega_{\mathrm{ce}}|$ followed by a nonlinear saturation phase. Furthermore, the numerical growth agrees very well with the analytical one (back dashed line) even for this rather coarse grid ($N_{\mathrm{el}} = 32$) and linear basis functions ($p = 1$). In order to analyze the real frequency ω_{r}, we compute the frequency spectrogram of the energy of the x-component of the magnetic field in the linear phase by using a discrete Fourier transform in time. The result is shown in fig. 4.2 where one can see that the field indeed most dominantly oscillates with the expected frequency[4] from the analytical theory.

Figure 4.2: Standard FEM with control variate (Run 1): Frequency spectrogram of the energy of the x-component of the magnetic field obtained by a fast Fourier transform and expected real frequency (black dashed line). This result corresponds to the simulation shown in fig. 4.1.

In summary, this test run already indicates that the developed algorithm leads to correct results in terms of growth rate and real frequency. Besides this, other simulations with the same setup put higher polynomial degrees ($p = 2, 3$) or more elements $N_{\mathrm{el}} \geq 32$ did not lead to visible changes. The same is true for more particles in the PIC part of the simulation ($N_{\mathrm{p}} \geq 1 \cdot 10^5$) and the used time step ($\Delta t = 0.0125 - 0.1 \, |\Omega_{\mathrm{ce}}|$) which means that the code is very robust regarding choices of numerical parameters.

Let us have a look at the distribution of the fast electrons in the respective directions at the end of the simulation at $t = 200 \, |\Omega_{\mathrm{ce}}|$ which is already in the nonlinear phase. The result is shown in fig. 4.3, where we compare the initial and final velocity distributions both in parallel and perpendicular direction. In parallel direction, we observe a flattening of the distribution function around the resonant velocities which are expected to be at $v_{\mathrm{R}} = (\omega_{\mathrm{r}} + |\Omega_{\mathrm{ce}}|)/k) \approx \pm 0.26 \, c$ for the wavenumber $k = 2 \, |\Omega_{\mathrm{ce}}|/c$. This means that electrons initially close to these resonant velocities gain energy in parallel direction which can more clearly be seen in the plot below where we show the difference in the parallel and final distribution. In contrast to that, electrons loose energy in perpendicular direction which is shown on the right-hand side as the final distribution function is larger for small velocities and slightly smaller for velocities $v_\perp \gtrsim 0.65 \, c$. A quantitative analysis yields that the fast electrons loose in total more energy in perpendicular direction than what they gain in parallel direction (which is why the blue curve in fig. 4.1 slightly drops) which is of course what we expect because the wave energies grow due to energy transfer from the fast electrons to the wave. In summary, the analysis of the distribution functions reveals that the dynamics of the system tends to reduce the temperature anisotropy of the fast electrons.
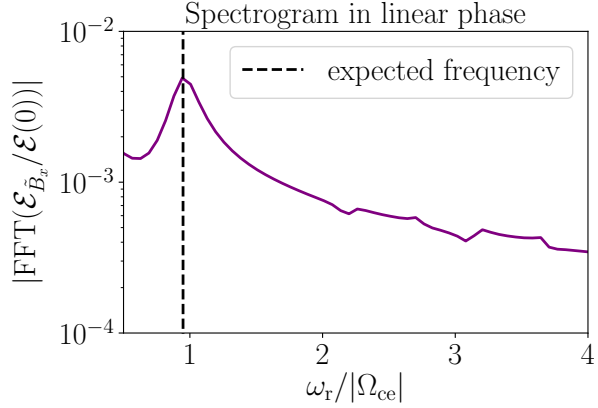
---

[4]Note that the expected frequency here is $2\omega_{\mathrm{r}}$ since the fields are squared in the case of energy computations. The same is true for the growth rate in fig. 4.1.
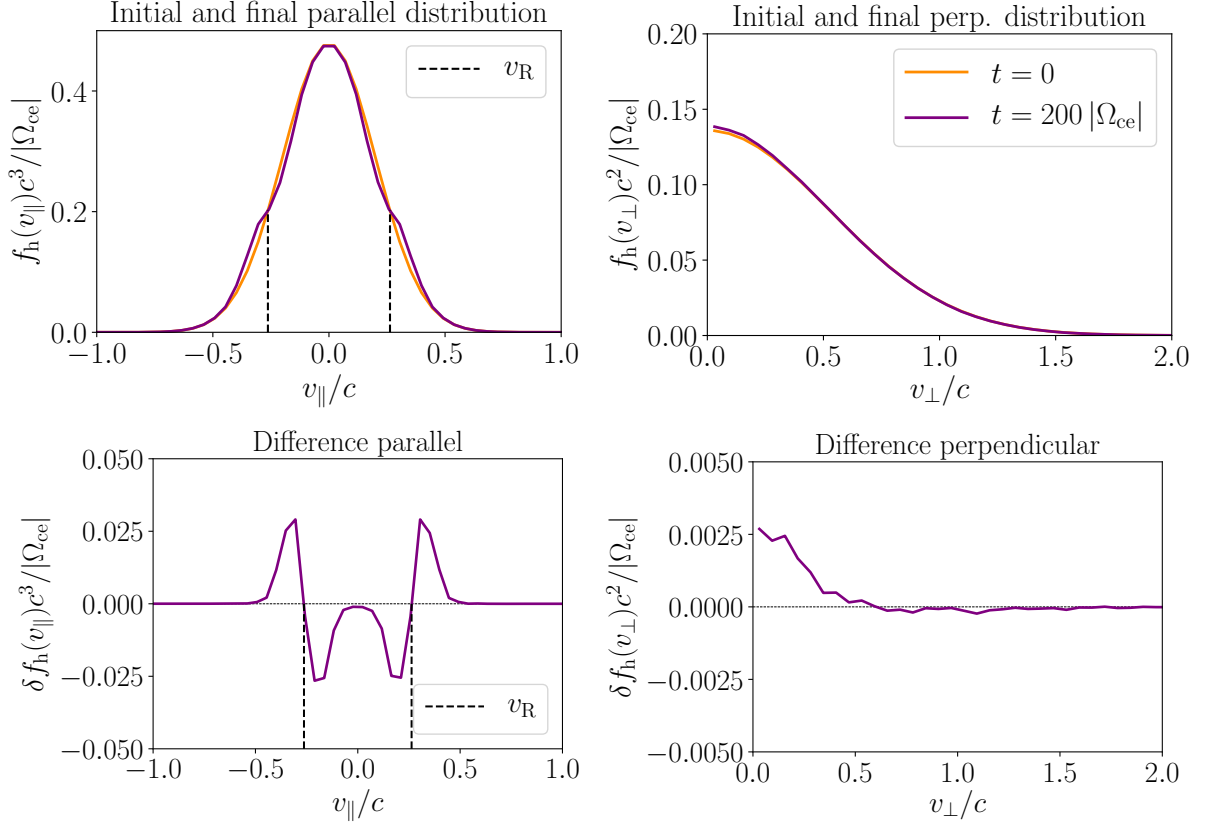
Figure 4.3: Standard FEM with control variate (Run 1): Top left: Initial (orange) and final (purple) velocity distribution of fast electrons in parallel direction with expected resonant velocities (black dashed). Top right: Initial (orange) and final (purple) velocity distribution of fast electrons in perpendicular direction. Bottom left: Difference of initial and final distribution in parallel direction. Bottom right: Difference of intial and final distribution in perpendicular direction.

Finally, we check the total energy conservation of this simulation since this should be the case according to the analytical theory. For this, we plot in fig. 4.4 the relative error of the total energy (i.e. the difference of the total energy to the initial total energy normalized to the latter one) with respect to time. One can observe that the order of the error is $\sim 10^{-7}$ in the very beginning of the simulation followed by a gradual increase to $\sim 10^{-3}$ in the nonlinear phase where the error seems to satu-
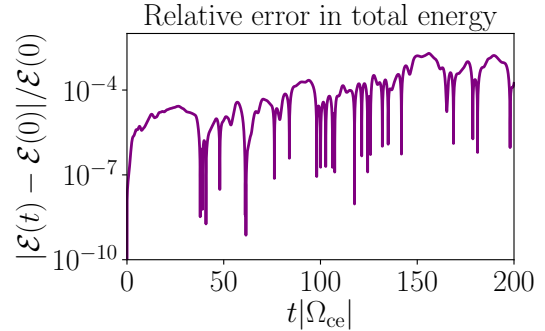

Figure 4.4: Standard FEM with control variate (Run 1): Time evolution of the relative error in the conservation of the total energy for the simulation shown in fig. 4.1.
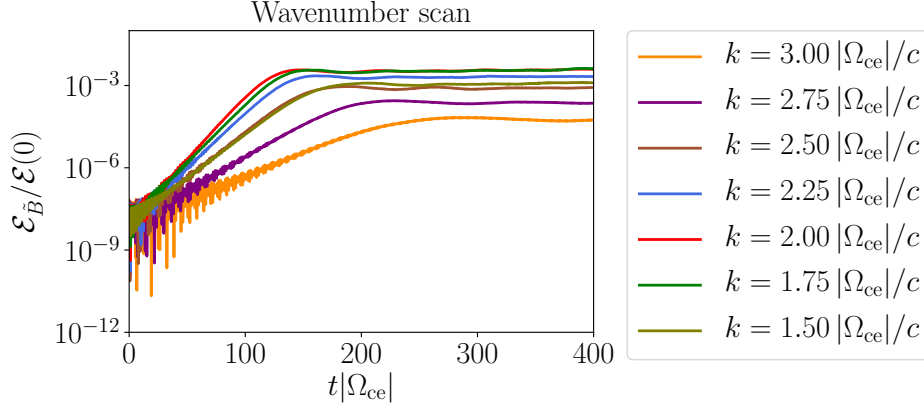
Figure 4.5: Standard FEM with control variate (Run 2): *Time evolution of the magnetic field energy for different wavenumbers k. The used parameters are $v_{th,\parallel} = 0.2\,c$, $v_{th,\perp} = 0.6\,c$, $\nu_h = 0.05$, $\Omega_{pe} = 2|\Omega_{ce}|$, $k = 1.5 - 3.0\,|\Omega_{ce}|/c$, $L = 2\pi/k$, $N_{el} = 200$, $p = 3$, $N_p = 5 \cdot 10^4$ and $\Delta t = 0.05\,|\Omega_{ce}|$.*

rate.

As a next step, in order to check whether the numerical output agrees with the linear theory for a certain range of wavenumbers, we run the code in the same way as before but successively for different k-values. The resulting time evolutions of the respective magnetic field energies $\mathcal{E}_{\tilde{B}}$ are shown in fig. 4.5. The analysis is done in two steps: First, we fit each curve linearly in the linear phase in order to get the growth rates γ for each k-value. Second, like in the analysis of the previous run, we compute the frequency spectrogram and look for a peak to which we relate the real frequency. Note that there is no specific reason for the choice of numerical parameters (especially the larger number of elements and the high polynomial degree). As already mentioned, no visible influence on the results by these parameters could be detected.
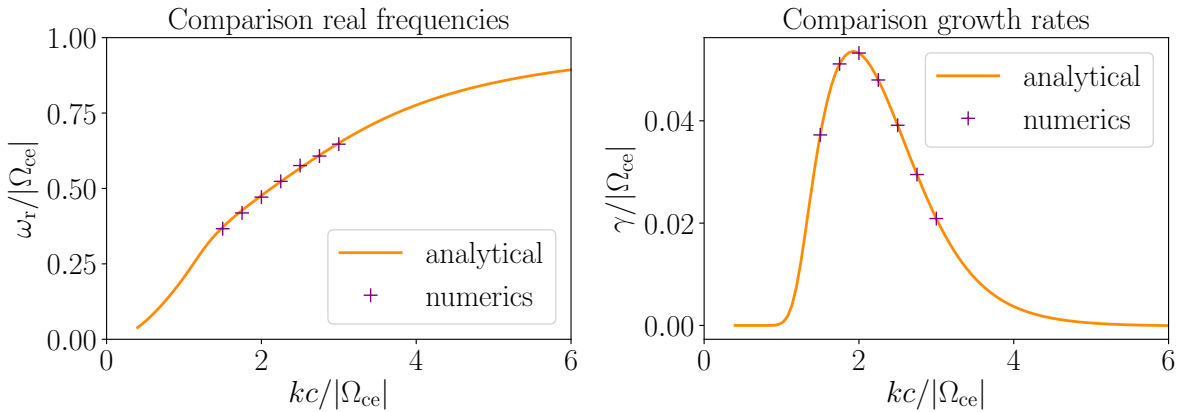

Figure 4.6: Standard FEM with control variate (Run 2): Left: *Comparison of expected real frequencies from the dispersion relation (2.46) with numerical ones.* **Right:** *Comparison of growth rates from the dispersion relation (2.46) with numerical ones.*
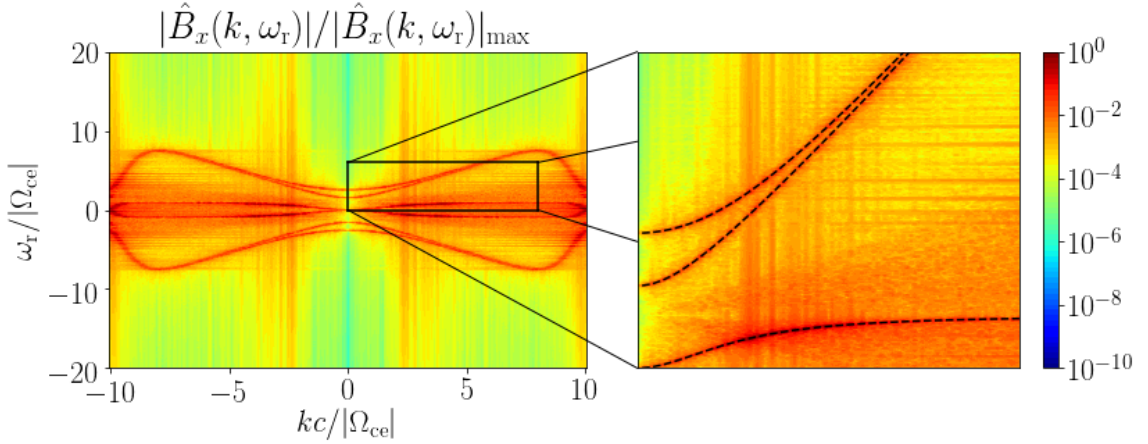
Figure 4.7: Standard FEM with control variate (Run 3): *Normalized 2D Fourier spectrum in the k-ω-plane for the x-component of the magnetic field $\tilde{B}_{h,x} = \tilde{B}_{h,x}(z,t)$ for a run with random noise induced by energetic electrons with an isotropic velocity distribution and comparison with the analytical dispersion relation (black dashed line on the right). The used parameters are $v_{th,\parallel} = 0.1\,c$, $v_{th,\perp} = 0.1\,c$, $\nu_h = 0.002$, $\Omega_{pe} = 2|\Omega_{ce}|$, $L = 80\,c/|\Omega_{ce}|$, $N_{el} = 256$, $p = 3$, $N_p = 5 \cdot 10^4$, $\Delta t = 0.05\,|\Omega_{ce}|^{-1}$. The simulation was run until $t_{end} = 300\,|\Omega_{ce}|^{-1}$.*

The results of this analysis can be seen in fig. 4.6, where we compare the numerical real frequencies (left) and growth rates (right) with the ones obtained by solving the linear dispersion relation (2.46). One notices the very good agreement between theory and numerics.

So far we have initialized the code with a small perturbation of the x-component of the magnetic field with a single wavenumber k. Next, we want to excite multiple k-modes of the system at the same time. This can be achieved by directly using the fact that the random initialization of the particles in phase space induces a low-level noise in the system. In fig. 4.7 one can see the two-dimensional Fourier transform of a run that has been initialized with a low density ($\nu_h = 0.002$), isotropic ($v_{th,\parallel} = v_{th,\perp} = 0.1\,c$,) Maxwellian for the fast electrons and no electromagnetic fields and cold current density. With this choice of parameters, there is no wave growth expected, however, by taking a look at the spectrum in the k-ω-plane, we see that the particle noise leads to an excitation of all three characteristic waves with a continuous spectrum in each quadrant. On the right-hand side, we compare the spectrum for certain ranges in the first quadrant with the analytical dispersion relation and again we find a very good agreement. However, for wavenumbers $k \gtrsim 8\,|\Omega_{ce}|/c$, we observe that the branches „bend downwards", which is of course not expected. This means that these wavelengths can not be resolved with this particular choice for the element size $h = 0.3125\,c/|\Omega_{ce}|$ and therefore we can state that $hk \lesssim 2.5$ must be taken into account for the spatial scales of interest.

To end this section, we perform a run without control variate in order to investigate its impact on the results. For this, we run the same simulation as in the beginning of this section (Run 1) but simply switch off the control variate by setting $\mathcal{M}_0(\mathbf{v}) = 0$. In fig. 4.8
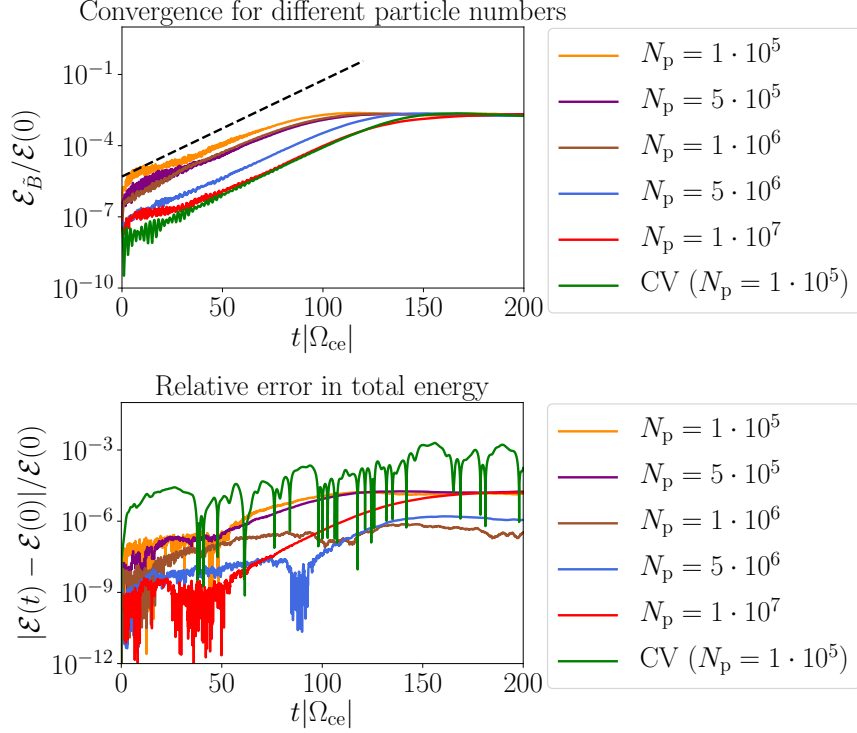
Figure 4.8: Standard FEM without control variate: Top: *Time evolution of magnetic field energy for paramters given in fig. 4.1 but different particle numbers and comparison with result obtained with control variate (CV).* ***Bottom:*** *Corresponding relative errors of the conservation of the energy with respect to time.*

on the top one can see the resulting time evolution of the magnetic field energy (orange line). One observes a rather large deviation from the result with control variate (green line) which is mostly due to a „jump" of the energy in the very beginning caused by the enhanced noise in the system. This can be understood by recalling that the weights are not zero in the beginning as it is the case with control variate. Thus, there is a „noisy" current which should not be there since the used equilibrium distribution function is a non-current carrying one. After the jump we observe that the curve runs parallel to the one with control variate, and both end up at the same saturation level.

In order to reduce the noise, we have performed the same runs, but with more and more particles up to $N_\mathrm{p} = 1 \cdot 10^7$. One can see in fig. 4.8 that the noise indeed reduces gradually, the jump in the beginning becomes smaller and smaller and the result converges to the one with control variate.

Furthermore, we compare in fig. 4.8 on the bottom the evolution of the error of the total energy conservation. It is interesting that the error is smaller without control variate although the qualitative result (magnetic energy) above is better. One can also observe a difference of linear and nonlinear phase in the case without control variate since the error oscillates on the same level in the beginning and at some point the error starts to grow until it saturates.

4.2 Geometric methods and comparison

In order to compare the geometric algorithm with the standard one, we perform a test run with the same parameters as the first run of the previous section (Run 1, see caption of fig. 4.1), however, first with the first order Lie-Trotter splitting (3.112). As already indicated, the derivation of the semi-discrete Hamiltonian structure and the time integrators was done with constant weights, i.e. without control variate. The result for this is shown in fig. 4.9 where one can see the time evolution of all energies together with the expected growth rate (dashed line) on the left and the error of the conservation of the total energy on the right. Qualitatively, we once more observe a good agreement of the wave growth with the analytical theory. Furthermore, one can see the that the energy error on the right oscillates constantly below $\sim 10^{-4}$ which is an improvement compared to the results shown in the previous section.

To demonstrate that this good behaviour is really due to the Hamiltonian structure of the semi-discrete system and the fact that we could subsequently construct Poisson time integrators by solving each sub-step of the splitting analytically, we run the same test, however, with the usual control variate switched on. As already indicated, this has the consequence that the semi-discrete equations can not be written in a Hamiltonian structure anymore and also the derivation of the time integrators is not fully correct since we assume there that the weights are constant in each time step. The control variate is applied such that the weights are adjusted every time the particle velocities change (which happens after applying the integrators $\Phi_{\Delta t}^E$, $\Phi_{\Delta t}^x$, $\Phi_{\Delta t}^y$ and $\Phi_{\Delta t}^z$). The results of this procedure are shown in fig. 4.10 where we still see the noise reduction due to the missing jump in the beginning (note that the energies start at $\sim 10^{-9}$ in fig. 4.10 compared to $\sim 10^{-7}$) in fig. 4.9). However, if we compare the resulting energy errors on the right-hand side, we observe that the error increases gradually (orange line) compared to the run without control variate (purple line).
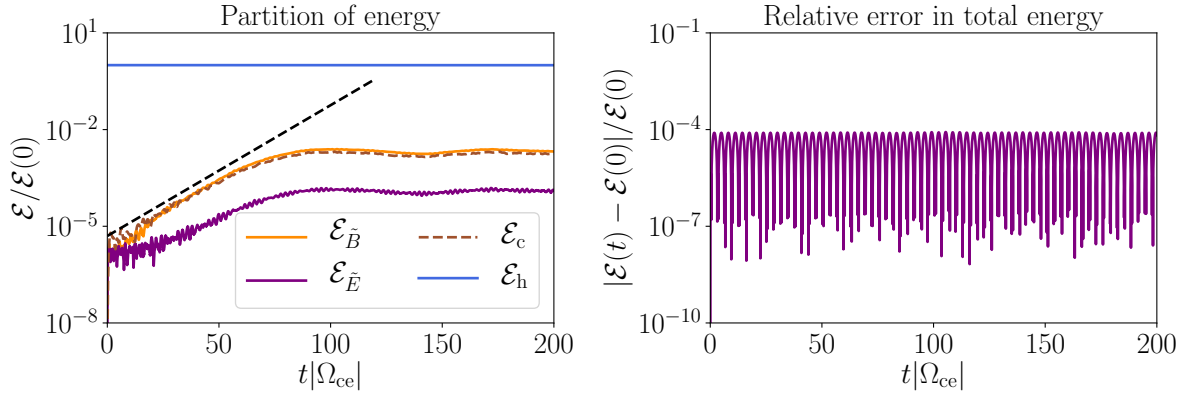

Figure 4.9: Geometric methods without control variate (Lie-Trotter): Left: Time evolution of all the energies involved in the system together with the expected growth rate (dashed black line) obtained with the geometric methods and the Lie-Trotter splitting. Right: Corresponding relative error in the total energy.
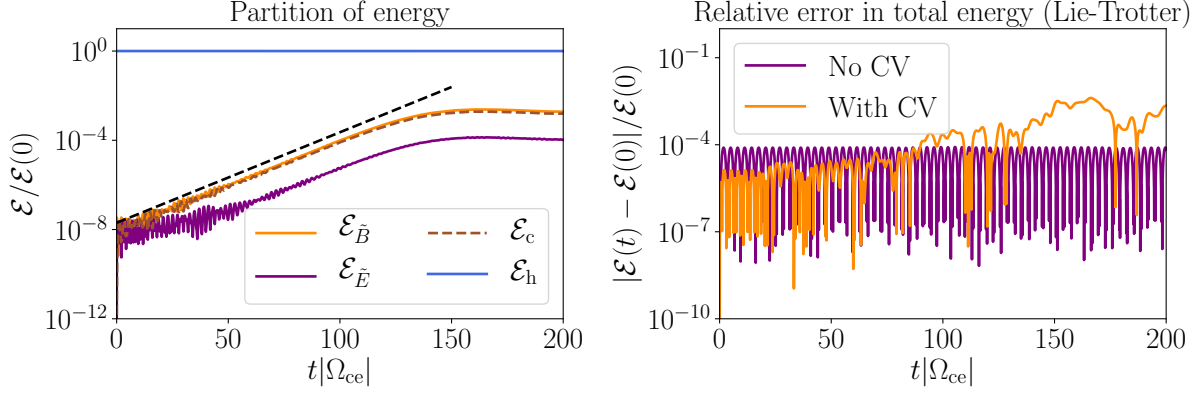
63

Figure 4.10: Geometric methods with control variate (Lie-Trotter): Left:
*Time evolution of all energies involved in the system together with the expected growth
rate (dashed black line) obtained with the geometric methods and the Lie-Trotter split-*
ting. ***Right:*** *Corresponding relative error in the conservation of the total energy and
comparison with the result without contol variate (fig. 4.9).*

Finally, we perform a simulation with the second order Strang splitting (3.113) which
should actually be used when comparing with the standard code since the used time
stepping scheme (Crank-Nicolson) there is also second order. In fig. 4.11 one can see
the results together with the ones obtained with the Lie-Trotter splitting and standard
FEM. We see that the Strang splitting reduces the error in the energy conservation by
about three orders of magnitude and shows a similar behavior as the Lie-Trotter splitting
in terms of non-increasing error in time. It can be observed that this happens in case of
standard FEM, especially at some point when nonlinearities probably start to play a role.
By having a look at the time evolution of the magnetic field energies we do not observe
a major difference for the three methods. In summary, one can therefore state that the
geometric methods are superior to the standard ones due to good energy conservation
properties for long-term simulations which is what such methods are designed for.
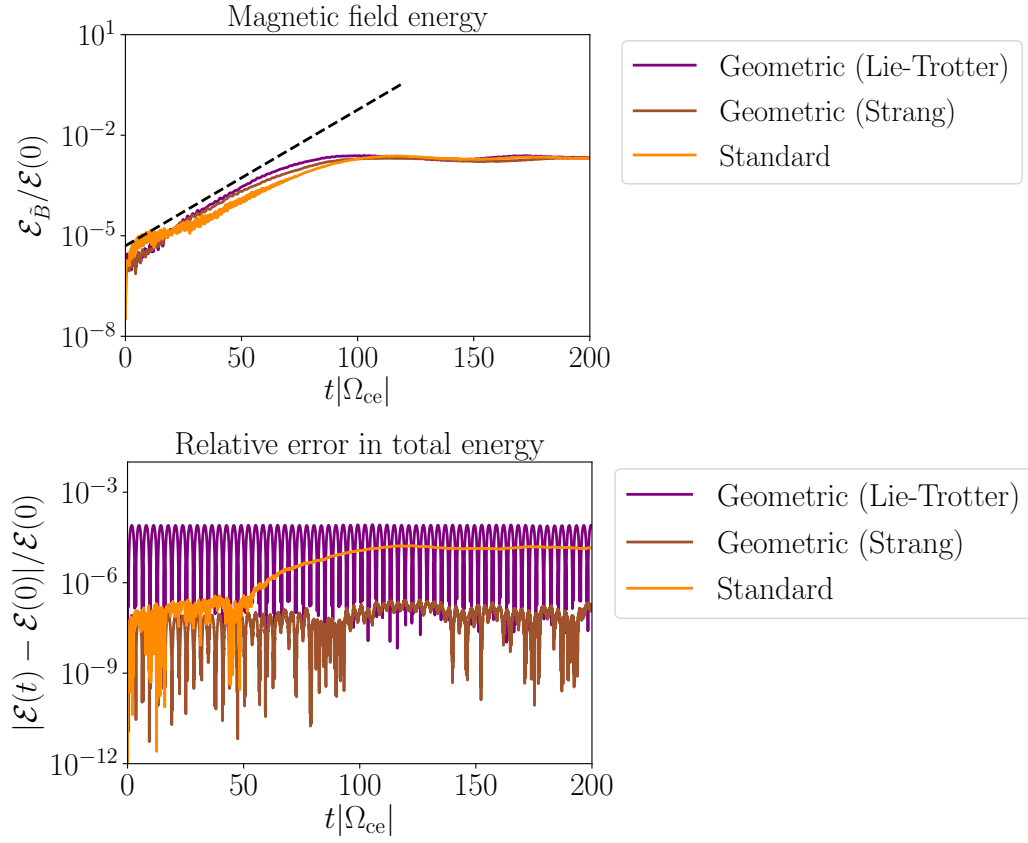
*Figure 4.11: Comparison of standard FEM with geometric methods: Top: Comparison of the time evolution of the magnetic field energy obtained with standard FEM and geometric methods (Lie-Trotter and Strang splitting). **Bottom:** Comparison of the relative errors in the conservation of the total energy.*

5 Conclusion and Outlook

In this master thesis two different finite element methods have been applied on a four-dimensional hybrid plasma model and implemented in Python in order to compare the performances of standard finite elements compared to the finite element exterior calculus. The considered hybrid plasma model is a combined kinetic/fluid description for a magnetized plasma which consists of cold (fluid) and energetic (kinetic) electrons which move in a stationary, neutralizing background of ions. The model's key physics content for wave propagation parallel to a uniform magnetic field is that it predicts the existence of growing/damped modes due to energy exchange between the energetic electrons and electromagnetic waves which propagate in the cold background plasma. The major parameter that determines the growth/damping is the anisotropy of the velocity distribution of the energetic electrons with respect to the direction of the background magnetic field.

For this case, first, a combination of one-dimensional B-spline finite elements for solving numerically Maxwell's equations and the momentum balance equation for the cold electrons and the particle-in-cell method for solving numerically the Vlasov equation (one dimension in space and three dimensions in velocity space) has been applied in an intuitive way and implemented in Python. The obtained simulation results showed an excellent agreement with the analytical theory for a wide range of numerical parameters. Therefore it can be stated that the advantage of this approach is its relative simplicity and robustness. However, the disadvantage is that this approach does not give any information about the preservation of certain conservation laws like the conservation of energy, for instance. Indeed, the results have shown that the error of the conservation of energy increased gradually in time.

Second, methods from the finite element exterior calculus have been applied on the same model. By choosing finite element spaces (Lagrange interpolation and Lagrange histopolation) which satisfy a so-called commuting diagram with the continuous function spaces, a semi-discrete system (discrete in space and continuous in time) with a non-canonical Hamiltonian structure has been derived for the time evolution of the finite element coefficients and particle configurations. It has been proven that, unlike the previous approach, this semi-discrete system conserves exactly the total energy of the system. The subsequent construction of Poisson time integrators by splitting the Hamiltonian has led to a bounded error in the conservation of energy with respect to time and could be decreased by orders of magnitude by using a higher-order time integration scheme. In summary, this approach is therefore superior to the previous one in a sense that is gives information about preserving conservation laws which is not the case for the standard FEM approach.

In principle, both codes form a basis to address physics questions which are related to the in section 2.1.1 mentioned Chorus wave generation in the earth's magnetosphere induced by fast electrons coming from space. For this, some extensions need to be done:

- **Non-uniform magnetic field**: Instead of taking a uniform magnetic field $\mathbf{B} = B_0 \mathbf{e}_z$, it has been shown that an appropriate approach for modeling the earth's magnetic field is to take a parabolic field of the form $B_{0z}(z) = B_0(1 + \xi z^2)$ (with the other components such that $\nabla \cdot \mathbf{B}_0 = 0$ is satisfied, see [14]) which acts as a magnetic

mirror. This leads to modified mass matrices in the finite element discretization. For instance, in the standard FEM version (3.59), an inhomogeneous background field $\mathbf{B}_0$ results in an equation of the form

$$\frac{\partial \mathbf{U}}{\partial t} + A_1 \frac{\partial \mathbf{U}}{\partial z} + A_2(z)\mathbf{U} = \mathbf{S}, \tag{5.1}$$

which means that the matrix A_2 remains in the integral when deriving the weak formulation.

- **Relativistic description for energetic electrons**: Since we have used energetic electron distributions with thermal velocities up to $60\,\%$ of the speed of light, a relativistic description would actually be the appropriate one. This can be achieved by working in momentum space instead of velocity space, i.e. the distribution function becomes

$$f_{\mathrm{h}} = f_{\mathrm{h}}(\mathbf{x}, \mathbf{p}, t), \tag{5.2}$$

  where $\mathbf{p} = \gamma_{\mathrm{L}}\mathbf{v}$ and γ_{L} is the well-known Lorentz factor. Solving the relativistic equations of motion for the PIC particles can easily be achieved by using a modified Boris algorithm ([22] p. 356-357).

- **Code acceleration**: Both codes are written in Python without any parallelization, which means that the computation times are rather large compared to programming languages like Fortran with/without parallelization. Taking a slightly enhanced number of elements ($N_{\mathrm{el}} \gtrsim 500$) together with higher polynomial degrees ($p > 2$) and a number of particles ($N_{\mathrm{p}} \gtrsim 1 \cdot 10^6$) already results in computation times of several days. This means that if one wants to be flexible in terms of numerical parameters, parts of the codes need to be converted e.g. to Fortran.

Finally, the knowledge gained from the FEEC code forms a basis to apply these methods to other physics models like hybrid magnetohydrodynamic (MHD)/kinetic models (e.g. ref. [10]) in order to study energetic particle effects in low-frequency regimes. This is in particular interesting for future fusion devices due to the fact that velocities of the formed α-particles will of the order of the so-called Alfvén velocity which is the characteristic speed of MHD-waves. As already indicated in the very beginning of this thesis, having codes with good conservation properties for long times is especially important for the nonlinear regime.

6 Appendix

Time integrators for Hamiltonian splitting

Problem 1. For $t \in [0, \Delta t]$ and $\mathbf{u}(t = 0) = \mathbf{u}^0$ we have,

$$\frac{\mathrm{d}\mathbf{u}}{\mathrm{d}t} = \mathbb{J}(\mathbf{u})\nabla_{\mathbf{u}}H_E(\mathbf{u}), \tag{6.1}$$

where

$$H_E(\mathbf{u}) = \frac{\epsilon_0}{2}(\mathbf{e}_x^\top \mathbb{M}^0 \mathbf{e}_x + \mathbf{e}_y^\top \mathbb{M}^0 \mathbf{e}_y). \tag{6.2}$$

This can be solved analytically as

$$\frac{\mathrm{d}\mathbf{e}_x}{\mathrm{d}t} = 0 \qquad \implies \quad \mathbf{e}_x(\Delta t) = \mathbf{e}_x^0, \tag{6.3a}$$

$$\frac{\mathrm{d}\mathbf{e}_y}{\mathrm{d}t} = 0 \qquad \implies \quad \mathbf{e}_y(\Delta t) = \mathbf{e}_y^0, \tag{6.3b}$$

$$\frac{\mathrm{d}\mathbf{b}_x}{\mathrm{d}t} = \frac{1}{\epsilon_0}\tilde{\mathbb{G}}(\mathbb{M}^0)^{-1}\epsilon_0 \mathbb{M}^0 \mathbf{e}_y \qquad \implies \quad \mathbf{b}_x(\Delta t) = \mathbf{b}_x^0 + \Delta t\tilde{\mathbb{G}}\mathbf{e}_y^0, \tag{6.3c}$$

$$\frac{\mathrm{d}\mathbf{b}_y}{\mathrm{d}t} = -\frac{1}{\epsilon_0}\tilde{\mathbb{G}}(\mathbb{M}^0)^{-1}\epsilon_0 \mathbb{M}^0 \mathbf{e}_x \qquad \implies \quad \mathbf{b}_y(\Delta t) = \mathbf{b}_y^0 - \Delta t\tilde{\mathbb{G}}\mathbf{e}_x^0, \tag{6.3d}$$

$$\frac{\mathrm{d}\mathbf{y}_x}{\mathrm{d}t} = \Omega_{\mathrm{pe}}^2(\mathbb{M}^0)^{-1}\epsilon_0 \mathbb{M}^0 \mathbf{e}_x \qquad \implies \quad \mathbf{y}_x(\Delta t) = \mathbf{y}_x^0 + \Delta t\epsilon_0\Omega_{\mathrm{pe}}^2\mathbf{e}_x^0, \tag{6.3e}$$

$$\frac{\mathrm{d}\mathbf{y}_y}{\mathrm{d}t} = \Omega_{\mathrm{pe}}^2(\mathbb{M}^0)^{-1}\epsilon_0 \mathbb{M}^0 \mathbf{e}_y \qquad \implies \quad \mathbf{y}_y(\Delta t) = \mathbf{y}_y^0 + \Delta t\epsilon_0\Omega_{\mathrm{pe}}^2\mathbf{e}_y^0, \tag{6.3f}$$

$$\frac{\mathrm{d}\mathbf{Z}}{\mathrm{d}t} = 0 \qquad \implies \quad \mathbf{Z}(\Delta t) = \mathbf{Z}^0, \tag{6.3g}$$

$$\frac{\mathrm{d}\mathbf{V}_x}{\mathrm{d}t} = \frac{q_{\mathrm{e}}}{\epsilon_0 m_{\mathrm{e}}}(\mathbb{Q}^0)^\top(\mathbb{M}^0)^{-1}\epsilon_0 \mathbb{M}^0 \mathbf{e}_x \quad \implies \quad \mathbf{V}_x(\Delta t) = \mathbf{V}_x^0 + \Delta t\frac{q_{\mathrm{e}}}{m_{\mathrm{e}}}(\mathbb{Q}^0)^\top(\mathbf{Z}^0)\mathbf{e}_x^0, \tag{6.3h}$$

$$\frac{\mathrm{d}\mathbf{V}_y}{\mathrm{d}t} = \frac{q_{\mathrm{e}}}{\epsilon_0 m_{\mathrm{e}}}(\mathbb{Q}^0)^\top(\mathbb{M}^0)^{-1}\epsilon_0 \mathbb{M}^0 \mathbf{e}_y \quad \implies \quad \mathbf{V}_y(\Delta t) = \mathbf{V}_x^0 + \Delta t\frac{q_{\mathrm{e}}}{m_{\mathrm{e}}}(\mathbb{Q}^0)^\top(\mathbf{Z}^0)\mathbf{e}_y^0, \tag{6.3i}$$

$$\frac{\mathrm{d}\mathbf{V}_z}{\mathrm{d}t} = 0 \qquad \implies \quad \mathbf{V}_z(\Delta t) = \mathbf{V}_z^0. \tag{6.3j}$$

The corresponding integrator is denoted by $\mathbf{u}(\Delta t) = \Phi_{\Delta t}^E(\mathbf{u}^0)$.
Note that the matrices $\mathbb{B}_x$ and $\mathbb{B}_y$ need to be updated after applying this integrator since the magnetic field coefficients $\mathbf{b}_x$ and $\mathbf{b}_y$ change.

Problem 2. For $t \in [0, \Delta t]$ and $\mathbf{u}(t = 0) = \mathbf{u}^0$ we have,

$$\frac{\mathrm{d}\mathbf{u}}{\mathrm{d}t} = \mathbb{J}(\mathbf{u})\nabla_{\mathbf{u}}H_B(\mathbf{u}), \tag{6.4}$$

where

$$H_B(\mathbf{u}) = \frac{1}{2\mu_0}(\mathbf{b}_x^\top \mathbb{M}^1 \mathbf{b}_x + \mathbf{b}_y^\top \mathbb{M}^1 \mathbf{b}_y). \tag{6.5}$$

This can be solved analytically as

$$\frac{\mathrm{d}\mathbf{e}_x}{\mathrm{d}t} = \frac{1}{\epsilon_0}(\mathbb{M}^0)^{-1}\tilde{\mathbb{G}}^\top \frac{1}{\mu_0}\mathbb{M}^1 \mathbf{b}_y \quad \implies \quad \mathbf{e}_x(\Delta t) = \mathbf{e}_x^0 + \Delta t c^2 (\mathbb{M}^0)^{-1}\tilde{\mathbb{G}}^\top \mathbb{M}^1 \mathbf{b}_y^0, \tag{6.6a}$$

$$\frac{\mathrm{d}\mathbf{e}_y}{\mathrm{d}t} = -\frac{1}{\epsilon_0}(\mathbb{M}^0)^{-1}\tilde{\mathbb{G}}^\top \frac{1}{\mu_0}\mathbb{M}^1 \mathbf{b}_x \quad \implies \quad \mathbf{e}_y(\Delta t) = \mathbf{e}_y^0 - \Delta t c^2 (\mathbb{M}^0)^{-1}\tilde{\mathbb{G}}^\top \mathbb{M}^1 \mathbf{b}_x^0, \tag{6.6b}$$

$$\frac{\mathrm{d}\mathbf{b}_x}{\mathrm{d}t} = 0 \quad \implies \quad \mathbf{b}_x(\Delta t) = \mathbf{b}_x^0, \tag{6.6c}$$

$$\frac{\mathrm{d}\mathbf{b}_y}{\mathrm{d}t} = 0 \quad \implies \quad \mathbf{b}_y(\Delta t) = \mathbf{b}_y^0, \tag{6.6d}$$

$$\frac{\mathrm{d}\mathbf{y}_x}{\mathrm{d}t} = 0 \quad \implies \quad \mathbf{y}_x(\Delta t) = \mathbf{y}_x^0, \tag{6.6e}$$

$$\frac{\mathrm{d}\mathbf{y}_y}{\mathrm{d}t} = 0 \quad \implies \quad \mathbf{y}_y(\Delta t) = \mathbf{y}_y^0, \tag{6.6f}$$

$$\frac{\mathrm{d}\mathbf{Z}}{\mathrm{d}t} = 0 \quad \implies \quad \mathbf{Z}(\Delta t) = \mathbf{Z}^0, \tag{6.6g}$$

$$\frac{\mathrm{d}\mathbf{V}_x}{\mathrm{d}t} = 0 \quad \implies \quad \mathbf{V}_x(\Delta t) = \mathbf{V}_x^0, \tag{6.6h}$$

$$\frac{\mathrm{d}\mathbf{V}_y}{\mathrm{d}t} = 0 \quad \implies \quad \mathbf{V}_y(\Delta t) = \mathbf{V}_y^0, \tag{6.6i}$$

$$\frac{\mathrm{d}\mathbf{V}_z}{\mathrm{d}t} = 0 \quad \implies \quad \mathbf{V}_z(\Delta t) = \mathbf{V}_z^0. \tag{6.6j}$$

The corresponding integrator is denoted by $\mathbf{u}(\Delta t) = \Phi_{\Delta t}^B(\mathbf{u}^0)$.

Problem 3. For $t \in [0, \Delta t]$ and $\mathbf{u}(t = 0) = \mathbf{u}^0$, we have

$$\frac{\mathrm{d}\mathbf{u}}{\mathrm{d}t} = \mathbb{J}(\mathbf{u})\nabla_{\mathbf{u}}H_Y(\mathbf{u}), \tag{6.7}$$

where

$$H_Y = \frac{1}{2\epsilon_0\Omega_{\mathrm{pe}}^2}(\mathbf{y}_x^\top\mathbb{M}^0\mathbf{y}_x + \mathbf{y}_y^\top\mathbb{M}^0\mathbf{y}_y). \tag{6.8}$$

This can be solved analytically as

$$\frac{\mathrm{d}\mathbf{e}_x}{\mathrm{d}t} = -\Omega_{\mathrm{pe}}^2(\mathbb{M}^0)^{-1}\frac{1}{\epsilon_0\Omega_{\mathrm{pe}}^2}\mathbb{M}^0\mathbf{y}_x$$

$$\implies \mathbf{e}_x(\Delta t) = \mathbf{e}_x^0 - \frac{1}{\epsilon_0}\int_0^{\Delta t}y_x(t')\mathrm{d}t' = \mathbf{e}_x^0 - \frac{1}{\epsilon_0\Omega_{\mathrm{ce}}}[\mathbf{y}_x^0\sin(\Omega_{\mathbf{ce}}t) - \mathbf{y}_y^0\cos(\Omega_{\mathbf{ce}}t) + \mathbf{y}_y^0], \tag{6.9a}$$

$$\frac{\mathrm{d}\mathbf{e}_y}{\mathrm{d}t} = -\Omega_{\mathrm{pe}}^2(\mathbb{M}^0)^{-1}\frac{1}{\epsilon_0\Omega_{\mathrm{pe}}^2}\mathbb{M}^0\mathbf{y}_y$$

$$\implies \mathbf{e}_y(\Delta t) = \mathbf{e}_y^0 - \frac{1}{\epsilon_0}\int_0^{\Delta t}y_y(t')\mathrm{d}t' = \mathbf{e}_y^0 - \frac{1}{\epsilon_0\Omega_{\mathrm{ce}}}[\mathbf{y}_y^0\sin(\Omega_{\mathbf{ce}}t) + \mathbf{y}_x^0\cos(\Omega_{\mathbf{ce}}t) - \mathbf{y}_x^0], \tag{6.9b}$$

$$\frac{\mathrm{d}\mathbf{b}_x}{\mathrm{d}t} = 0 \qquad\qquad \implies \quad \mathbf{b}_x(\Delta t) = \mathbf{b}_x^0, \tag{6.9c}$$

$$\frac{\mathrm{d}\mathbf{b}_y}{\mathrm{d}t} = 0 \qquad\qquad \implies \quad \mathbf{b}_y(\Delta t) = \mathbf{b}_y^0, \tag{6.9d}$$

$$\frac{\mathrm{d}\mathbf{y}_x}{\mathrm{d}t} = \epsilon_0\Omega_{\mathrm{pe}}^2\Omega_{\mathrm{ce}}(\mathbb{M}^0)^{-1}\frac{1}{\epsilon_0\Omega_{\mathrm{pe}}^2}\mathbb{M}^0\mathbf{y}_y \implies \quad \mathbf{y}_x(\Delta t) = \mathbf{y}_x^0\cos(\Omega_{\mathbf{ce}}\Delta t) + \mathbf{y}_y^0\sin(\Omega_{\mathbf{ce}}\Delta t), \tag{6.9e}$$

$$\frac{\mathrm{d}\mathbf{y}_y}{\mathrm{d}t} = -\epsilon_0\Omega_{\mathrm{pe}}^2\Omega_{\mathrm{ce}}(\mathbb{M}^0)^{-1}\frac{1}{\epsilon_0\Omega_{\mathrm{pe}}^2}\mathbb{M}^0\mathbf{y}_x \implies \quad \mathbf{y}_y(\Delta t) = \mathbf{y}_y^0\cos(\Omega_{\mathbf{ce}}\Delta t) - \mathbf{y}_x^0\sin(\Omega_{\mathbf{ce}}\Delta t), \tag{6.9f}$$

$$\frac{\mathrm{d}\mathbf{Z}}{\mathrm{d}t} = 0 \qquad\qquad \implies \quad \mathbf{Z}(\Delta t) = \mathbf{Z}^0, \tag{6.9g}$$

$$\frac{\mathrm{d}\mathbf{V}_x}{\mathrm{d}t} = 0 \qquad\qquad \implies \quad \mathbf{V}_x(\Delta t) = \mathbf{V}_x^0, \tag{6.9h}$$

$$\frac{\mathrm{d}\mathbf{V}_y}{\mathrm{d}t} = 0 \qquad\qquad \implies \quad \mathbf{V}_y(\Delta t) = \mathbf{V}_y^0, \tag{6.9i}$$

$$\frac{\mathrm{d}\mathbf{V}_z}{\mathrm{d}t} = 0 \qquad\qquad \implies \quad \mathbf{V}_z(\Delta t) = \mathbf{V}_z^0. \tag{6.9j}$$

The corresponding integrator is denoted by $\mathbf{u}(\Delta t) = \Phi_{\Delta t}^Y(\mathbf{u}^0)$.

Problem 4. For $t \in [0, \Delta t]$ and $\mathbf{u}(t = 0) = \mathbf{u}^0$ we have,

$$\frac{\mathrm{d}\mathbf{u}}{\mathrm{d}t} = \mathbb{J}(\mathbf{u})\nabla_{\mathbf{u}}H_x(\mathbf{u}), \tag{6.10}$$

where

$$H_x = \frac{m_{\mathrm{e}}}{2}\mathbf{V}_x^{\top}\mathbb{W}\mathbf{V}_x. \tag{6.11}$$

This can be solved analytically as

$$\frac{\mathrm{d}\mathbf{e}_x}{\mathrm{d}t} = -\frac{q_{\mathrm{e}}}{\epsilon_0 m_{\mathrm{e}}}(\mathbb{M}^0)^{-1}\mathbb{Q}^0 m_{\mathrm{e}}\mathbb{W}\mathbf{V}_x \implies \mathbf{e}_x(\Delta t) = \mathbf{e}_y^0 - \Delta t\frac{q_{\mathrm{e}}}{\epsilon_0}(\mathbb{M}^0)^{-1}\mathbb{Q}^0(\mathbf{Z}^0)\mathbb{W}\mathbf{V}_x^0, \tag{6.12a}$$

$$\frac{\mathrm{d}\mathbf{e}_y}{\mathrm{d}t} = 0 \qquad\qquad \implies \mathbf{e}_y(\Delta t) = \mathbf{e}_y^0, \tag{6.12b}$$

$$\frac{\mathrm{d}\mathbf{b}_x}{\mathrm{d}t} = 0 \qquad\qquad \implies \mathbf{b}_x(\Delta t) = \mathbf{b}_x^0, \tag{6.12c}$$

$$\frac{\mathrm{d}\mathbf{b}_y}{\mathrm{d}t} = 0 \qquad\qquad \implies \mathbf{b}_y(\Delta t) = \mathbf{b}_y^0, \tag{6.12d}$$

$$\frac{\mathrm{d}\mathbf{y}_x}{\mathrm{d}t} = 0 \qquad\qquad \implies \mathbf{y}_x(\Delta t) = \mathbf{y}_x^0, \tag{6.12e}$$

$$\frac{\mathrm{d}\mathbf{y}_y}{\mathrm{d}t} = 0 \qquad\qquad \implies \mathbf{y}_y(\Delta t) = \mathbf{y}_y^0, \tag{6.12f}$$

$$\frac{\mathrm{d}\mathbf{Z}}{\mathrm{d}t} = 0 \qquad\qquad \implies \mathbf{Z}(\Delta t) = \mathbf{Z}^0, \tag{6.12g}$$

$$\frac{\mathrm{d}\mathbf{V}_x}{\mathrm{d}t} = 0 \qquad\qquad \implies \mathbf{V}_x(\Delta t) = \mathbf{V}_x^0, \tag{6.12h}$$

$$\frac{\mathrm{d}\mathbf{V}_y}{\mathrm{d}t} = -\frac{\Omega_{\mathrm{ce}}}{m}\mathbb{W}^{-1}m_{\mathrm{e}}\mathbb{W}\mathbf{V}_x \qquad \implies \mathbf{V}_y(\Delta t) = \mathbf{V}_y^0 - \Delta t\Omega_{\mathrm{ce}}\mathbf{V}_x^0, \tag{6.12i}$$

$$\frac{\mathrm{d}\mathbf{V}_z}{\mathrm{d}t} = \frac{q_{\mathrm{e}}}{m_{\mathrm{e}}^2}\mathbb{B}_y\mathbb{W}^{-1}m_{\mathrm{e}}\mathbb{W}\mathbf{V}_x \qquad \implies \mathbf{V}_z(\Delta t) = \mathbf{V}_z^0 + \Delta t\frac{q_{\mathrm{e}}}{m_{\mathrm{e}}}\mathbb{B}_y(\mathbf{Z}^0, \mathbf{b}_y^0)\mathbf{V}_x^0. \tag{6.12j}$$

The corresponding integrator is denoted by $\mathbf{u}(\Delta t) = \Phi_{\Delta t}^y(\mathbf{u}^0)$.

Problem 5. For $t \in [0, \Delta t]$ and $\mathbf{u}(t = 0) = \mathbf{u}^0$ we have,

$$\frac{\mathrm{d}\mathbf{u}}{\mathrm{d}t} = \mathbb{J}(\mathbf{u})\nabla_{\mathbf{u}}H_y(\mathbf{u}), \tag{6.13}$$

where

$$H_y = \frac{m_{\mathrm{e}}}{2}\mathbf{V}_y^{\top}\mathbb{W}\mathbf{V}_y. \tag{6.14}$$

This can be solved analytically as

$$\frac{\mathrm{d}\mathbf{e}_x}{\mathrm{d}t} = 0 \qquad\qquad \implies \quad \mathbf{e}_x(\Delta t) = \mathbf{e}_x^0, \tag{6.15a}$$

$$\frac{\mathrm{d}\mathbf{e}_y}{\mathrm{d}t} = -\frac{q_{\mathrm{e}}}{\epsilon_0 m_{\mathrm{e}}}(\mathbb{M}^0)^{-1}\mathbb{Q}^0 m_{\mathrm{e}}\mathbb{W}\mathbf{V}_y \implies \quad \mathbf{e}_y(\Delta t) = \mathbf{e}_y^0 - \Delta t\frac{q_{\mathrm{e}}}{\epsilon_0}(\mathbb{M}^0)^{-1}\mathbb{Q}^0(\mathbf{Z}^0)\mathbb{W}\mathbf{V}_y^0, \tag{6.15b}$$

$$\frac{\mathrm{d}\mathbf{b}_x}{\mathrm{d}t} = 0 \qquad\qquad \implies \quad \mathbf{b}_x(\Delta t) = \mathbf{b}_x^0, \tag{6.15c}$$

$$\frac{\mathrm{d}\mathbf{b}_y}{\mathrm{d}t} = 0 \qquad\qquad \implies \quad \mathbf{b}_y(\Delta t) = \mathbf{b}_y^0, \tag{6.15d}$$

$$\frac{\mathrm{d}\mathbf{y}_x}{\mathrm{d}t} = 0 \qquad\qquad \implies \quad \mathbf{y}_x(\Delta t) = \mathbf{y}_x^0, \tag{6.15e}$$

$$\frac{\mathrm{d}\mathbf{y}_y}{\mathrm{d}t} = 0 \qquad\qquad \implies \quad \mathbf{y}_y(\Delta t) = \mathbf{y}_y^0, \tag{6.15f}$$

$$\frac{\mathrm{d}\mathbf{Z}}{\mathrm{d}t} = 0 \qquad\qquad \implies \quad \mathbf{Z}(\Delta t) = \mathbf{Z}^0, \tag{6.15g}$$

$$\frac{\mathrm{d}\mathbf{V}_x}{\mathrm{d}t} = \frac{\Omega_{\mathrm{ce}}}{m}\mathbb{W}^{-1}m_{\mathrm{e}}\mathbb{W}\mathbf{V}_y \qquad \implies \quad \mathbf{V}_x(\Delta t) = \mathbf{V}_x^0 + \Delta t\Omega_{\mathrm{ce}}\mathbf{V}_y^0, \tag{6.15h}$$

$$\frac{\mathrm{d}\mathbf{V}_y}{\mathrm{d}t} = 0 \qquad\qquad \implies \quad \mathbf{V}_y(\Delta t) = \mathbf{V}_y^0, \tag{6.15i}$$

$$\frac{\mathrm{d}\mathbf{V}_z}{\mathrm{d}t} = -\frac{q_{\mathrm{e}}}{m_{\mathrm{e}}^2}\mathbb{B}_x\mathbb{W}^{-1}m_{\mathrm{e}}\mathbb{W}\mathbf{V}_y \qquad \implies \quad \mathbf{V}_z(\Delta t) = \mathbf{V}_z^0 - \Delta t\frac{q_{\mathrm{e}}}{m_{\mathrm{e}}}\mathbb{B}_x(\mathbf{Z}^0, \mathbf{b}_x^0)\mathbf{V}_y^0. \tag{6.15j}$$

The corresponding integrator is denoted by $\mathbf{u}(\Delta t) = \Phi_{\Delta t}^y(\mathbf{u}^0)$.

Problem 6. For $t \in [0, \Delta t]$ and $\mathbf{u}(t = 0) = \mathbf{u}^0$ we have,

$$\frac{\mathrm{d}\mathbf{u}}{\mathrm{d}t} = \mathbb{J}(\mathbf{u})\nabla_{\mathbf{u}}H_z(\mathbf{u}), \tag{6.16}$$

where

$$H_z = \frac{m_{\mathrm{e}}}{2}\mathbf{V}_z^\top\mathbb{W}\mathbf{V}_z. \tag{6.17}$$

This can be solved analytically as

$$\frac{\mathrm{d}\mathbf{e}_x}{\mathrm{d}t} = 0 \qquad\qquad \implies \quad \mathbf{e}_x(\Delta t) = \mathbf{e}_x^0, \tag{6.18a}$$

$$\frac{\mathrm{d}\mathbf{e}_y}{\mathrm{d}t} = 0 \qquad\qquad \implies \quad \mathbf{e}_y(\Delta t) = \mathbf{e}_y^0, \tag{6.18b}$$

$$\frac{\mathrm{d}\mathbf{b}_x}{\mathrm{d}t} = 0 \qquad\qquad \implies \quad \mathbf{b}_x(\Delta t) = \mathbf{b}_x^0, \tag{6.18c}$$

$$\frac{\mathrm{d}\mathbf{b}_y}{\mathrm{d}t} = 0 \qquad\qquad \implies \quad \mathbf{b}_y(\Delta t) = \mathbf{b}_y^0, \tag{6.18d}$$

$$\frac{\mathrm{d}\mathbf{y}_x}{\mathrm{d}t} = 0 \qquad\qquad \implies \quad \mathbf{y}_x(\Delta t) = \mathbf{y}_x^0, \tag{6.18e}$$

$$\frac{\mathrm{d}\mathbf{y}_y}{\mathrm{d}t} = 0 \qquad\qquad \implies \quad \mathbf{y}_y(\Delta t) = \mathbf{y}_y^0, \tag{6.18f}$$

$$\frac{\mathrm{d}\mathbf{Z}}{\mathrm{d}t} = \frac{1}{m}\mathbb{W}^{-1}m_{\mathrm{e}}\mathbb{W}\mathbf{V}_z \qquad \implies \quad \mathbf{Z}(\Delta t) = \mathbf{Z}^0 + \Delta t\mathbf{V}_z^0, \tag{6.18g}$$

$$\frac{\mathrm{d}\mathbf{V}_x}{\mathrm{d}t} = -\frac{q_{\mathrm{e}}}{m_{\mathrm{e}}^2}\mathbb{B}_y\mathbb{W}^{-1}m_{\mathrm{e}}\mathbb{W}\mathbf{V}_z \implies \quad \mathbf{V}_x(\Delta t) = \mathbf{V}_x^0 - \frac{q_{\mathrm{e}}}{m_{\mathrm{e}}}\int_0^{\Delta t}\mathbb{B}_y(\mathbf{Z}(s), \mathbf{b}_y^0)\mathrm{d}s\mathbf{V}_z^0 \tag{6.18h}$$

$$\frac{\mathrm{d}\mathbf{V}_y}{\mathrm{d}t} = \frac{q_{\mathrm{e}}}{m_{\mathrm{e}}^2}\mathbb{B}_x\mathbb{W}^{-1}m_{\mathrm{e}}\mathbb{W}\mathbf{V}_z \quad \implies \quad \mathbf{V}_y(\Delta t) = \mathbf{V}_y^0 + \frac{q_{\mathrm{e}}}{m_{\mathrm{e}}}\int_0^{\Delta t}\mathbb{B}_x(\mathbf{Z}(s), \mathbf{b}_x^0)\mathrm{d}s\mathbf{V}_z^0 \tag{6.18i}$$

$$\frac{\mathrm{d}\mathbf{V}_z}{\mathrm{d}t} = 0 \qquad\qquad \implies \quad \mathbf{V}_z(\Delta t) = \mathbf{V}_z^0. \tag{6.18j}$$

The corresponding integrator is denoted by $\mathbf{u}(\Delta t) = \Phi_{\Delta t}^z(\mathbf{u}^0)$.

Steps (6.18h) and (6.18i) involve integrals of the form

$$\int_0^{\Delta t}\varphi_{j+1/2}^1(z_k^0 + sv_{k,z}^0)\mathrm{d}s, \tag{6.19}$$

which can be computed exactly for a particle r starting in the element $\Omega_k = [c_k, c_{k+1}]$, i.e. $z_r^0 \in \Omega_k$, and the non-vanishing basis functions in this elements as follows:

1. Change of variables $s'(s) = z_r^0 + sv_{r,z}^0$:

$$\int_0^{\Delta t}\varphi_{j+1/2}^1(z_r^0 + sv_{r,z}^0)\mathrm{d}s = \frac{1}{v_{r,z}^0}\int_{z_r^0}^{z_r^0 + \Delta t v_{r,z}^0}\varphi_{j+1/2}^1(s')\mathrm{d}s' \tag{6.20}$$

2. Change of variables $s''(s') = \frac{2(s'-c_k)}{c_{k+1}-c_k}$ on the reference interval $I = [-1,1]$ in order to get an integral over the shape functions χ:

$$\frac{1}{v_{r,z}^0} \int_{z_r^0}^{z_r^0 + \Delta t v_{r,z}^0} \varphi_{j+1/2}^1(s') \mathrm{d}s' = \frac{1}{v_{r,z}^0} \frac{c_{k+1} - c_k}{2} \int_{s''(z_r^0)}^{s''(z_r^0 + \Delta t v_{r,z}^0)} \chi_{n+1/2}(s'') \mathrm{d}s'' \quad (6.21)$$

3. Use that LH shape functions χ are linear combinations of first order derivatives of LP shape functions η of degree p:

$$\chi_{n+1/2}(s'') = \sum_{m=n+1}^{p} \frac{\mathrm{d}}{\mathrm{d}s''} \eta_m(s'') \quad (6.22)$$

$$\Rightarrow \frac{1}{v_{r,z}^0} \frac{c_{k+1} - c_k}{2} \int_{s''(z_r^0)}^{s''(z_r^0 + \Delta t v_{r,z}^0)} \chi_{n+1/2}(s'') \mathrm{d}s'' \quad (6.23)$$

$$= \frac{1}{v_{r,z}^0} \frac{c_{k+1} - c_k}{2} \sum_{m=n+1}^{p} \int_{s''(z_r^0)}^{s''(z_r^0 + \Delta t v_{r,z}^0)} \frac{\mathrm{d}}{\mathrm{d}s''} \eta_m(s'')(s'') \mathrm{d}s'' \quad (6.24)$$

$$= \frac{1}{v_{r,z}^0} \frac{c_{k+1} - c_k}{2} \sum_{m=n+1}^{p} [\eta_m(s''(z_r^0 + \Delta t v_{r,z}^0)) - \eta_m(s''(z_r^0))] \quad (6.25)$$

4. Finally, if the particle reaches the right $(v_{r,z}^0 > 0)$ or the left $(v_{r,z}^0 < 0)$ element boundary within the time step Δt, set

$$z_r^0 + \Delta t v_{r,z}^0 = \begin{cases} c_{k+1}, & \text{if } v_{r,z}^0 > 0 \\ c_k, & \text{if } v_{r,z}^0 < 0 \end{cases} \quad (6.26)$$

since the basis functions of V_1 are not zero only in one element. On the other hand, such a particle entering an adjacent element, contributes to the non-vanishing basis functions in this element, where the integration now must be started at

$$z_r^0 = \begin{cases} c_{k+1}, & \text{if } v_{r,z}^0 > 0 \\ c_k, & \text{if } v_{r,z}^0 < 0. \end{cases} \quad (6.27)$$

Of course, it can happen that a particle propagates through multiple elements (e.g. for large time steps Δt or large particle velocities $v_{r,z}^0$). Then the integration boundaries need to be adjusted in the above way every time the particle crosses an element boundary.

Note that the matrices $\mathbb{Q}^0$, $\mathbb{Q}^1$, $\mathbb{B}_x$ and $\mathbb{B}_y$ need to be updated after applying this integrator since the particle positions $\mathbf{Z}$ change.

References

[1]   D. N. Arnold, R. S. Falk, R. Winther: *Finite Element exterior calculus, homological techniques, and applications*, Acta Numerica **15**, 1-155 (2006).

[2]   D. N. Arnold, R. S. Falk, R. Winther: *Finite Element exterior calculus: From Hodge theory to numerical stability*, Bulletin of the American mathematical society, **47(2)**, 281-354 (2010).

[3]   P. J. Morrison: *Structure and structure-preserving algorithms for plasma physics*, Physics of Plasma **24**, 055502 (2017).

[4]   R. I. McLachlan, G. R. W. Quispel: *Splitting methods*, Acta Numerica **11**, 341-434 (2002).

[5]   U. Stroth: *Plasmaphysik*, Viehweg + Teubner Verlag, Wiesbaden, 1. Auflage, 2011.

[6]   Y. Horibe, N. Ogura: *Deuterium Content as a Parameter of Water Mass in the Ocean*, J. Geophys. Res. **73**, 1239-1249 (1968).

[7]   J. D. Lawson: *Some Criteria for a Power Producing Thermonuclear Reactor*, Proc. Phys. B **70**, 6-10 (1957).

[8]   D. Keefe, *Inertial Confinement*, Ann. Rev. Nucl. Part. Sci. **32**, 391-441 (1982).

[9]   O. A. Hurricane: *Fuel gain exceeding unity in an inertially confined fusion implosion*, Nature **506**, 343-348 (2014).

[10]   L. Chen, F. Zonca: *Physics of Alfvén waves and energetic particles in burning plasmas*, Rev. Mod. Phys. **88**, 015008 (2016).

[11]   W. W. Heidbrink: *Basic physics of Alfvén instabilities driven by energetic particles in toroidally confined plasmas*, Physics of Plasmas **15**, 055501 (2008).

[12]   P. Lauber: *Linear Gyrokinetic Description of Fast Particle Effects on the MHD Stability in Tokamaks*, Dissertation TU München, 2003.

[13]   Y. Katoh, Yoshiharu: *Computer simulation of chorus wave generation in the Earth's inner magnetosphere*, Geophys. Res. Lett. **34**, L03102 (2007).

[14]   X. Tao: *A numerical study of chorus generation and the related variation of wave intensity using the DAWN code*, J. Geophys. Res. Space Physics **119**, 3362-3372 (2014).

[15]   M. Brambilla: *Kinetic Theory of Plasma Waves: Homogeneous Plasmas*, Oxford University Press, Oxford, 1998.

[16]   S. I. Braginskii: *Transport processes in a plasma*, in: Reviews of Plasma Physics (M. A. Leontovich, Editor), Consultants Bureau, New York, Vol. 1, 205-311 (1966).

[17] G. T. A. Huysmans, O. Czarny: *MHD stability in X-point geometry: simulation of ELMs*, Nucl. Fusion **47**, 659-666 (2007).

[18] J. Donea, A. Huerta: *Finite Element Methods for Flow Problems*, John Wiley & Sons, Ltd., 2003.

[19] M. Kraus, K. Kormann, P. J. Morrison, E. Sonnendrücker: *GEMPIC: geometric electromagnetic particle-in-cell methods*, J. Plasma Phys. **83**, 905830401 (2015).

[20] F. Xiao, R. M. Thorne, D. Summers: *Instability of electromagnetic R-mode waves in a relativistic plasma*, Physics of Plasmas **5**, 2489-2497 (1998).

[21] I. N. Bronstein, K. A. Semendjajew, G. Musiol, H. Mühlig: *Taschenbuch der Mathematik*, Harri Deutsch Verlag, Frankfurt am Main, 8. Auflage, 2012.

[22] K. Birdsall, A. Langdon: *Plasma physics via computer simulation*, CRC press, 2004.

[23] H. Qin, S. Zhang, J. Xiao, J. Liu, Y. Sun, W. M. Tang: *Why is Boris algorithm so good?*, Physics of Plasmas **20**, 084503 (2013).

[24] A. Ratnani, E. Sonnendrücker: *Arbitrary High-Order Spline Finite Element Solver for the Time Domain Maxwell equations*, Journal of Scientific Computing, Springer Verlag, 2011.

[25] L. L. Schumaker: *Spline Functions - Computational Methods*, Society for Industrial and Applied Mathematics, Philadelphia, 2015.

[26] P. J. Roache: *Code Verification by the Method of Manufactured Solutions*, J. of Fluids Eng. **124**, 4-10 (2002).

[27] J. H. Bramble, J. E. Pasciak, O. Steinbach, *On the stability of the L^2-projection in $H^1(\Omega)$*, Mathematics of Computation **71**, 147-156 (2001).

[28] J. Crank, P. Nicolson: *A practical method for numerical evaluation of solutions of partial differential equations of the heat-conduction type*, Advances in Computational Mathematics **6**, 207-226 (1997).

[29] A. Y. Aydemir: *A unified Monte Carlo interpretation of particle simulations and applications to non-neutral plasmas*, Physics of Plasmas **1**, 822-831 (1994).

[30] H. F. Trotter: *On the product of semi-groups of operators*, Proc. Am. Math. Soc. **10**, 545-551 (1959).

[31] G. Strang: *On the construction and comparison of differences schemes*, SIAM . Numeri. Anal. **5**, 506-517 (1968).

Ackknowledgements

To end this thesis, I would like to thank everybody who has supported me in the last year and without whom this work would not have been possible: